Charles University in Prague
Faculty of Mathematics and Physics

DIPLOMA THESIS

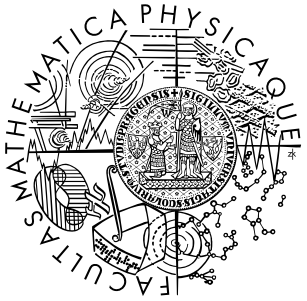

Richard Řezníček

Influence of cationic substitution on hyperfine interactions in magnetite

Department of Low Temperature Physics

Supervisor: prof. RNDr. Helena Štěpánková, CSc.
Study program: Physics of Condensed Matter and Materials

2010

I would like to express my gratitude to my supervisor prof. RNDr. Helena Štěpánková, CSc. for her guidance and for provided advice. I am also obliged to my consultant Mgr. Vojtěch Chlan. I wish to thank those who kindly provided the samples: prof. V. A. M. Brabers from Technical University of Eindhoven, prof. J. M. Hönig from Purdue University in West Lafayette, prof. dr hab. Ing. Andrzej Kozłowski and prof. dr hab. Ing. Zbigniew Kakol from AGH University of Kraków. I am grateful to Ing. Pavel Novák, DSc. for his hints. Finally, I wish to thank my sister Alena for language corrections.

Prohlašuji, že jsem svou diplomovou práci napsal samostatně a výhradně s použitím citovaných pramenů. Souhlasím se zapůjčováním práce.

I hereby confirm that the diploma thesis submitted is entirely my own work and all other sources used are cited appropriately. I agree with lending of the thesis.

Prague, 12th April 2010 Richard Řezníček

Contents

Název práce: Vliv substituce kationtů na hyperjemné interakce v magnetitu
Autor: Richard Řezníček
Katedra (ústav): Katedra fyziky nízkých teplot
Vedoucí diplomové práce: prof. RNDr. Helena Štěpánková, CSc.
e-mail vedoucího: Helena.Stepankova@mff.cuni.cz

Abstrakt: Tématem předložené práce je studium souborů monokrystalických vzorků magnetitu se substitucemi zinku a titanu metodami NMR. Ionty substituce zinku Zn^{2+} nahrazují část železitých iontů v tetraedrických (A) pozicích, zatímco ionty titanu Ti^{4+} obsazují oktaedrické (B) pozice nahrazujíce ionty železa $Fe^{2.5+}$. Hyperjemné interakce a lokální elektronová struktura jsou citlivé na přítomnost substituce. Obzvláště zajímavý je případ, když valence iontů substituce je odlišná od valence nahrazovaného iontu. Resonanční frekvence jader v okolí substituce jsou posunuty v důsledku změněného hyperjemného pole, je tedy možné pozorovat satelitní čáry ve spektrech NMR. Teplotní závislosti spekter nad Verweyovým přechodem byly měřeny v nulovém vnějším magnetickém poli a byla také změřena spektra NMR při teplotě 4,2 K. Sestavené teplotní závislosti frekvencí hlavních čar a satelitních signálů ve spektrech nad Verweyovým přechodem byly porovnány s daty pro čistý magnetit a magnetit s dalšími substitucemi a kationtovými vakancemi. Dále byly nad Verweyovým přechodem nalezeny a diskutovány změny šířek A čar s teplotou.

Klíčová slova: NMR, magnetit, substituce Zn, substituce Ti, elektronová struktura

Title: Influence of cationic substitution on hyperfine interactions in magnetite
Author: Richard Řezníček
Department: Department of Low Temperature Physics
Supervisor: prof. RNDr. Helena Štěpánková, CSc.
Supervisor's e-mail address: Helena.Stepankova@mff.cuni.cz

Abstract: The subject matter of the present work is a study of a series of single crystal samples of magnetite with substitutions of zinc and titanium by means of the NMR method. Ions of the zinc substitution Zn^{2+} replace a part of ferric ions at tetrahedral (A) sites, while the titanium ions Ti^{4+} occupy octahedral (B) sites replacing iron ions $Fe^{2.5+}$. Hyperfine interactions and local electronic structure are sensitive to the presence of substitution. The case when the valence of the substitution ion is different from that of the replaced ion is of a particular interest. Resonance frequencies of nuclei in the neighbourhood of the substitution are shifted due to the modified hyperfine field, thus satellite lines can be observed in NMR spectra. Temperature dependences of spectra above the Verwey transition were measured in a zero external magnetic field. Additionally, NMR spectra were also acquired at the temperature of 4.2 K. Temperature dependences of frequencies of main lines and satellite signals in the spectra above the Verwey transition were constructed and compared to the data for pure magnetite and magnetite with other substitutions and with cationic vacancies. Furthermore, variations of widths of A lines against the temperature above the Verwey transition were found and discussed.

Keywords: NMR, magnetite, Zn substitution, Ti substitution, electronic structure

Chapter 1

Introduction

Magnetite (Fe_3O_4), one of the first discovered magnetic materials, exhibits many interesting physical properties. The most characteristic feature of this compound is a structural phase transition of the first order at ≈ 120 K, which is known as the Verwey transition. During this transition, changes of other physical properties of this substance occur, e.g. specific heat anomaly and an abrupt change of electrical conductivity. Despite the longstanding research of magnetite, its electronic structure and the principle of the Verwey transition are still not completely resolved. A broad range of applications of magnetite-derived ferrites, especially in electrotechnics and electronics, and a recent utilization of these materials in other fields, e.g. in biomedical applications, represent another cogent argument for both fundamental and applied physical research of magnetite.

Physical properties, especially the electronic structure and the Verwey transition, are influenced by the presence of substitution or vacancies in a sample. Thus a systematical study of substituted and non-stoichiometric magnetite can bring new information important for our understanding of the physical properties and processes related to this compound. Nuclear magnetic resonance is particularly suitable for microstructure investigation of magnetite as the resonating ^{57}Fe nuclei serve as a local hyperfine field probe. Moreover, the NMR method provides the highest resolution of all hyperfine methods, which makes it possible to observe even fine structures in spectra. The contribution of NMR in the magnetite research can be documented for example by articles [1] and [2], which propose the charge density wave model of charge ordering in magnetite below the Verwey transition based on NMR experiments.

Existing works employing NMR on substituted magnetite focused mainly on substitution of aluminium ions Al^{3+} [3], [4] and gallium ions Ga^{3+} [5]. NMR spectrum of magnetite substituted by titanium ions Ti^{4+} at 273 K was published only in [6], spectra and relaxation times of zinc substituted magnetite at 4.2 K, 198 K and 273 K were measured in [7]. This work aims to measure temperature dependence of NMR spectra above the Verwey transition of titanium and zinc substituted magnetite samples. Results of performed experiments are analyzed and compared to data for magnetite with other substitutions and for non-stoichiometric magnetite in order to obtain information about the impact of substitutions on the NMR spectra and on the magnetic and electronic structure of magnetite.

Chapter 2

NMR Method

2.1 NMR Principles

2.1.1 Nuclear Magnetic Moment

Vector sum of spin and orbital angular momenta of nucleons is called nuclear spin $\vec{I}$. Absolute value of nuclear spin $|\ \vec{I}\ |$ is connected to nuclear spin quantum number I (0, 1/2, 1, 3/2, ...) by relation

$$|\ \vec{I}\ | = \hbar\sqrt{I\,(I+1)}. \tag{2.1}$$

The z-component is given by nuclear spin magnetic quantum number m ($-I$, $-I+1$, ..., $I-1$, I)

$$I_z = \hbar m. \tag{2.2}$$

Nuclear magnetic moment is related to nuclear spin and gyromagnetic ratio γ

$$\hat{\vec{\mu}} = \gamma \hat{\vec{I}}, \tag{2.3}$$

for z-component applies

$$\hat{\mu}_z = \gamma \hat{I}_z. \tag{2.4}$$

2.1.2 Interaction with Magnetic Field

Interaction of the nuclear magnetic moment $\vec{\mu}$ with an external (static) magnetic field $\vec{B}_0$ is described by Hamiltonian

$$\hat{H}_0 = -\hat{\vec{\mu}} \cdot \vec{B}_0. \tag{2.5}$$

Let $\vec{B}_0 = (0, 0, B_0)$ and rewrite the Hamiltonian as

$$\hat{H}_0 = -\gamma \hat{I}_z B_0. \tag{2.6}$$

Energy eigenvalues are then determined by the values of magnetic quantum number m (see (2.2)):

$$E_m = -\gamma \hbar m B_0. \tag{2.7}$$

The set of $2I+1$ energy eigenvalues forms Zeeman multiplet of equidistant energy levels corresponding to particular space orientations of the nuclear magnetic moment.

2.1.3 Effect of RF Field

If we consider the presence of an external radio-frequency (RF) magnetic field $\vec{B}_1 = (B_1 \cos\omega_z t, B_1 \sin\omega_z t, 0)$ (ω_z is angular frequency) in addition to the static magnetic field $\vec{B}_0 = (0, 0, B_0)$, we can write the Hamiltonian of the interaction of the nuclear magnetic moment with the magnetic field in the form

$$\hat{H} = \hat{H}_0 + \hat{H}_1(t), \tag{2.8}$$

where

$$\hat{H}_1 = -\hat{\vec{\mu}} \cdot \vec{B}_1 = -\gamma B_1 \left(\hat{I}_x \cos\omega_z t + \hat{I}_y \sin\omega_z t\right) = -\frac{\gamma B_1}{2}\left(\hat{I}^- e^{i\omega_z t} + \hat{I}^+ e^{-i\omega_z t}\right) \tag{2.9}$$

($\hat{I}^-$ and $\hat{I}^+$ are lowering and raising operators).

The RF field can induce transitions between the levels of Zeeman multiplet. This effect is called the nuclear magnetic resonance (NMR). The probability of transition between states with quantum numbers m and m' is in approximation of perturbation theory (valid for $B_1 << B_0$) proportional to perturbation matrix element

$$P_{m',m} \sim |\langle m'|\hat{H}_1|m\rangle|^2. \tag{2.10}$$

Considering the form of Hamiltonian (2.9) and the properties of ladder operators, we notice that only transitions between neighbouring levels are allowed, i.e. $m' = m \pm 1$.

The transition between neighbouring levels of Zeeman multiplet is accompanied by emission or absorption of energy quantum $|\Delta E| = \gamma\hbar B_0$ (see (2.7)). This energy quantum can be written as $\Delta E = \hbar\omega_0$ and thus we obtain the resonance condition [8]

$$\omega_0 = \gamma B_0, \tag{2.11}$$

where ω_0 is called Larmor frequency.

2.1.4 Nuclear Magnetization

Macroscopic nuclear magnetization $\vec{M}$ can be understood as a sum of magnetic moments $\vec{\mu}_i$ of nuclei in volume V

$$\vec{M} = \sum_{i=1}^{N} \frac{\vec{\mu}_i}{V}, \tag{2.12}$$

where N is the number of nuclei in the specified volume.

Assuming the thermal equilibrium with lattice at temperature T, the occupation probability p_m for level E_m of Zeeman multiplet corresponding to magnetic quantum number m is determined by Boltzmann distribution

$$p_m = \frac{e^{-\frac{E_m}{k_B T}}}{\sum_{m'=-I}^{I} e^{-\frac{E_{m'}}{k_B T}}}, \tag{2.13}$$

where k_B is the Boltzmann constant. The equilibrium nuclear magnetization $\vec{M}_0 = (0, 0, M_0)$ in external magnetic field $\vec{B}_0 = (0, 0, B_0)$ can be obtained by employing relations (2.4) and (2.2):

$$M_0 = \sum_{i=1}^{N} \frac{\gamma\hbar}{V} \sum_{m=-I}^{I} m p_m = \frac{N\gamma\hbar}{V} \frac{\sum_{m=-I}^{I} m e^{-\frac{E_m}{k_B T}}}{\sum_{m=-I}^{I} e^{-\frac{E_m}{k_B T}}} = \frac{N\gamma\hbar}{V} I B_I \left(\frac{I\gamma\hbar B_0}{k_B T} \right), \quad (2.14)$$

where $B_I(x)$ stands for Brillouin function. For $\frac{I\gamma\hbar B_0}{k_B T} << 1$ we get the equation

$$M_0 = \frac{N\gamma^2\hbar^2}{V} \frac{I(I+1) B_0}{3 k_B T} \quad (2.15)$$

corresponding to Curie's law.

2.1.5 Bloch equations

Now we consider a condensed matter placed in an external magnetic field $\vec{B} = \vec{B}_0 + \vec{B}_1(t)$, where $B_1 << B_0$, $\vec{B}_0 = (0, 0, B_0)$, $\vec{B}_1 = (B_1 \cos\omega_z t, B_1 \sin\omega_z t, 0)$ and $\vec{\omega}_z$ is the frequency of the RF field. The motion of nuclear magnetization $\vec{M}$ is phenomenologically described by Bloch equations:

$$\frac{dM_x}{dt} = \gamma \left(\vec{M} \times \vec{B} \right)_x - \frac{M_x}{T_2} \quad (2.16)$$

$$\frac{dM_y}{dt} = \gamma \left(\vec{M} \times \vec{B} \right)_y - \frac{M_y}{T_2} \quad (2.17)$$

$$\frac{dM_z}{dt} = \gamma \left(\vec{M} \times \vec{B} \right)_z - \frac{M_z - M_0}{T_1} \quad (2.18)$$

where T_1 is called spin-lattice (longitudinal) relaxation time, T_2 is spin-spin (transverse) relaxation time and $\vec{M}_0 = (0, 0, M_0)$ is equilibrium magnetization in the field $\vec{B}_0$.

The first term at the right side of Bloch equations describes how the nuclear magnetization is influenced by torsional moment of the external field. In the absence of an RF field (i.e. $B_1 = 0$), nuclear magnetization exercises Larmor precession around the direction of the static field $\vec{B}_0$ at Larmor frequency

$$\vec{\omega}_0 = -\gamma \vec{B}_0. \quad (2.19)$$

When the RF field is present, we should take advantage of the transformation of equations (2.16), (2.17) and (2.18) into the system of coordinates rotating with the RF field, which replaces the time-dependent field $\vec{B}$ in the expressions by a time-independent effective field

$$\vec{B}_{ef} = \left(B_1, 0, B_0 + \frac{\omega_z}{\gamma} \right). \quad (2.20)$$

In the rotating system of coordinates, nuclear magnetization precedes around the effective field $\vec{B}_{ef}$ at a frequency $\vec{\omega}_1 = -\gamma \vec{B}_{ef}$.

Now we consider the RF field in the form of a single pulse of length τ. We start at $B_1 = 0$ and $\vec{M} \,||\vec{B}_0$, then we apply the RF pulse and at the end of the pulse the nuclear magnetization is tilted at an angle (referenced to z-axis)

$$\theta = \gamma B_1 \tau. \tag{2.21}$$

This principle can be used to adjust the precession angle.

The second term at the right side of Bloch equations describes how the nuclear magnetization returns to equilibrium. The last term at the right side of equation (2.18) corresponds to the interaction of nuclear spins and lattice. The rate of energy transfer from spin system to lattice after tilting nuclear magnetization from equilibrium is characterized by spin-lattice relaxation time T_1. The second terms at the right side of equations (2.16) and (2.17) describe the decay of transverse components of nuclear magnetization caused by fluctuations of Larmor precession frequencies of particular nuclear magnetic moments. In the ideal case of an absolutely homogenous field $\vec{B}_0$, the decay is characterized by spin-spin relaxation time T_2. In reality, however, Larmor frequencies of individual nuclear magnetic moments differ due to local inhomogeneities of the field $\vec{B}_0$, which results in faster decay characterized by time $T_2^\star$ because of out-of-phase motion of individual moments.

2.2 Pulse Sequences

Today's NMR experiments are almost exclusively based on pulse methods, i.e. RF field $\vec{B}_1(t)$ is applied in the form of short pulses and the response of nuclear magnetization is detected in the time after or between pulses. The length of pulses is assumed to be far shorter than spin-lattice and spin-spin relaxation times. This chapter contains short characteristics of two basic pulse sequences (FID and spin echo) and CPMG sequence, which was employed in performed experiments.

2.2.1 Free Induction Decay

Pulse sequence for free induction decay measurements consists of a single RF pulse at Larmor frequency of length corresponding to $\pi/2$ tilt of nuclear magnetization according to (2.21). Such pulse is called $\pi/2$-pulse. Transverse component of nuclear magnetization can be detected after the end of the pulse as a free induction decay signal. In case of an absolutely homogenous field $\vec{B}_0$, the amplitude A of the signal would decay in time t ($t = 0$ set at the start of pulse) as

$$A(t) \sim \exp\left(-\frac{t}{T_2}\right). \tag{2.22}$$

However, local inhomogeneities of the magnetic field $\vec{B}_0$ cause much faster decay

$$A(t) \sim \exp\left(-\frac{t}{T_2^\star}\right). \tag{2.23}$$

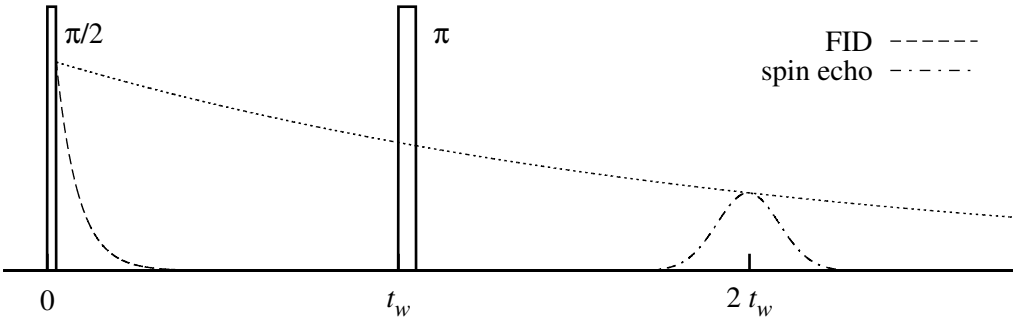

Figure 2.1: Free induction decay and spin echo sequences

2.2.2 Spin Echo

The sequence for spin echo signal measurement can be obtained by appending the second RF pulse at Larmor frequency of length corresponding to π tilt of nuclear magnetization (see (2.21)) to the FID sequence. Time interval t_w between the $\pi/2$-pulse and this π-pulse should be shorter than spin-spin relaxation time T_2. The application of π-pulse flips the transverse component of nuclear magnetization through π angle around the $\vec{B}_1$ direction. Thus the local magnetization vectors get aligned in the time $2t_w$ and the transverse component of nuclear magnetization can be observed as a spin echo signal. Amplitude of spin echo signal follows the relation (2.22).

2.2.3 CPMG Sequence

Spin echo sequence can be further extended by appending additional π-pulses while keeping $2t_w$ time spacing between adjacent π-pulses. In this case, the spin echo signal can be detected in each time window between π-pulses (and of course also after the last π-pulse), while the amplitudes of these echoes correspond to relation (2.22). This pulse sequence, which is named Carr-Purcell sequence, is very sensitive to improperly adjusted π-pulse length and intensity, because any deviation causes nuclear magnetization to point slightly out of the transverse plane and these errors cumulate through the sequence. The abovementioned problem is solved in Carr–Purcell–Meiboom–Gill (CPMG) pulse sequence by introducing $\pi/2$ phase shift of $\pi/2$-pulse relative to π-pulses' phase. As was shown in [9], the described errors are not cumulative in CPMG sequence.

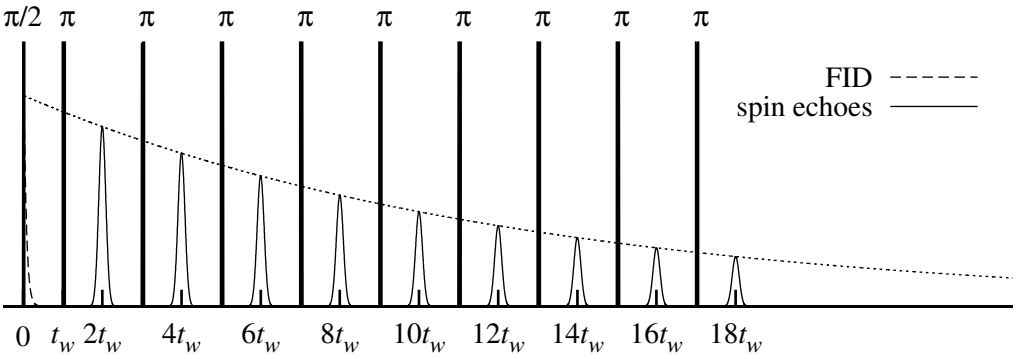

Figure 2.2: CPMG pulse sequence

2.3 NMR Spectrum

NMR spectrum is a distribution of resonance (Larmor) frequencies of nuclear magnetic moments in an investigated sample excited by the pulse sequence. In order to obtain the spectrum, Fourier transform has to be applied to signal in the time domain acquired during pulse method experiments. Free induction decay or spin echo signal can be usually transformed directly, whereas in case of the signal from the CPMG experiment, it is useful to average corresponding data points from detected echoes in order to obtain waveform similar to the signal of one spin echo while taking advantage of significantly better signal-to-noise ratio (SNR). However, the shape of the spectrum can be influenced by frequency dependence of spin-spin relaxation time T_2 if averaged echoes originate from time interval of length comparable to T_2.

2.4 NMR Spectrometer

Pulse NMR spectrometer, a simplified block diagram of which is in figure 2.3, is used to apply the desired sequence of RF pulses to a sample and to record the nuclear magnetization response.

A pulse generator is responsible both for the proper length and timing of excitation pulses and for triggering of signal acquisition. An RF signal at desired frequency and with appropriate phase is generated by a frequency synthesizer. A modulator transforms this signal into RF pulses, which are then appropriately attenuated and led into a (fixed gain) power amplifier in order to achieve requested pulse intensity. During excitation period, the power amplifier output is connected to the probe consisting of an LC resonance circuit (sample is placed in the coil) through the RX/TX switch, while the preamplifier input is isolated. Throughout the detection period, the power amplifier output is isolated from the probe and a signal induced in the LC circuit by the motion of transverse component of nuclear magnetization is connected to the preamplifier input. Amplified NMR signal is mixed with the second RF signal provided by the frequency synthesizer at frequency higher (or lower) by intermediate frequency (IF) than the excitation frequency. The resulting signal is further amplified in an IF amplifier and then sent into an I/Q detector. In-phase and quadrature signals from the outputs of the

detector are digitized by an A/D converter and stored in a memory. An important feature of this data acquisition is the ability to perform coherent summation of the signal, i.e. the pulse sequence is repeated many times and the corresponding data points from all scans are summed in order to improve the signal-to-noise ratio (SNR is proportional to a square root of number of scans). Acquired data are transferred into a computer for subsequent processing. This computer serves also for control of the spectrometer by operator. The purpose of a stable frequency reference is to ensure that all RF signals are coherent and that clock signals for relevant logic circuits are synchronous.

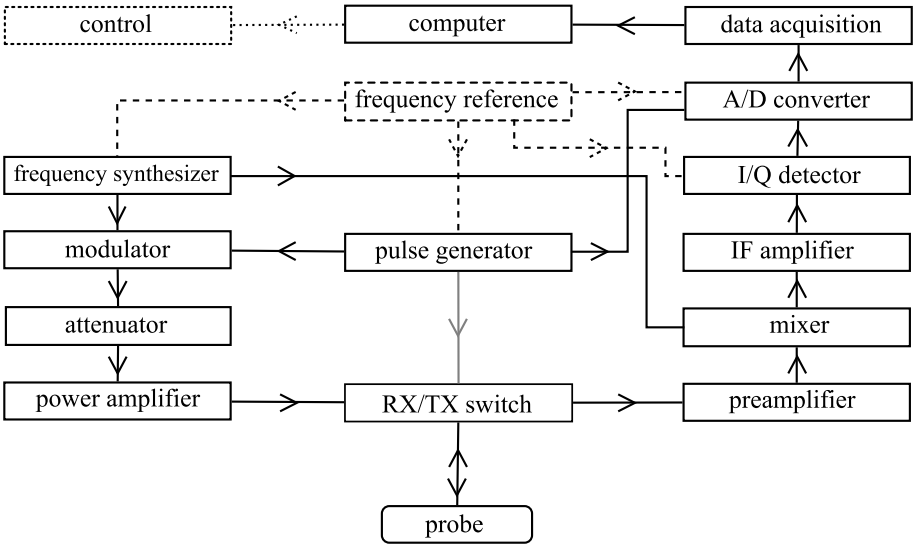

Figure 2.3: Simplified block diagram of pulse NMR spectrometer

2.5 NMR in Magnetics

A major part of a local magnetic field at nuclei in magnetically ordered matter is represented by hyperfine field originating from electron magnetic moments:

$$\vec{B}_h = -\frac{\mu_0 \mu_B}{2\pi} \sum_i \left(\frac{\hat{\vec{l}}_i}{r_i^3} + \frac{\hat{\vec{s}}_i}{r_i^3} - \frac{3\left(\hat{\vec{s}}_i \cdot \vec{r}_i\right)\vec{r}_i}{r_i^5} + \frac{8\pi}{3}\hat{\vec{s}}_i \delta\left(\vec{r}_i\right) \right), \tag{2.24}$$

where $\vec{r}_i$ are positions (relative to nucleus), $\hat{\vec{l}}_i$ stand for orbital moments and $\hat{\vec{s}}_i$ are spins of particular electrons, μ_0 denotes permeability of vacuum and μ_B is Bohr magneton. The first term in this equation is the magnetic field coming from electron orbital moments, other terms describe field corresponding to interaction between nucleus and electron spins, where the last term belongs to Fermi contact interaction. Time mean value of hyperfine field in magnetic substances is high even in a zero external magnetic field, which allows us to perform NMR experiments in these materials without the need for an external static magnetic field.

Hyperfine field is strongly dependent on crystal, electronic and magnetic structure of the sample in the vicinity of a nucleus. As a result, splitting of energy

levels of nuclei in crystallographically or magnetically nonequivalent positions is different. Also the presence of a defect near a nucleus influences the energy level splitting. Differences in splitting of both origins can be observed in a measured NMR spectrum. However, significant differences of hyperfine field strength in distinct crystallographic positions imply a wide spectral range.

The interaction of an external RF field with nuclear magnetic moments was described in previous paragraphs, but we also have to mention the interaction of this field with electron magnetic moments, which produces the oscillating component of a hyperfine field. Thus total RF field interacting with nuclear moments in magnetics is much stronger than an external RF field. Ratio of the total RF field amplitude B_2 and the external RF field amplitude B_1 is called enhancement (amplification) factor

$$\eta = \frac{B_2}{B_1}. \tag{2.25}$$

Values of η depend on the material and typically fall in the range from 1 to 10^4. This factor is usually different for nuclei in magnetic domains, where enhancement is caused by rotation of electron magnetization, than for those in walls, where enhancement process is based on wall motion.

The coupling between nuclear and electron systems is also responsible for the amplification of the detected signal.

Chapter 3

Structure of Magnetite

3.1 Crystal Structure

Chemical formula for magnetite is Fe_3O_4. The most typical feature of this compound is the Verwey phase transition at $T_V \approx 120$ K. This transition is accompanied by a change of crystal structure, specific heat anomaly and an abrupt change of electrical conductivity by two orders of magnitude. Detailed review can be found in [10] and [11].

At a temperature above the Verwey transition, magnetite has a cubic inverse spinel structure belonging to a space group $Fd\bar{3}m - O_h^7$. Elementary cell (lattice parameter $a = 8.398$ Å [12]) contains 32 oxygen ions O^{2-} arranged in a face centered cubic lattice. There are 64 tetrahedral and 32 octahedral interstitial positions between the oxygen ions in this lattice. Ferric ions Fe^{3+} occupy 8 tetrahedral (A) sites, while iron ions with mixed valency $Fe^{2.5+}$ are located at 16 octahedral (B) sites. Elementary cubic cell can be divided into 8 octants of two types with different iron ion positions as shown in figure 3.1. (See [13], [14] for details.) The symmetry of occupied crystallographic positions can be found in table 3.1 [15].

The structure of magnetite below the Verwey transition is monoclinic of space group Cc. Axes of elementary monoclinic cell $\vec{a}_m$, $\vec{b}_m$ a $\vec{c}_m$ correspond to directions $[1\bar{1}0]$, [110] a [001] in cubic lattice above the Verwey transition and the dimensions of the monoclinic cell expressed using the cubic cell parameter are $\sqrt{2}a \times \sqrt{2}a \times 2a$. Lattice parameters at temperature 10 K are $a_m = 11.868$ Å, $b_m = 11.851$ Å and $c_m = 16.752$ Å [16]. Angle between the monoclinic and $\vec{a}_m$ axes is $\beta = 90.2365\,(2)^\circ$ [17].

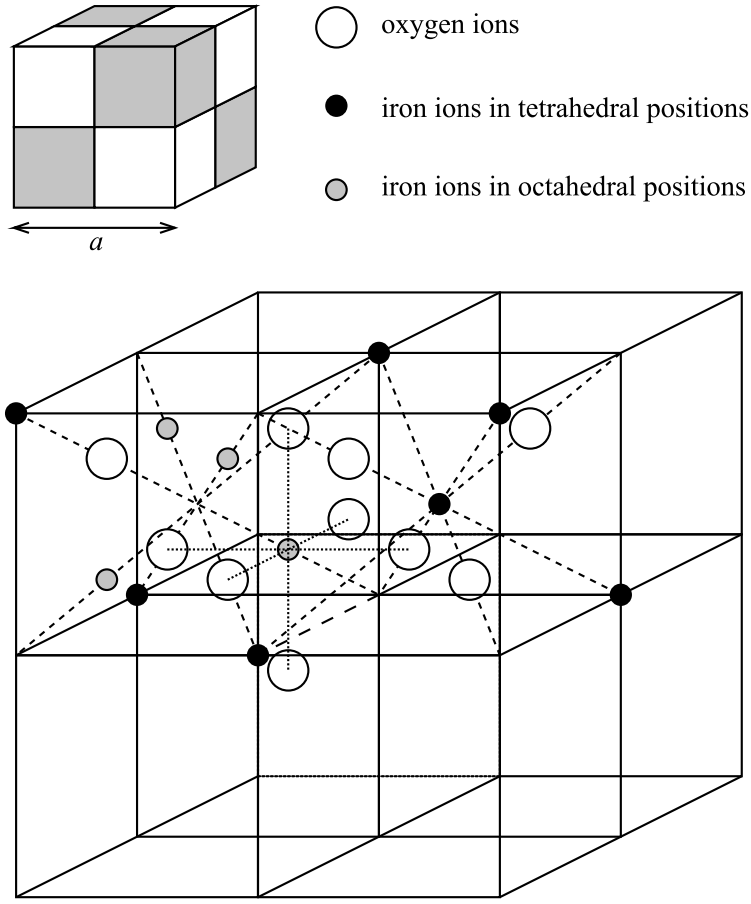

Figure 3.1: Magnetite elementary cell above the Verwey transition

Table 3.1: Occupied crystallographic sites in cubic magnetite structure (origin at tetrahedral site) [15]

Occupied positions	**Multiplicity**	**Wyckoff symbol**	**Symmetry**	**Coordinates**			
O^{2-} ion sites	32	e	3m	μ, μ, μ; μ, μ, μ; μ, μ, μ; μ, μ, μ;	1/4 -μ, 1/4 - μ, 1/4 - μ; 1/4 - μ, 1/4 + μ, 1/4+ μ; 1/4 + μ, 1/4 - μ, 1/4+μ; 1/4 + μ, 1/4+ μ, 1/4 - μ;		
$Fe^{2.5+}$ ion B sites	16	d	$\bar{3}$m	5/8,5/8,5/8;	5/8,7/8,7/8;	7/8,5/8,7/8;	7/8,7/8,5/8;
Fe^{3+} ion A sites	8	a	$\bar{4}$3m	0,0,0;	1/4,1/4,1/4;		

3.2 Magnetic Structure

Magnetite is a ferrimagnetic material with paramagnetic transition at a temperature $T_C \approx 860$ K. Magnetic moments of iron ions in A sites are anti-parallel to those of iron ions in B sites [14]. Total magnetic moment has a direction of moments of iron ions in B positions. The principal interactions responsible for magnetic ordering in magnetite are double exchange and superexchange interactions. Both the experimental data [18] for temperature dependence of magnetizations of A and B sublattices and the curves calculated [19] using Kubo-Ohata mean field theory [20] are shown in figure 3.2.

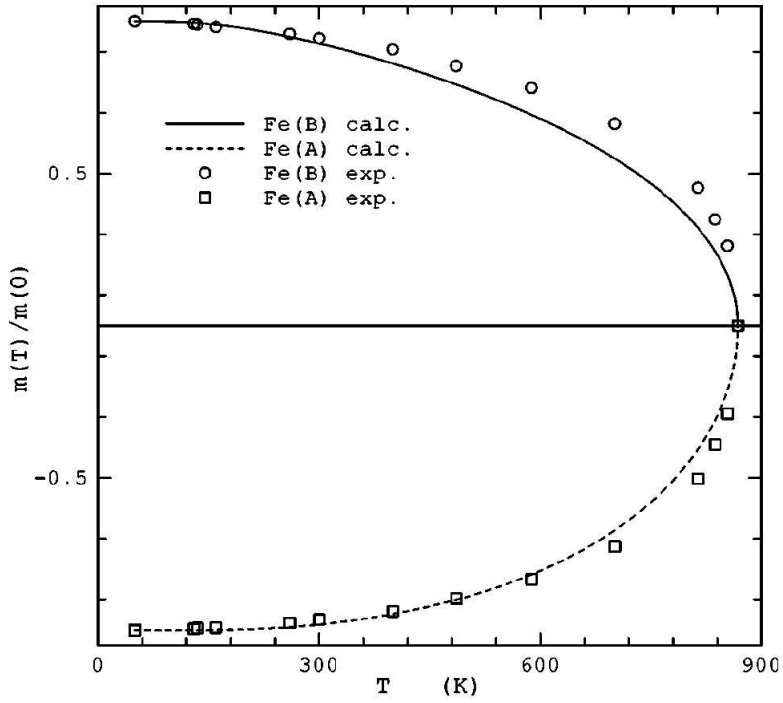

Figure 3.2: Comparison of the calculated and experimental reduced magnetizations in magnetite [19]

An easy magnetization direction in monoclinic lattice of magnetite below the Verwey transition is [001]. The number of magnetically nonequivalent positions then equals the number of crystallographically non-equivalent positions, i.e. there are 8 magnetically non-equivalent A positions and 16 magnetically non-equivalent B positions.

In the temperature range between the Verwey transition and the spin reorientation transition ($\approx 125 - 130$ K), the easy magnetization direction in cubic lattice is [001]. In this case all A positions are magnetically equivalent and also all B positions are magnetically equivalent.

Easy magnetization direction above spin reorientation transition is [111]. In this situation all A positions are magnetically equivalent, while B positions are divided into two groups of magnetically equivalent positions B_1 a B_2 in ratio 1:3.

3.3 NMR in Magnetite

NMR is a very suitable method for a study of crystal, electronic and magnetic structure of magnetite as the resonating nuclei ^{57}Fe represent a local hyperfine magnetic field probe. Each group of magnetically equivalent crystallographic positions of iron ions gives rise to one spectral line, the intensity of which is proportional to the count of resonating nuclei in this group. Considering the aforementioned phase transitions in magnetite, different structure of spectra can be expected for temperatures below the Verwey transition, between the Verwey and the spin reorientation transitions and above the spin reorientation transition, as can be seen in figure 3.3 [21]. The structure of spectra in figure 3.3 corresponds to the crystal and magnetic structure of magnetite at particular temperature. There are 8 A lines (two of them are overlapping) and 16 B lines (one of them is overlapped by A lines) resolved in the spectrum below the Verwey transition. One A line and one B line can be found in the spectrum measured at temperature in between the Verwey and the spin reorientation transitions. The spectrum acquired above the temperature of the spin reorientation transition contains one A line and two B lines (B_1 and B_2) with an intensity ratio 1:3.

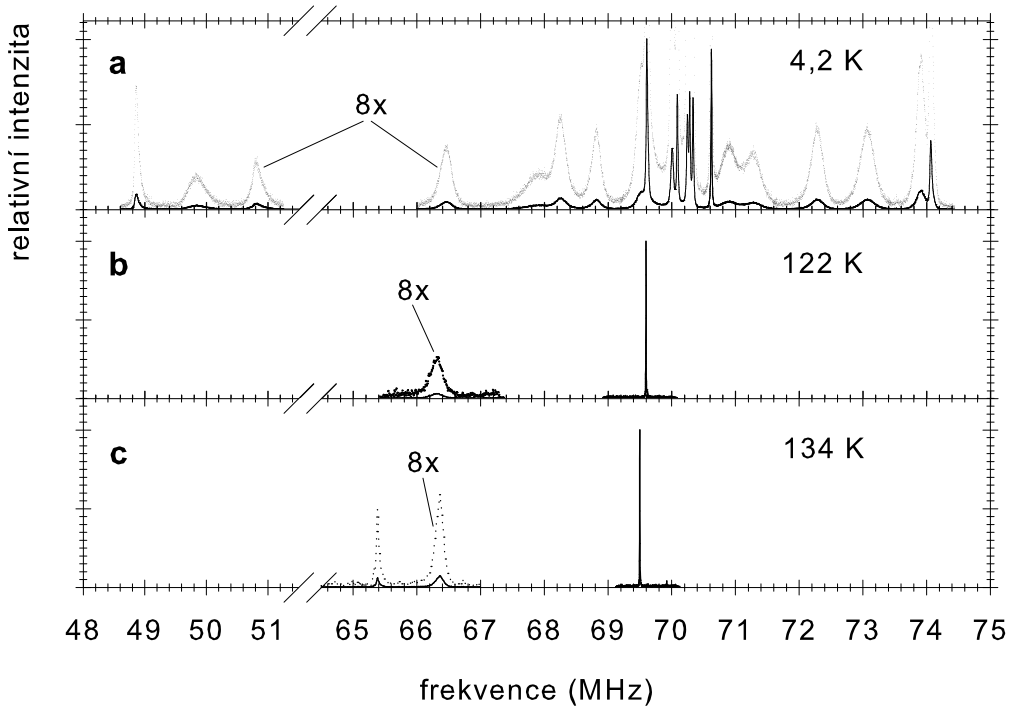

Figure 3.3: NMR spectra of pure magnetite measured at temperature below the Verwey transitions (a), between the Verwey and the spin reorientation transition (b) and above spin reorientation transition (c) [21]

Individual lines in NMR spectra of magnetite were identified in papers [2] and [1]. Temperature dependence of frequencies of individual lines in the range from 4,2 K to 135 K can be also found in [2], while the dependences above the Verwey transition up to 400 K for A line and up to 320 K for both A and B lines were published in [3] for pure and Al-substituted samples and in [22] for pure magnetite and magnetite with vacancies, respectively. Angular variations of frequencies of

spectral lines in an external magnetic field were reported in [1].

Spin-lattice relaxation times of particular spectral lines measured at temperature 4,2 K in [2] are comparable, whereas spin-spin relaxation times differ by orders of magnitude. Temperature dependences of both spin-lattice and spin-spin relaxation times below the Verwey transition were published in [23]. Dependences of relaxation times of all A lines are of similar character, the same applies for the B lines.

3.4 Substitution and Defects in Magnetite

Physical properties of magnetite can be strongly influenced by the presence of structural defects and substitutions at cation sites. In particular, the temperature of the Verwey transition decreases with increasing concentration of substitution or vacancies in a sample – see figure 3.4 [24]. Moreover, when the concentration reaches a limit marked in figure 3.4 by vertical line, a change of the Verwey transition from the transition of the first order to the transition of a higher order was reported [24], [25].

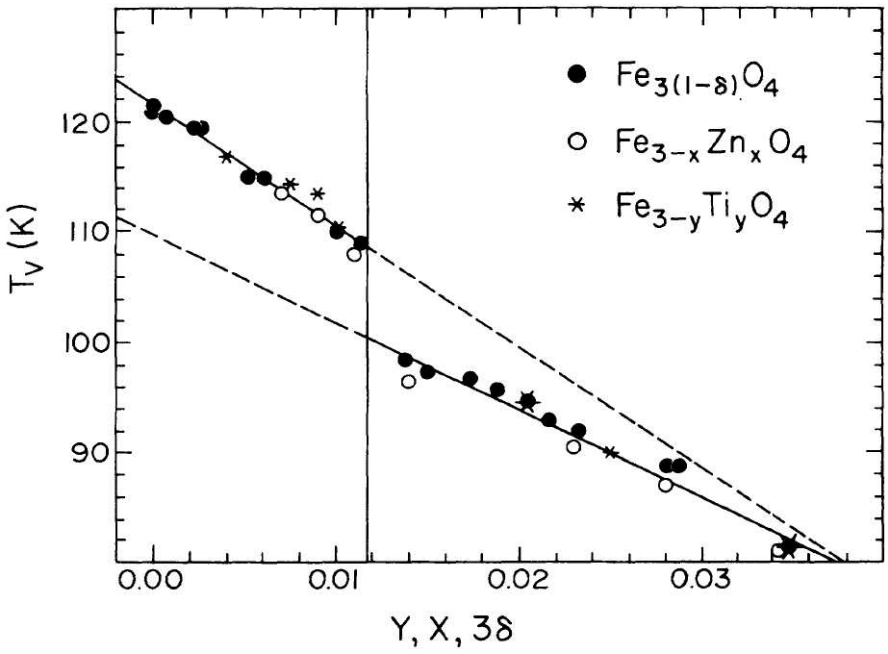

Figure 3.4: Variation of the Verwey transition temperature against sample composition. The region on the left from a vertical line corresponds to the first order transition. [24]

Existing NMR studies of samples with substitutions or structural defects concern mainly substitution of aluminium ions Al^{3+} [3], [4] and gallium ions Ga^{3+} [5] and vacancies in non-stoichiometric magnetite [22]. NMR spectra and relaxation times of magnetite with substitution of zinc Zn^{2+} ions measured at 4.2 K, 198 K and 273 K were published in [7]. Spectrum of magnetite substituted by titanium ions Ti^{4+} at 273 K was reported in [6].

The shape of NMR spectra is significantly influenced by the preference of substitution ions for a particular cationic position. Ions of zinc substitution Zn^{2+}

enter in magnetite into A sites, whereas titanium ions Ti^{4+} occupy B sites. Partial replacement of iron ions by ions of the substitution induces a change of the hyperfine field at iron nuclei in the vicinity. If the concentration of substitution is low, satellite structure in ^{57}Fe NMR spectra can be observed. (In case of a higher concentration of defects, main lines become broader and may overlap the satellite signals.) Relative intensity of satellite signals is proportional to the substitution concentration. The number of satellite lines corresponding to a particular set of crystallographically equivalent configurations of resonating nuclei and substituent can be determined by considering the number of magnetically equivalent configurations contained within this set. Crystallographical configurations of a resonating iron nucleus and a substitution ion in magnetite above the Verwey transition temperature are listed in table 3.2 [26]. Rows b) and d) in the table correspond to the zinc substitution, while rows a) and c) apply to the titanium substitution. Figures 3.5 and 3.6 displaying the surrounding of the resonating iron nuclei in magnetite are provided for better understanding.

Table 3.2: Configurations of a resonating iron nucleus and a substitution ion in magnetite above the Verwey transition temperature [26]

Notation	Position of resonating nucleus	Position of substitution	Iron surrounding (within 5 Å)
a)	8*a* = A	16*d* = B	12 x 3.453 Å
b)		8*a* = A	4 x 3.607 Å
c)	16*d* = B	16*d* = B	6 x 2.945 Å
d)		8*a* = A	6 x 3.453 Å

In the case noted in table 3.2 as a), the substitution ion is situated in the plane of symmetry for the position of a resonating nucleus and a corresponding tensor of local field anisotropy A has three independent terms α, β and γ:

$$A = \begin{pmatrix} \alpha & \beta & \gamma \\ \beta & \alpha & \gamma \\ \gamma & \gamma & -2\alpha \end{pmatrix}. \tag{3.1}$$

The case b) denotes the situation when the substitution ion is located in the plane of symmetry and on the 3-fold axis. The corresponding local field anisotropy tensor has only one independent term:

$$A = \begin{pmatrix} 0 & \gamma & \gamma \\ \gamma & 0 & \gamma \\ \gamma & \gamma & 0 \end{pmatrix}. \tag{3.2}$$

In the cases c) and d), the substitution is placed in the plane of symmetry for the position of a resonating nucleus as in the case a). Satellite structure of spectra corresponding to a particular configuration of a resonating iron nucleus and a substitution ion for a given magnetization direction can be found in table 3.3 [26].

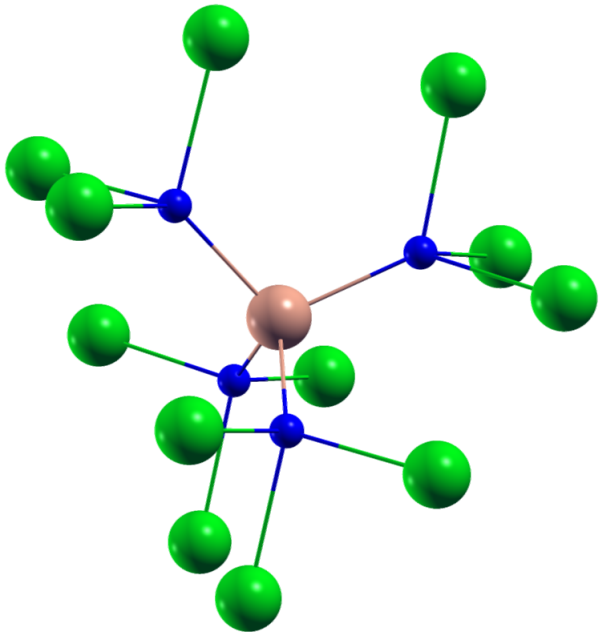

Figure 3.5: Surrounding of the resonating iron nucleus at the A site in a pure magnetite (oxygen ions are drawn blue, iron ions at the A sites red and iron ions at the B sites green; central ion is highlighted). Created by V. Chlan using XCrySDen [27].

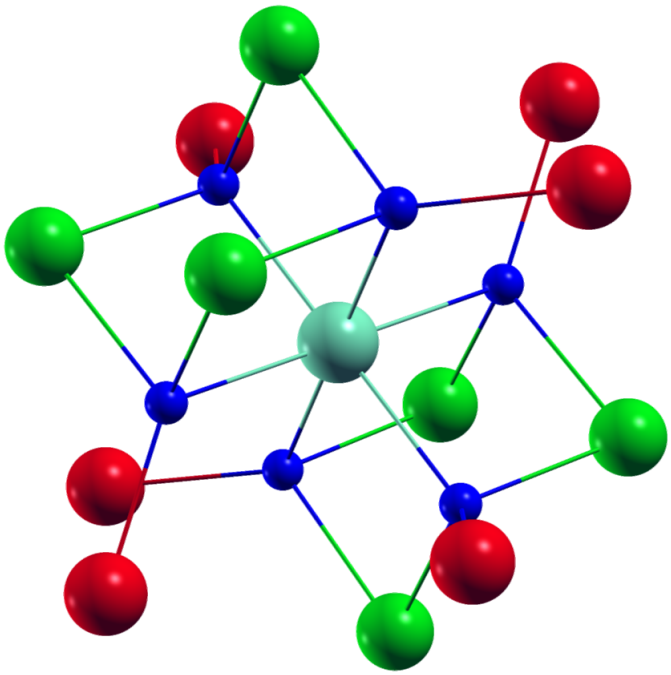

Figure 3.6: Surrounding of the resonating iron nucleus at the B site in a pure magnetite (oxygen ions are drawn blue, iron ions at the A sites red and iron ions at the B sites green; central ion is highlighted). Created by V. Chlan using XCrySDen [27].

Table 3.3: Satellite structure of spectra corresponding to various configurations of a resonating iron nucleus and a substitution ion in magnetite above the Verwey transition for different magnetization directions [26]

Magnetization direction	$\sum_{i,j=1}^{3} A_{ij}^{s} n_i n_j$	**Notation from the previous table**	**Number of satellites**	**Ratio of intensities of satellites**	**Positions of the satellites** (in order of the previous column)
[100]	A_{xx}	a), c), d)	2	2 : 1	$I + \alpha$ $I - 2\alpha$
		b)	1		I
[110]	$A_{xx} + A_{yy} + 2A_{xy}$	a), c), d)	4	1 : 1 : 2 : 2	$I + 2\alpha + 2\beta$ $I + 2\alpha - 2\beta$ $I - \alpha + 2\gamma$ $I - \alpha - 2\gamma$
		b)	2	1 : 1	$I + 2\gamma$ $I - 2\gamma$
[111]	$2A_{xy} + 2A_{xz} + 2A_{yz}$	a), c), d)	3	1 : 2 : 1	$I + 2\beta + 4\gamma$ $I - 2\beta$ $I + 2\beta - 4\gamma$
		b)	2	1 : 3	$I + 6\gamma$ $I - 2\gamma$

Chapter 4

Experiments and Discussion

4.1 Samples

NMR experiments were performed on a series of zinc substituted and titanium substituted magnetite single crystal samples. Chemical formulae of zinc substituted and titanium substituted samples are $Fe_{3-xZn}Zn_{xZn}O_4$ and $Fe_{3-xTi}Ti_{xTi}O_4$, respectively, where the xZn and xTi parameters denote the concentration of substitution. Investigated samples are listed in tables 4.1 and 4.2. Typical dimensions of samples were of the order of millimeters.

Table 4.1: List of investigated zinc substituted samples

Sample number	**Sample label**	**Nominal zinc substitution** xZn	**Verwey transition temperature** T_V [K]	**Note**
Zn1	SM459J#1	0.0075	113.8	small piece cut from SM459J
Zn2	SM448#4	0.0086	112.3	
Zn3	459-1#22 mg3	0.0174	104.9	xZn according to electron microprobe measurement in [28]

Samples Ti1 and Ti6 were prepared in the laboratory of professor V. A. M. Brabers at Eindhoven University of Technology using the floating zone method [29]. First of all, stoichiometric polycrystalline rods of desired composition were prepared using ceramic techniques. These rods were then melted in a floating zone apparatus, using an arc-image furnace, in a nitrogen atmosphere. Additional annealing in an oxygen atmosphere was performed in order to improve the mechanical quality of the crystals.

Table 4.2: List of investigated titanium substituted samples

Sample number	**Sample label**	**Nominal titanium substitution** xTi	**Verwey transition temperature** T_V [K]	**Note**
Ti1	$Fe_{2.992}Ti_{0.008}O_4$	0.008	≈ 116	
Ti2	392P2#1	0.0065 – 0.0098	109 – 116	
Ti3	394-1	0.008 – 0.02	< 95	
Ti4	391P4#1	0.0032 – 0.0040		NMR spectra measured only at 144 K
Ti5	447#3A-1	0.01 – 0.026		NMR spectra measured only at 4.2 K
Ti6	S255-4	0.1		

All the remaining samples come from the laboratory of Dr. J. Hönig at Purdue University, USA [28]. Single crystals were grown from the melt by using the cold crucible method (skull melter). Subsequently, the crystals were exposed to sub-solidus annealing under CO/CO_2 gas mixtures in order to establish the appropriate oxygen stoichiometry, and then quickly quenched to room temperature to freeze in the high temperature thermodynamic equilibrium. In spite of the presence of defects generated by this procedure, reflecting the high temperature disorder, the sharp transition and the high Verwey transition temperature demonstrate that most of the low-temperature electronic processes are not affected.

4.2 Experimental Settings and the Data Processing

NMR spectra of ^{57}Fe nuclei were measured in a zero external magnetic field using the CPMG pulse sequence. Typical length of $\pi/2$-pulse in the pulse sequence was $1 - 2$ μs. Typical number of π-pulses (and thus also the number of echoes) was of the order of 10 or 100, as determined by a spin-spin relaxation time and by a time window between π-pulses ($= 2t_w$ – see figure 2.2), which was adjusted to values of the order of 10 or 100 μs to accommodate the whole width of the echo. Pulse sequence repetition time (i.e. time between consecutive scans) was in the range from 5 ms to 6 s, while being set long enough with respect to a spin-lattice relaxation time. The amplitude of RF pulses was properly adjusted before taking each spectrum to ensure that only the nuclei in domains would be excited. The chosen number of scans was of the order from 10 to 10,000, depending on the signal-to-noise ratio. Receiver gain was adjusted to properly utilize the input range of the A/D converter. The sample rate of detected signal data was 0.7 or 2 MSps and the length of the sampled interval was of the order of 1 or 10 ms, depending on the number of π-pulses and on a width of the time window between them.

A wide range of spectra makes it practically impossible to excite the whole spectrum in a single step. Thus, the spectra were acquired step-by-step with a typical frequency step in the range of $30 - 75$ kHz, depending on the width of the spectral lines. Resulting spectra were constructed as an envelope of spectra (Fourier transform modules) corresponding to particular steps – see an illustration figure 4.1. In a few cases, the spectra were plotted as Fourier transform modules at the excitation frequency of particular steps.

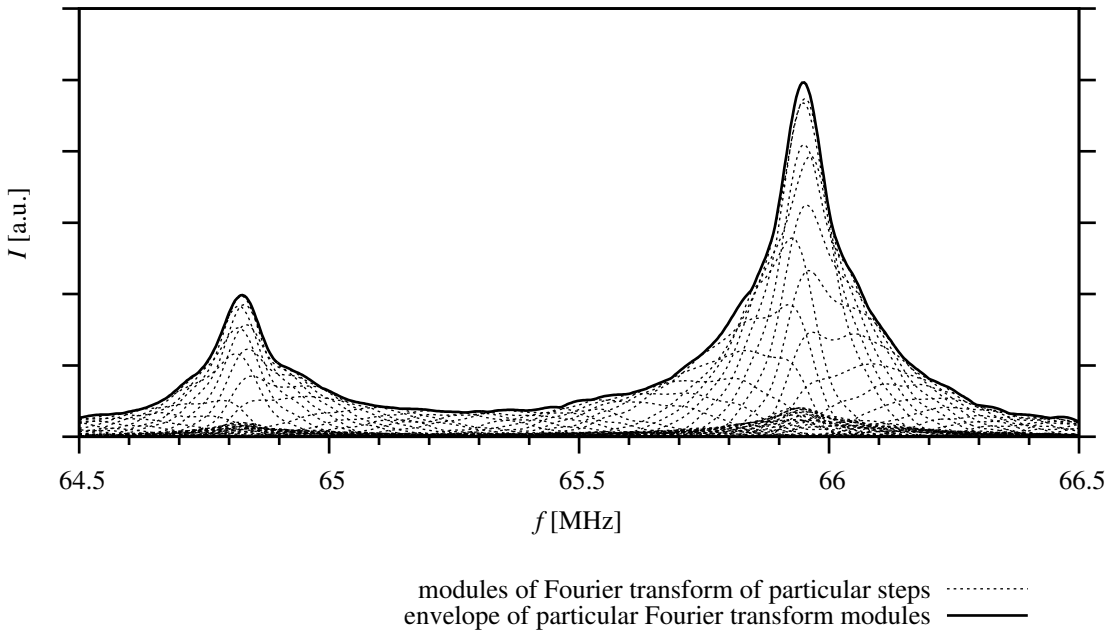

Figure 4.1: Illustration of the construction of the spectrum from particular steps (B lines, sample Ti2 at 168 K)

Parameters of subsequent data processing are just as important as the acquisition parameters. Employed data processing involves a selection of echoes which will be averaged. The first and the second echoes are disqualified as they are usually affected by a higher noise level and by a distorted phase. The choice of the last processed echo is limited by a spin-spin relaxation time and by a noise level. Comparison of spectra obtained from different rounds of processing with different choices of the last echo provides a qualitative measure of the influence of a frequency dependence of a spin-spin relaxation time on the shape of the spectra – see figure 4.2. The waveform obtained by the abovementioned averaging contains the desired signal in the center and a noise at the sides. Thus, the data points containing mostly the noise are cut off to reduce the noise level in a Fourier transform result. However, the decision about which points belong to noise and which still represent the signal depends on the line width and on the intensity of the signal of interest. For example, the echo corresponding to a narrow spectral line is broader than an echo belonging to a broad line and thus fewer points can be discarded than in the latter case. The echo of a weak satellite signal is located in a narrow region in the center of the waveform and a noise prevails in the rest, so it may be necessary in some cases to drop a large number of data points in order to enhance the signal-to-noise ratio of satellite signals in spectrum – the use

of this approach in the reported spectra is denoted by an asterisk ("*") in the key. An illustration is provided in figure 4.3.

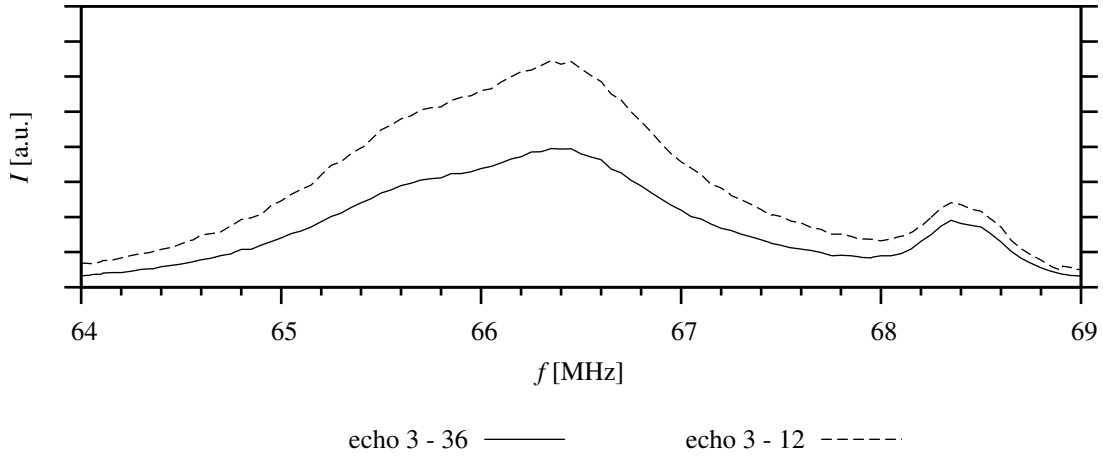

Figure 4.2: Illustrative comparison of spectra based on the same data processed with different choices of the last echo. The difference between spin-spin relaxation rates of signals at 66.39 MHz and at 68.37 MHz is apparent. (B lines and satellite signals, sample Ti3 at 128 K)

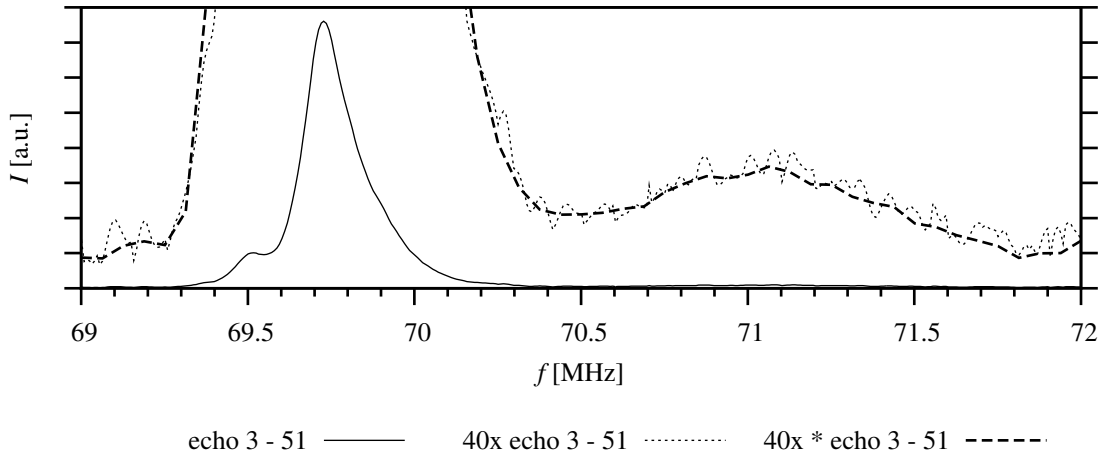

Figure 4.3: Illustration of the effect of discarding data points with prevailing noise during the data processing – see the text for details (A line and sat 20, sample Zn3 at 106 K)
solid line – processing suitable for the main spectral line at 69.73 MHz. Only a small amount of data points at the sides of a broad echo signal was dropped.
dotted line – same as above magnified by a factor of 40
dashed line – processing suitable for the weak broad signal at 71.06 MHz. The signal-to-noise ratio of this spectral signal was improved by cutting off a large number of data points containing mostly the noise at the sides of a weak narrow echo.

Several approaches were used to provide the defined temperature during NMR experiments. During the measurements of spectra at 4.2 K, the probe with the sample was submerged in liquid helium in a Dewar vessel. Several measurements at 198 K were performed in a mixture of solid carbon dioxide and ethanol in a polystyrene container (temperature deviation was within ±2 K, which was acceptable). The temperature of 273 K was achieved by placing the probe in a mixture of ice and water in a polystyrene vessel. Spectra were also acquired at the ambient temperature of 299 K. In all the remaining cases, desired temperatures were provided by helium continuous flow cryostat.

4.3 Results on Zinc Substituted Magnetite Samples

4.3.1 Spectra below the Verwey Transition Temperature

NMR spectra of zinc substituted samples Zn1 and Zn2 measured at the temperature of 4.2 K are shown in figures 4.6 and 4.7. There are no significant differences between the spectra of these samples. The structure of the spectra corresponds to the structure of spectra of pure magnetite at this temperature – see figures 4.4 and 4.5 for reference. However, the spectral lines are substantially broadened due to the presence of the zinc substitution. (See figures 4.3 and 4.4 in [7] for comparison with spectra of samples with higher concentrations of the zinc substitution.) Typical line widths in spectra of the pure magnetite single crystals at 4.2 K are of the order of 10 kHz for A lines and of the order of 10 to 100 kHz for B lines [2]. The presence of the substitution causes broadening of all spectral lines. Satellite signals cannot be observed as they are overlaid by the dense structure of broadened main lines. The processing of the same experimental data with different numbers of averaged echoes exhibits different spin-spin relaxation rates of individual spectral lines. Similarly to pure magnetite, the spin-spin relaxation times of the B lines are shorter than those of the A lines. However, the relaxation rates in substituted magnetite are generally faster than those in pure magnetite.

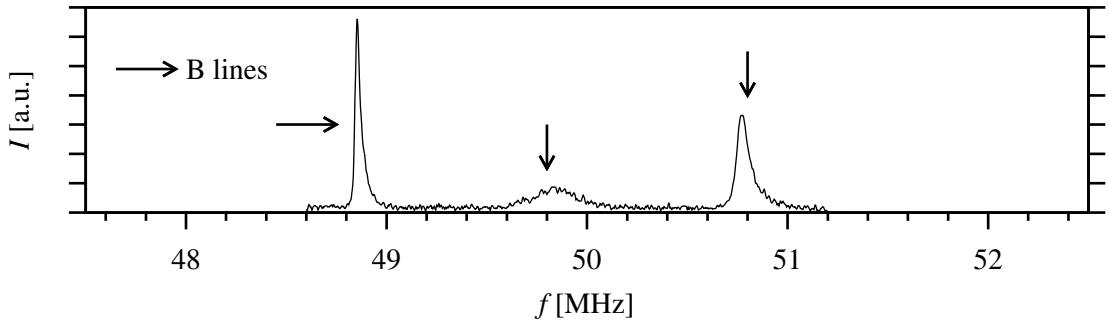

Figure 4.4: NMR spectrum of a pure magnetite single crystal at 4.2 K in the range 47.5 – 52.5 MHz (measured by V. Chlan)

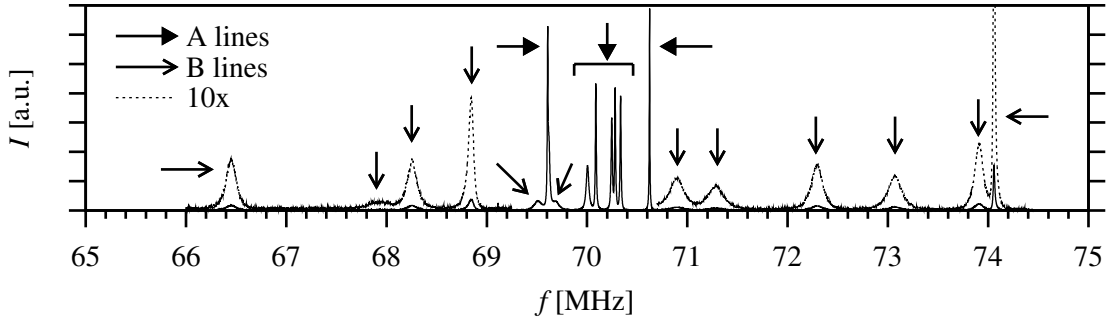

Figure 4.5: NMR spectrum of a pure magnetite single crystal at 4.2 K in the range 65 – 75 MHz (measured by V. Chlan)

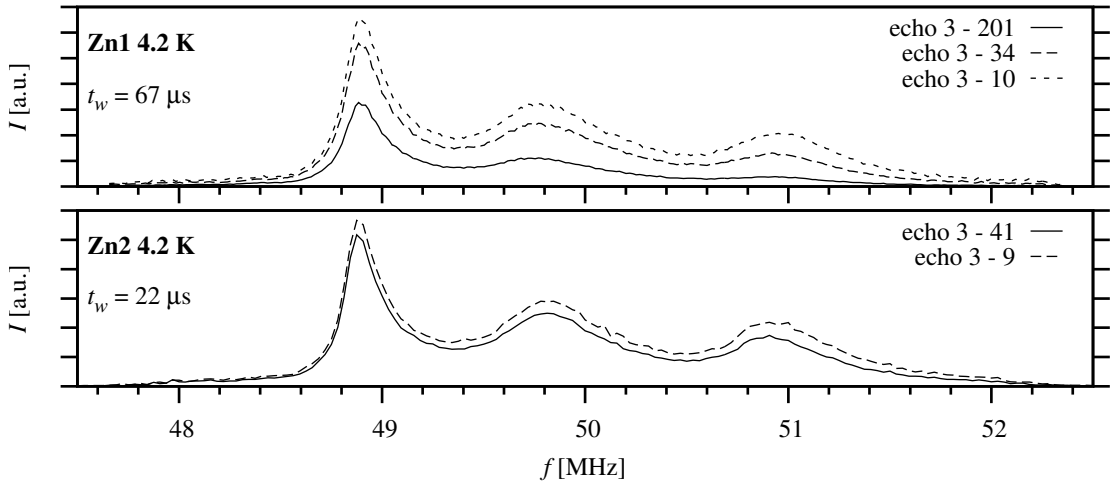

Figure 4.6: Comparison of NMR spectra of zinc substituted samples at 4.2 K in the range 47.5 – 52.5 MHz (the meaning of t_w is illustrated in figure 2.2)

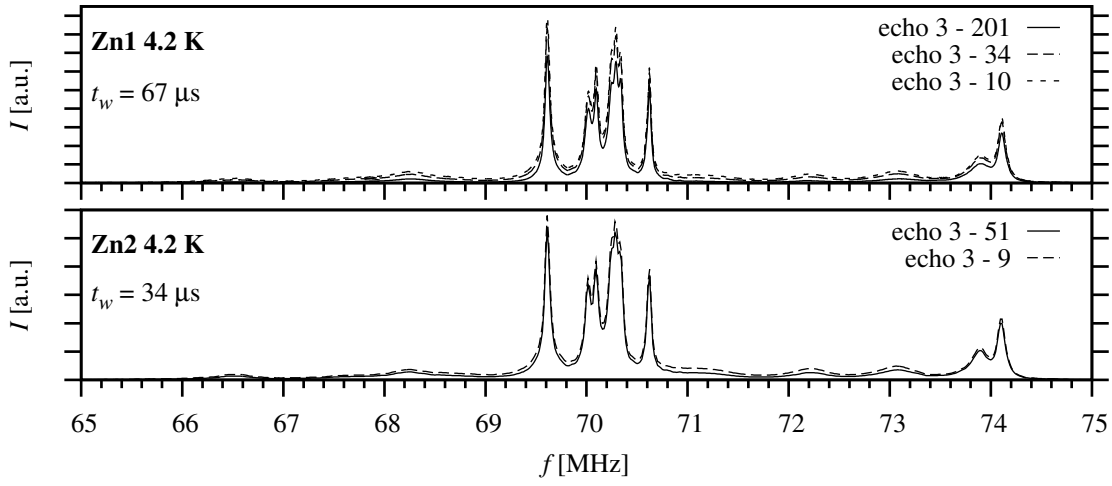

Figure 4.7: Comparison of NMR spectra of zinc substituted samples at 4.2 K in the range 65 – 75 MHz

4.3.2 Spectra above the Verwey Transition Temperature

Comparisons of NMR spectra of samples Zn1, Zn2 and Zn3 acquired at temperatures of 144 K, 216 K and 273 K are depicted in figures 4.10 to 4.15. (Spectra of samples with higher concentrations of the zinc substitution at 273 K can be found in figures 4.9 and 4.10 in [7].) Positions of the main lines in the spectra correspond to those in the spectrum of pure magnetite above the spin reorientation transition – see figures 4.9 and 4.8 for reference. Several satellite signals were observed near the B lines and a complex satellite structures were found in the vicinity of the A lines in the spectra of these three samples.

As expected, the sample Zn3, which has the highest substitution concentration, exhibits the broadest spectral lines of these three samples. On the other hand, the lines in the spectra of the sample Zn2 are apparently narrower than those of the sample Zn1, which has slightly lower nominal concentration of the zinc substitution. Deviation of the actual zinc content from the claimed one in one of these two samples or the presence of inhomogeneities in the sample Zn1 can be considered as the most plausible explanations.

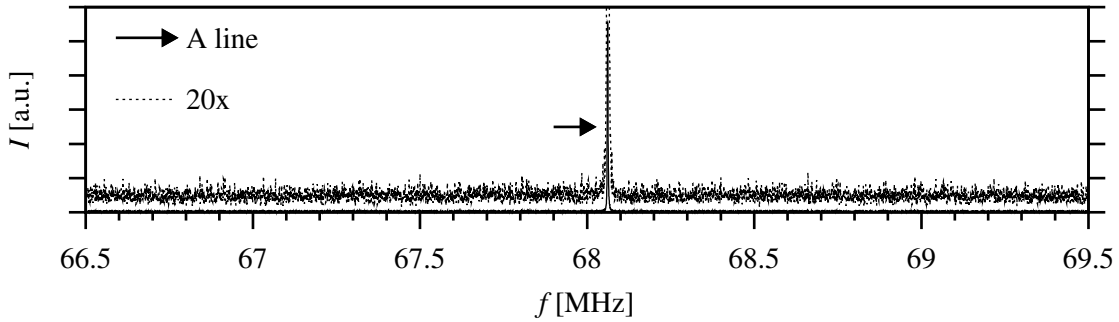

Figure 4.8: NMR spectrum of a pure magnetite single crystal at 273 K – A line (measured by V. Chlan)

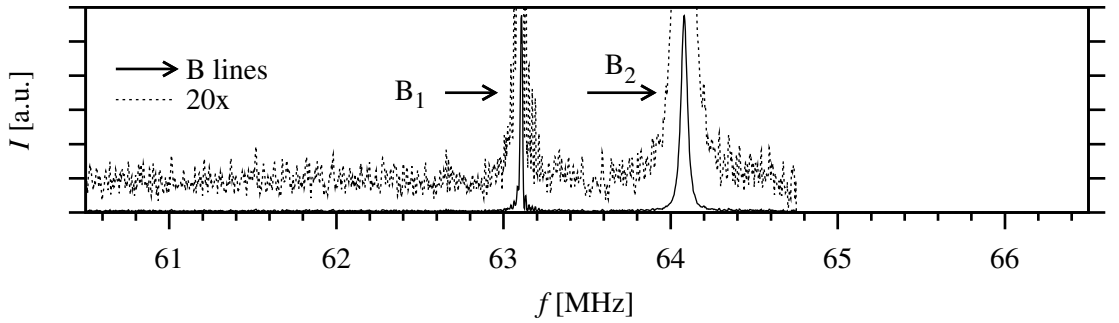

Figure 4.9: NMR spectrum of a pure magnetite single crystal at 273 K – B lines (measured by V. Chlan)

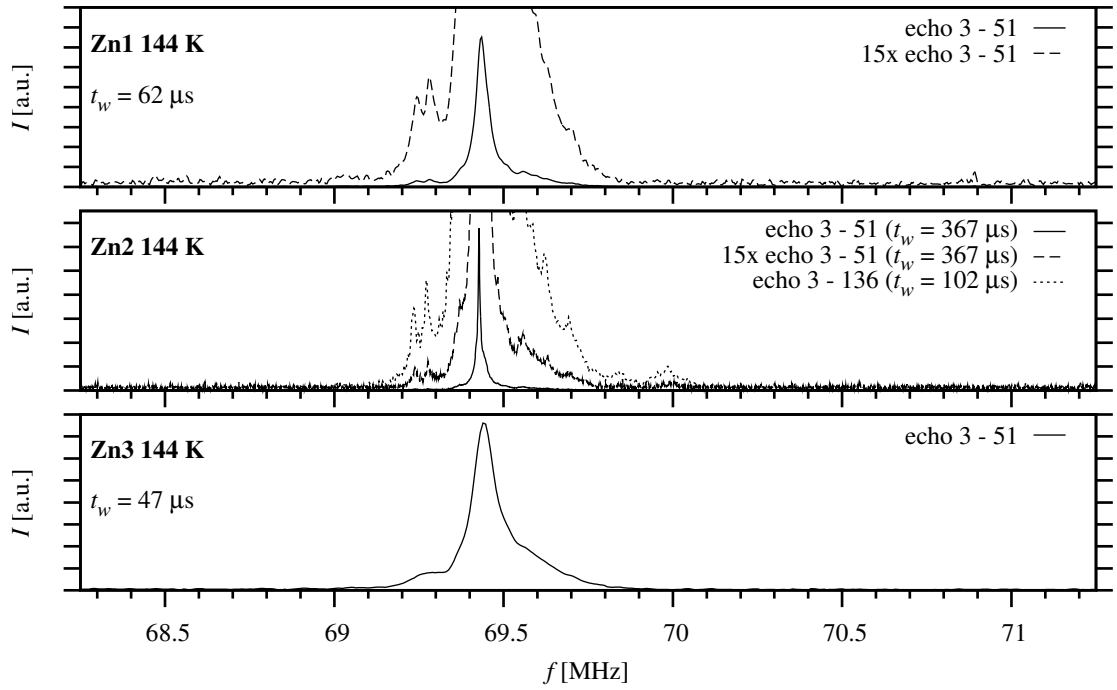

Figure 4.10: Comparison of NMR spectra of zinc substituted samples at 144 K – A lines

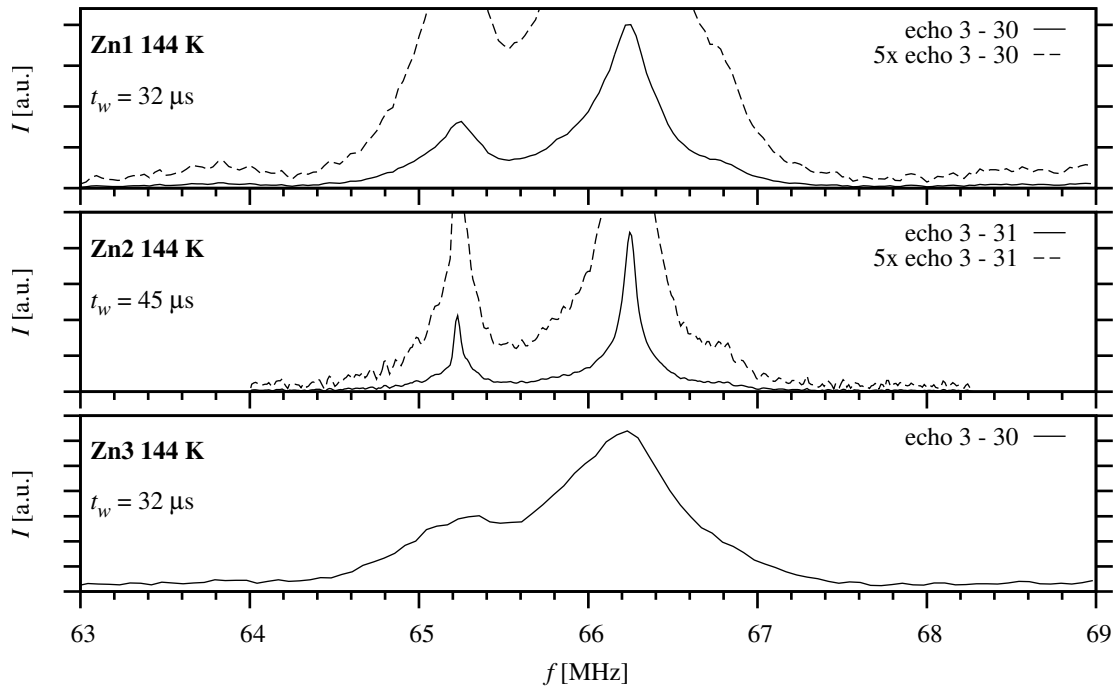

Figure 4.11: Comparison of NMR spectra of zinc substituted samples at 144 K – B lines

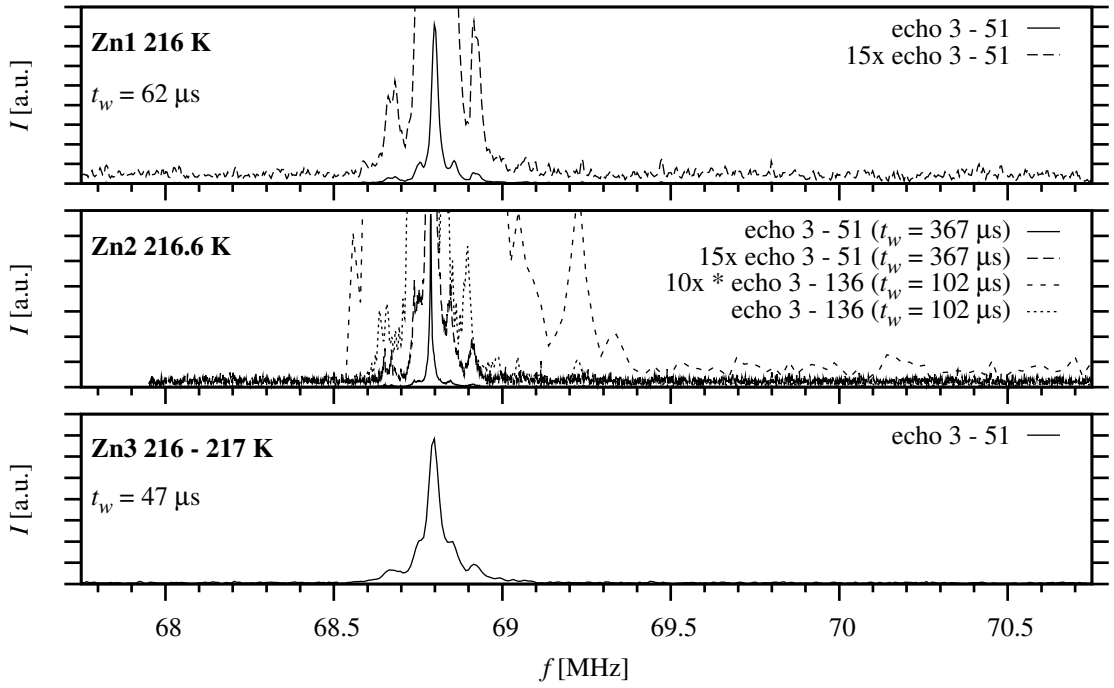

Figure 4.12: Comparison of NMR spectra of zinc substituted samples at 216 K – A lines

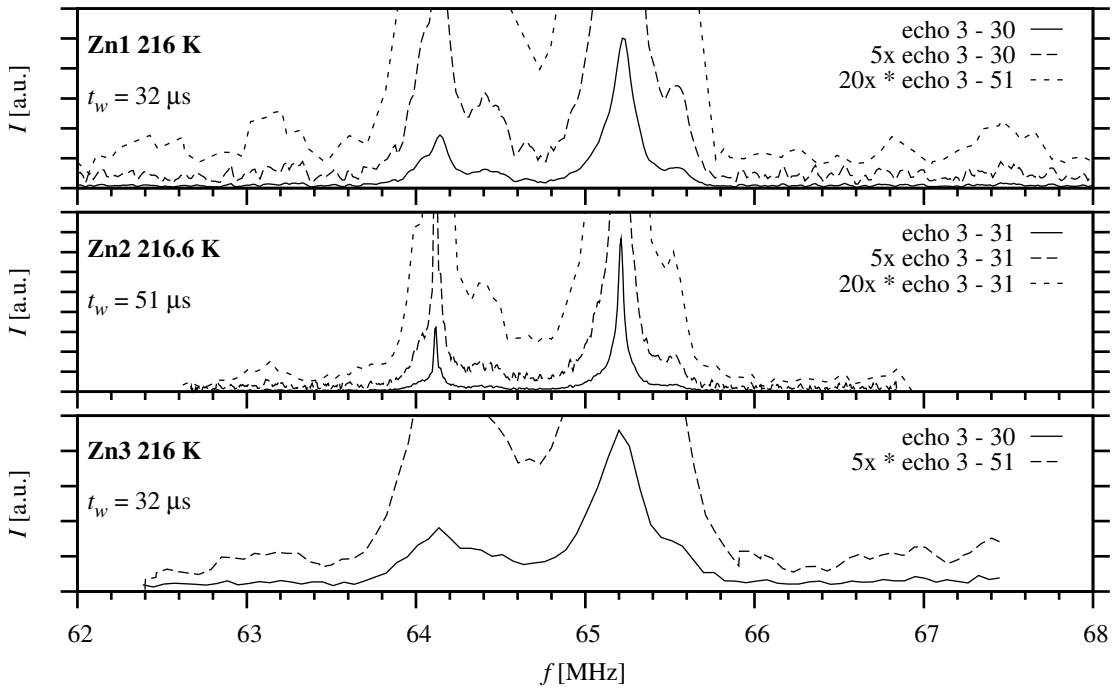

Figure 4.13: Comparison of NMR spectra of zinc substituted samples at 216 K – B lines

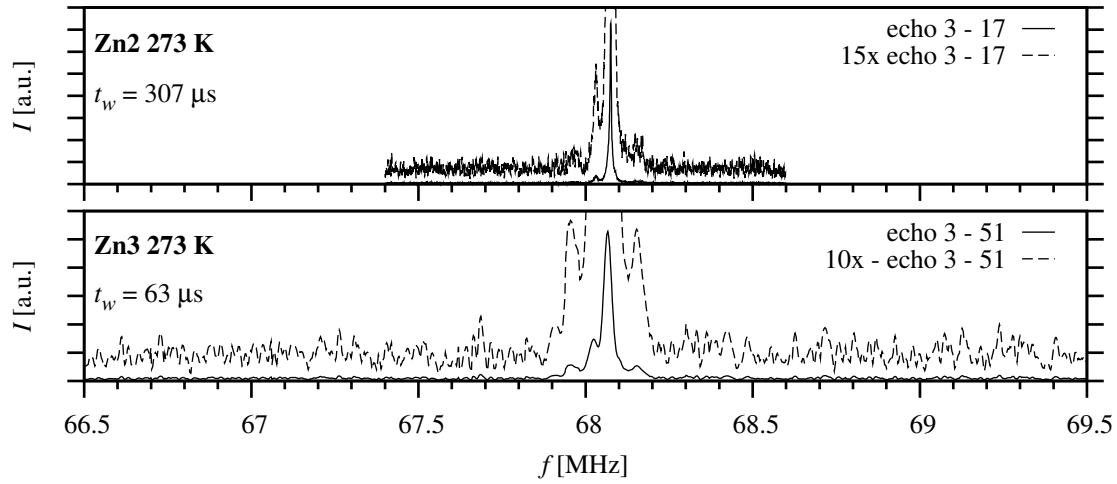

Figure 4.14: Comparison of NMR spectra of zinc substituted samples at 273 K – A lines

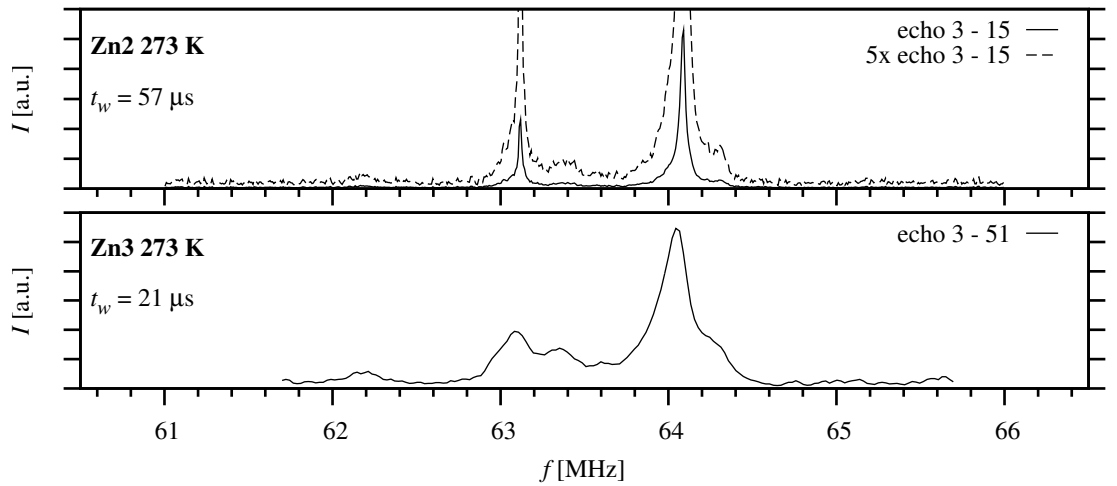

Figure 4.15: Comparison of NMR spectra of zinc substituted samples at 273 K – B lines

4.3.3 Temperature Dependences of Spectra above the Verwey Transition Temperature

Temperature dependences of NMR spectra of zinc substituted magnetite samples Zn1, Zn2 and Zn3 were measured from temperatures slightly above the Verwey transition up to 299 K. The acquired spectra are plotted in figures A.1 to A.9 in Appendix, while figures 4.16 to 4.21 show the spectra plotted relative to the most intensive line in the displayed spectral range, thus making it easier to qualitatively evaluate the temperature evolution of relative position, line width and shape of spectral signals. In accordance with the fact that the Verwey transition temperature decreases with increasing concentration of substitution and defects (see figure 3.4), spectra corresponding to a cubic phase were observed to lower temperatures compared to pure magnetite (≈ 115 K for samples Zn1 and Zn2, ≈ 106 K for sample Zn3). The most apparent changes in the spectra are the spin reorientation transition and the narrowing of the main lines with the increasing temperature. Special care was taken to find the satellite lines in the spectra in order to be able to track the variation of their frequencies against the temperature.

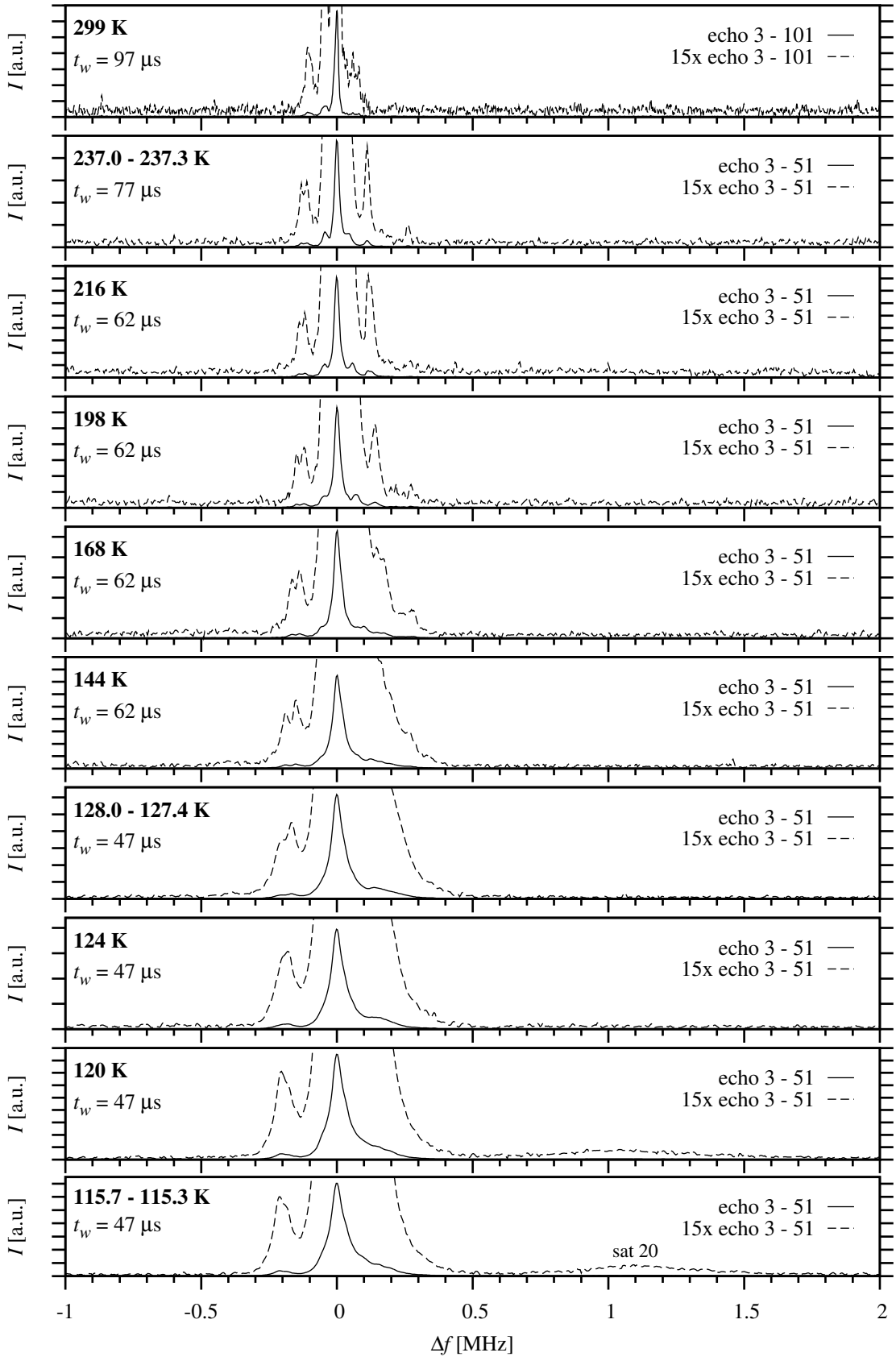

Figure 4.16: Temperature dependence of NMR spectra of sample Zn1 – spectra plotted relative to the A lines

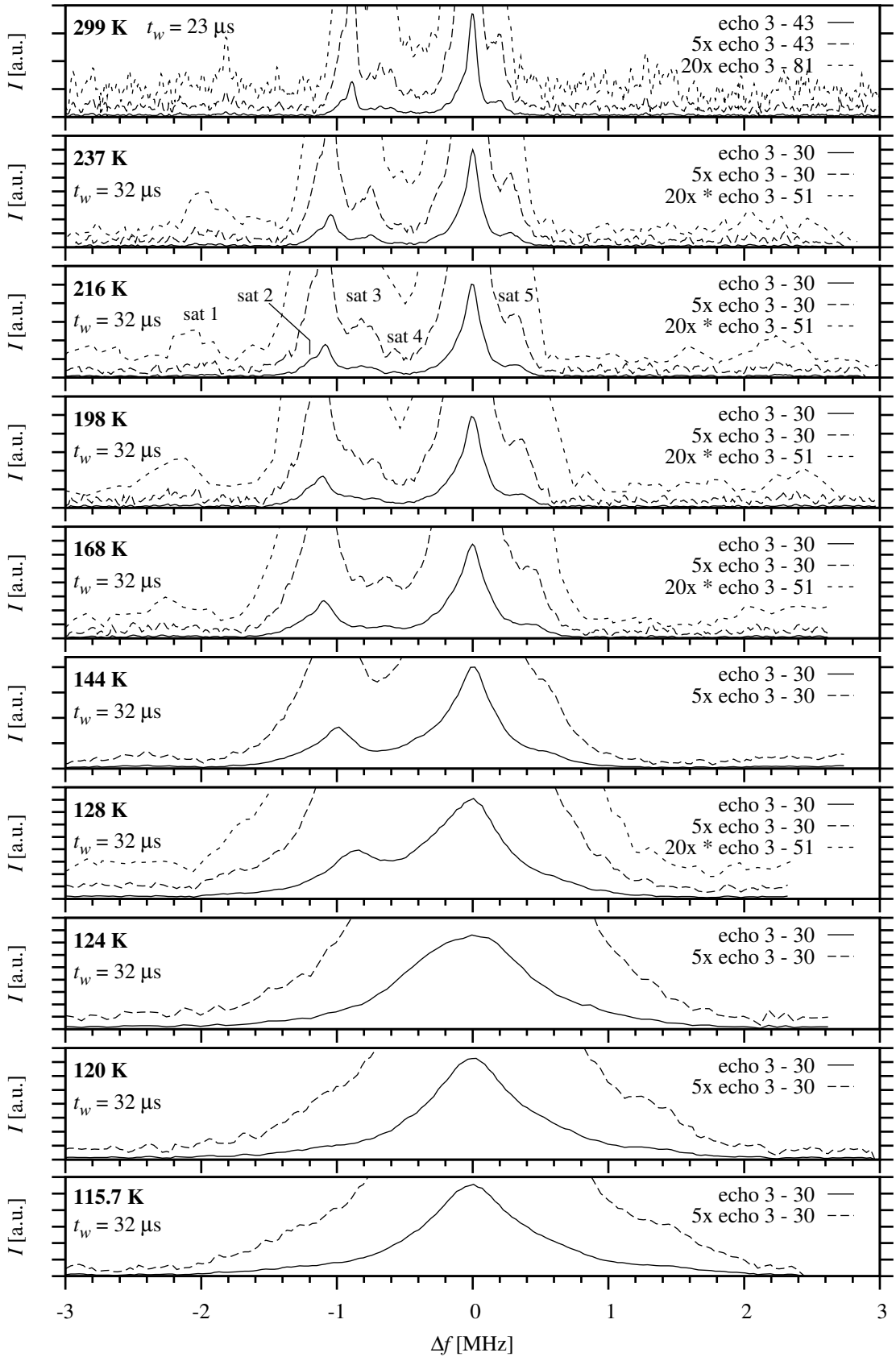

Figure 4.17: Temperature dependence of NMR spectra of sample Zn1 – spectra plotted relative to the B, B_2 lines

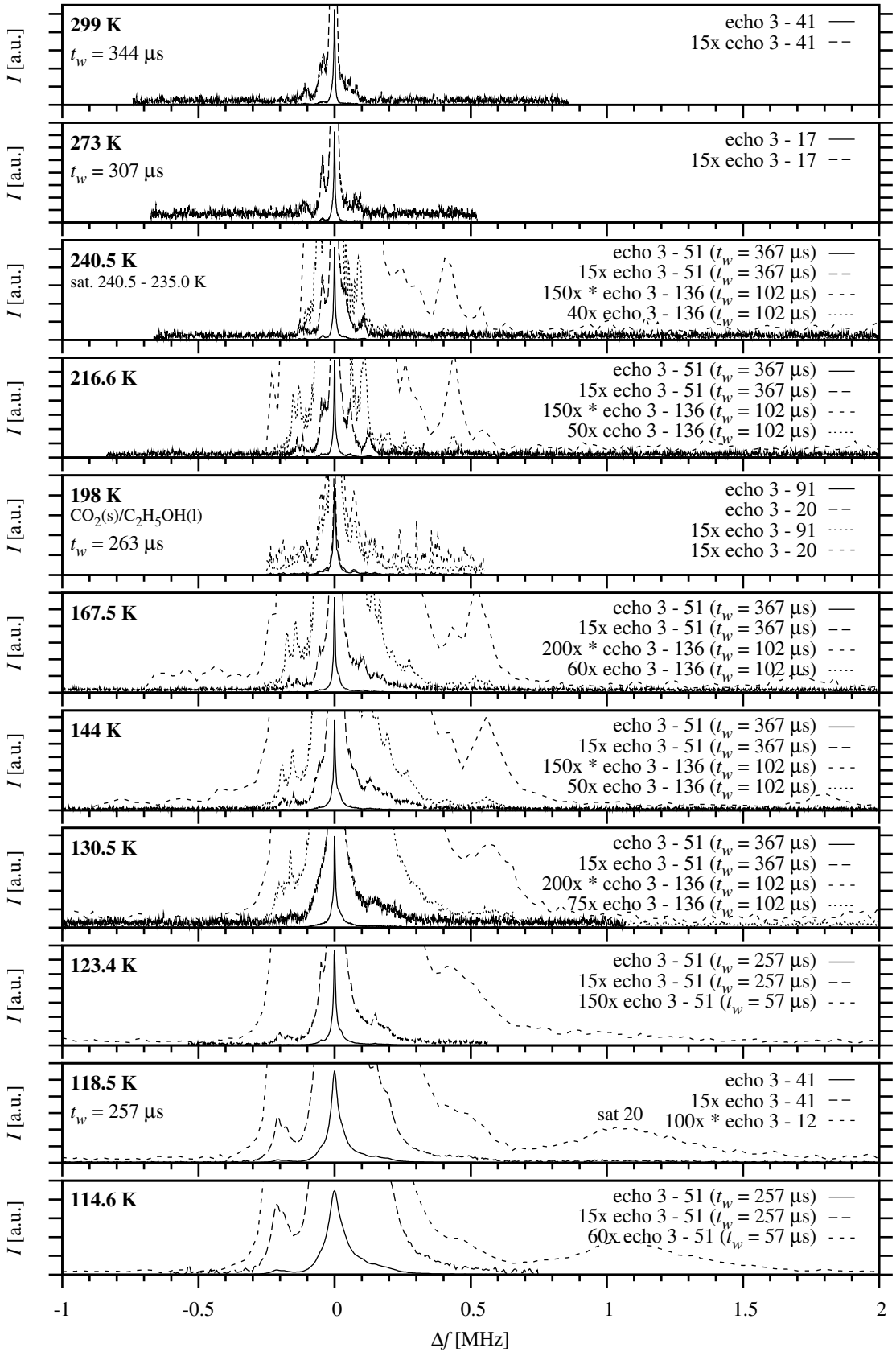

Figure 4.18: Temperature dependence of NMR spectra of sample Zn2 – spectra plotted relative to the A lines

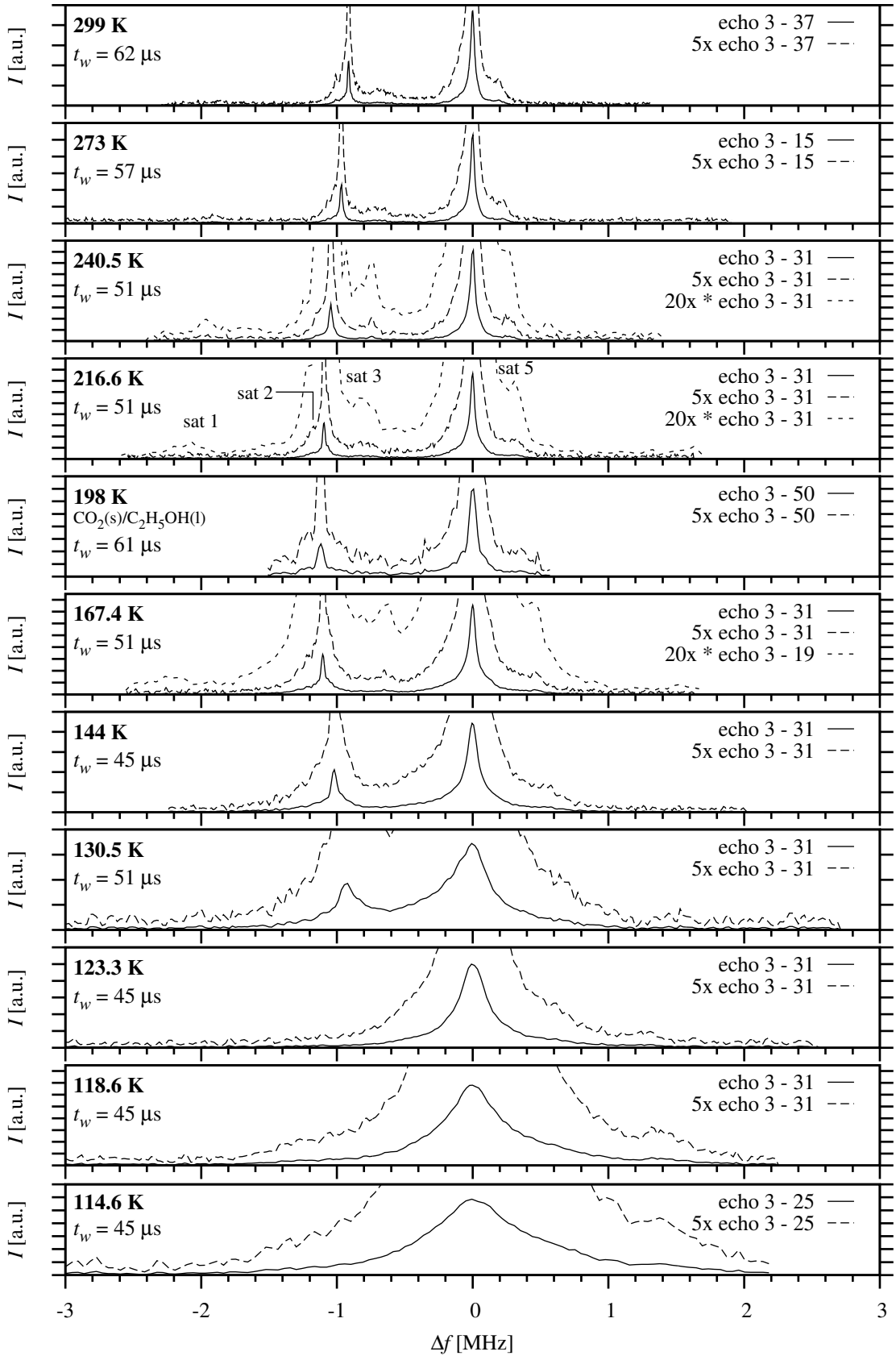

Figure 4.19: Temperature dependence of NMR spectra of sample Zn2 – spectra plotted relative to the B, B_2 lines

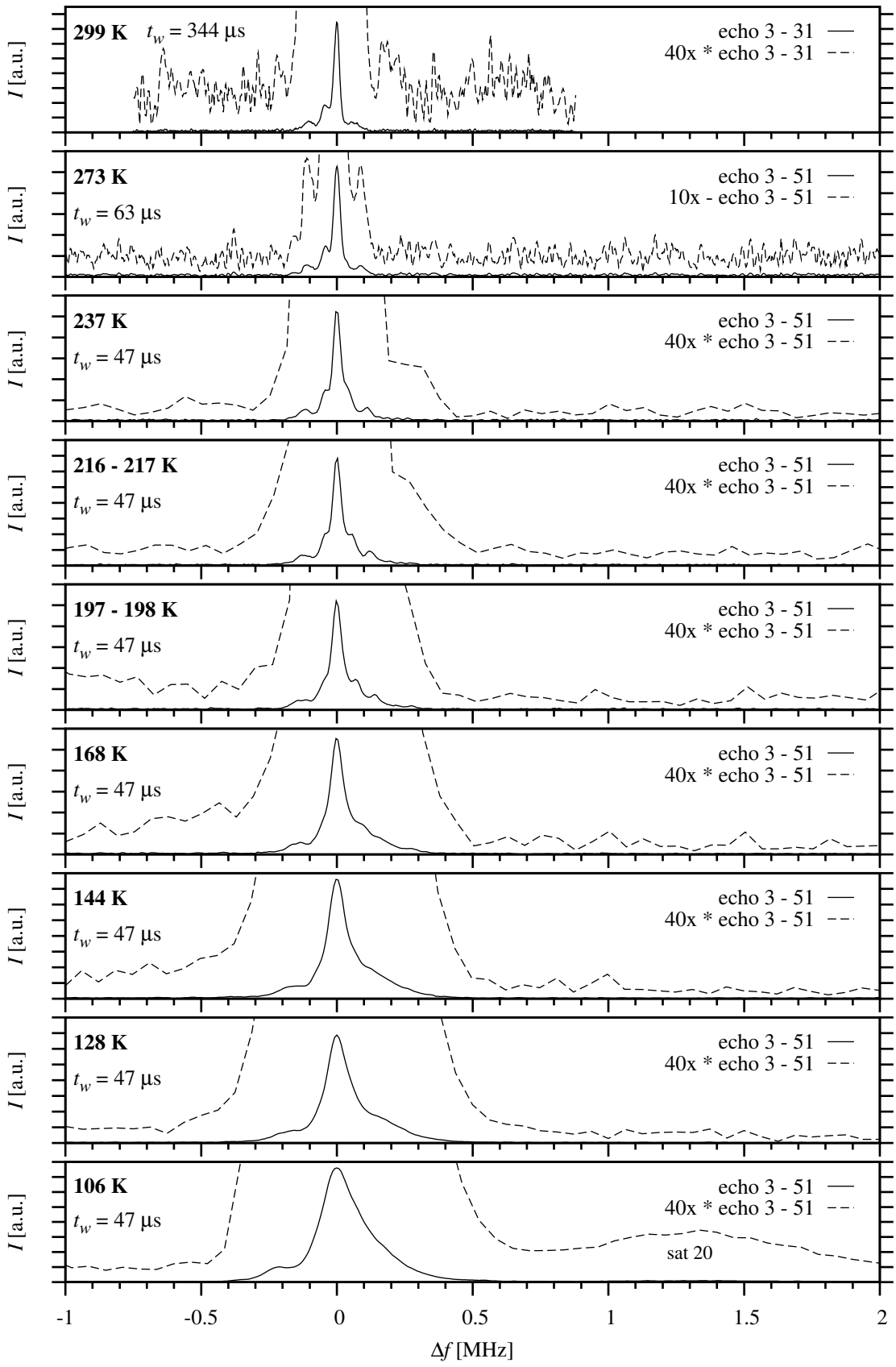

Figure 4.20: Temperature dependence of NMR spectra of sample Zn3 – spectra plotted relative to the A lines

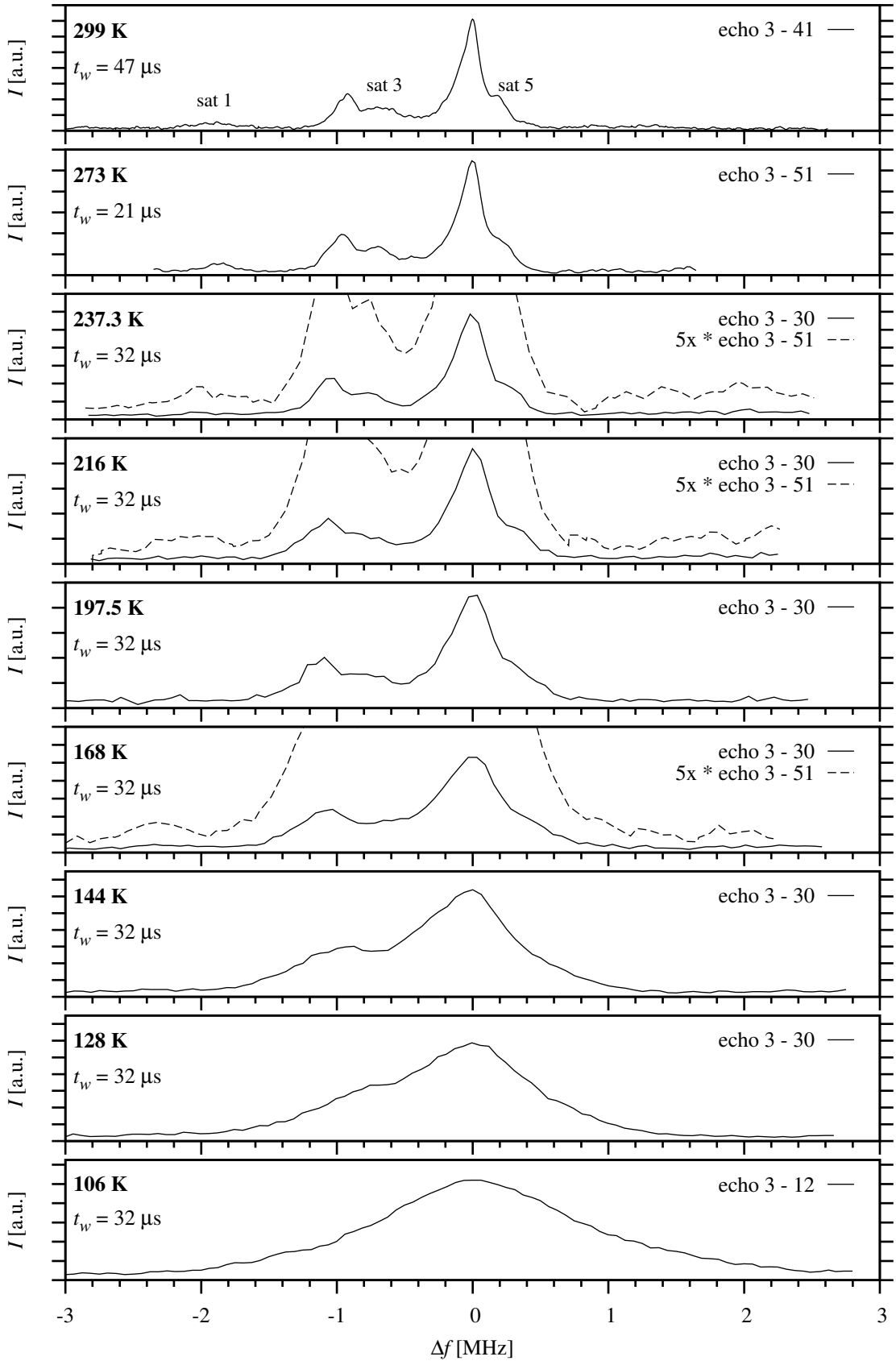

Figure 4.21: Temperature dependence of NMR spectra of sample Zn3 – spectra plotted relative to the B, B_2 lines

4.3.4 Temperature Dependences of Spectral Signal Frequencies

The results of the measurements of the temperature dependences of spectra were used to find the positions of the main lines and of the satellite signals in order to construct the temperature dependences of their frequencies. Assembled data can be found in tables B.1 to B.6 in Appendix, while the graphical representation is shown in figure 4.22.

Several satellite lines found near the B lines probably arise from the presence of a zinc ion Zn^{2+} in the A position nearest to the resonating nuclei at the B sites. A complex satellite pattern in the vicinity of the A line is localized close to the main line because the distance between the substitution at the A site and the resonating nuclei at the A sites is higher and thus the corresponding change of the hyperfine field is lower. A high number of satellite lines in this pattern indicates that many of these signals are induced by the substitution in the distant surrounding of the resonating nuclei.

Satellite signals in the spectra of the sample Zn2 which are denoted in table B.4 by an asterisk ("*") were not found in the spectra of the other zinc substituted magnetite samples. However, these signals coincide with the satellite lines in the spectra of the non-stoichiometric magnetite reported in [22] – see figure 4.23. Thus the presence of vacancies in the sample is evidenced. Concentration of the vacancies is of the order of 10^{-4} vacancies per formula unit, as estimated from intensities of the corresponding satellite signals.

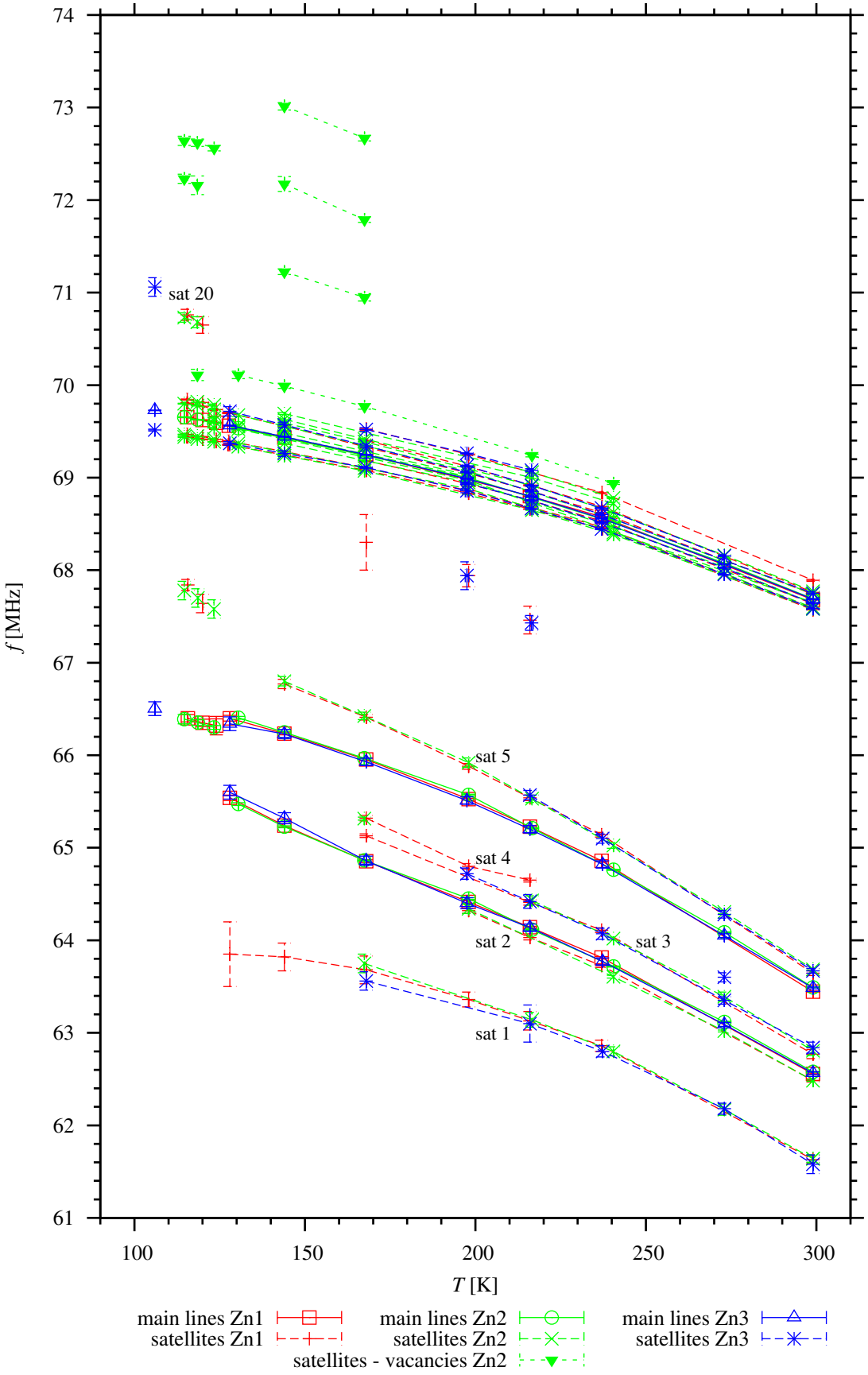

Figure 4.22: Temperature dependences of frequencies of the main lines and of the satellite signals in the spectra of the zinc substituted samples

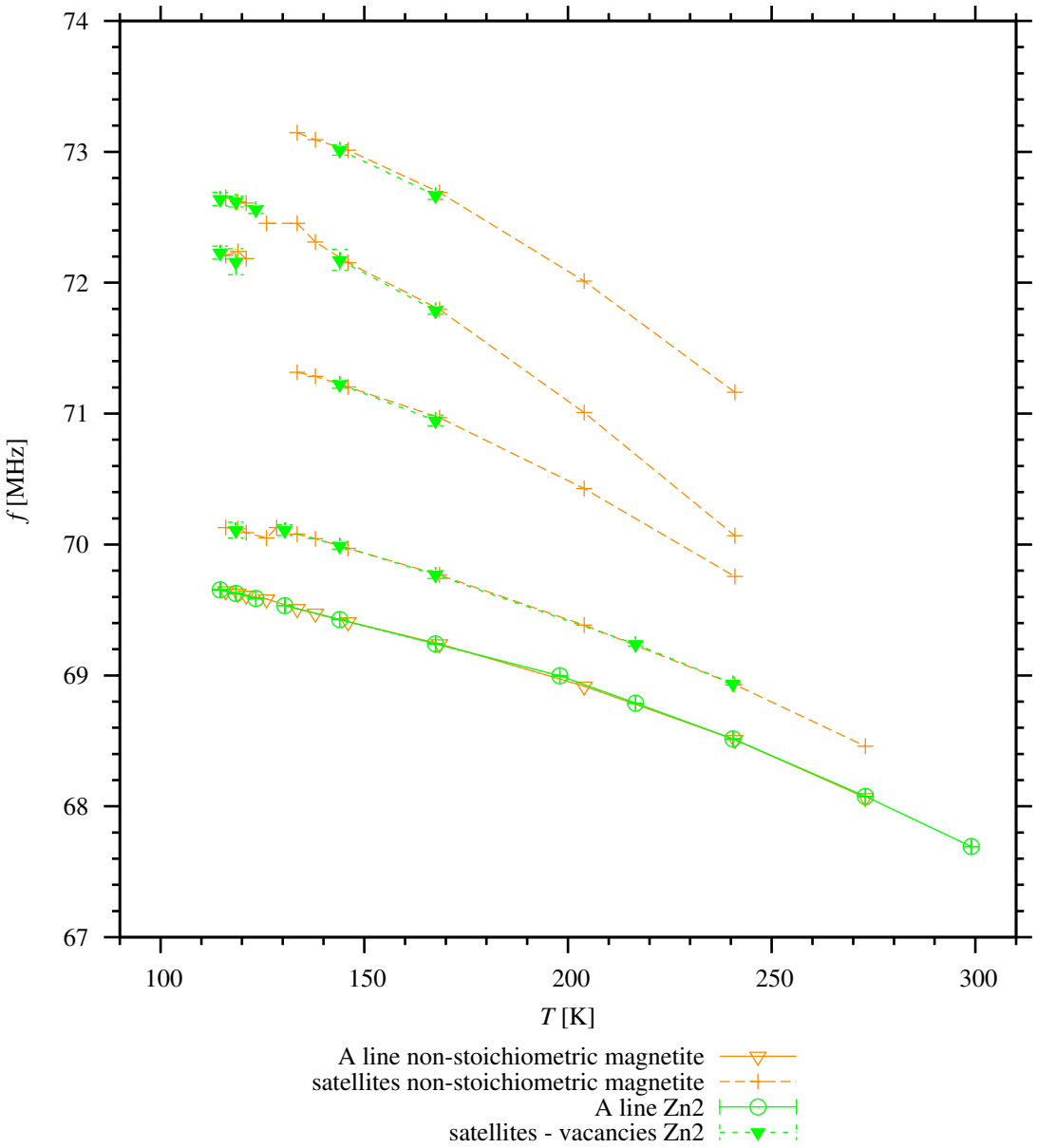

Figure 4.23: Comparison of the temperature dependences of frequencies of the A line and of the satellite signals corresponding to the presence of vacancies in the spectra of the sample Zn2 with the data for non-stoichiometric magnetite $Fe_{3(1-0.0025)}O_4$ [22]

4.3.5 Temperature Dependences of HWHM of the A Lines

The half widths of the A lines in the temperature dependences of the spectra of the samples Zn1, Zn2 and Zn3 are listed in tables C.1 to C.3 in Appendix. The variation of HWHM of the A lines against the temperature is plotted in figure 4.24. Significant differences between the curves for particular samples can be clearly seen: especially the curve for the sample Zn2 suggests lower actual concentration of the zinc substitution than the nominal one.

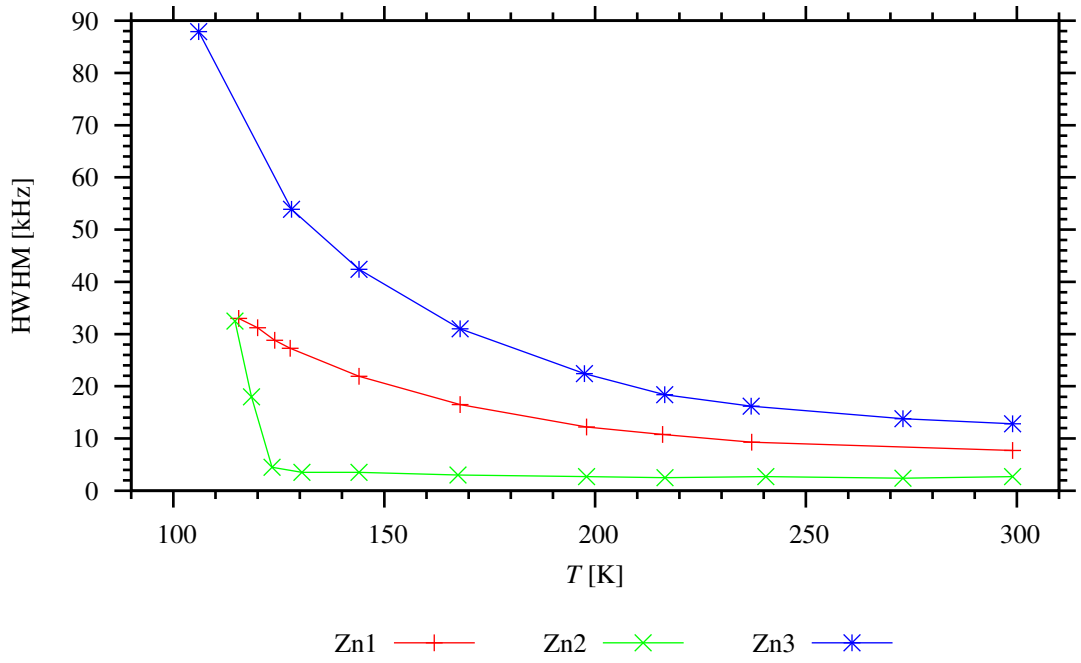

Figure 4.24: Temperature dependences of half width at half maximum of the A lines in the spectra of the zinc substituted samples

4.4 Results on Titanium Substituted Magnetite Samples

4.4.1 Spectra below the Verwey Transition Temperature

Spectra of titanium substituted samples Ti1, Ti5 and Ti6 acquired at 4.2 K are presented in figures 4.25 and 4.26. Just like in the case of the zinc substituted samples, the structure of the spectra matches the structure of the spectra of pure magnetite at the same temperature (see figures 4.6 and 4.7). The presence of titanium substitution causes a broadening of the spectral lines, especially in the spectrum of the sample Ti6, which has relatively high substitution concentration. Satellite signals are overlaid by the dense structure of broadened main lines and thus they cannot be observed.

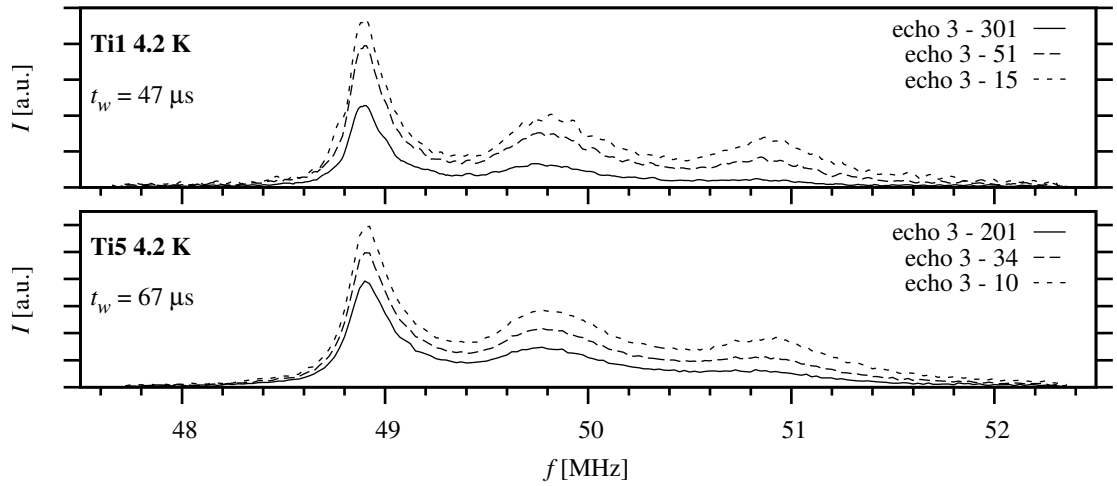

Figure 4.25: Comparison of NMR spectra of titanium substituted samples at 4.2 K in the range 47.5 – 52.5 MHz

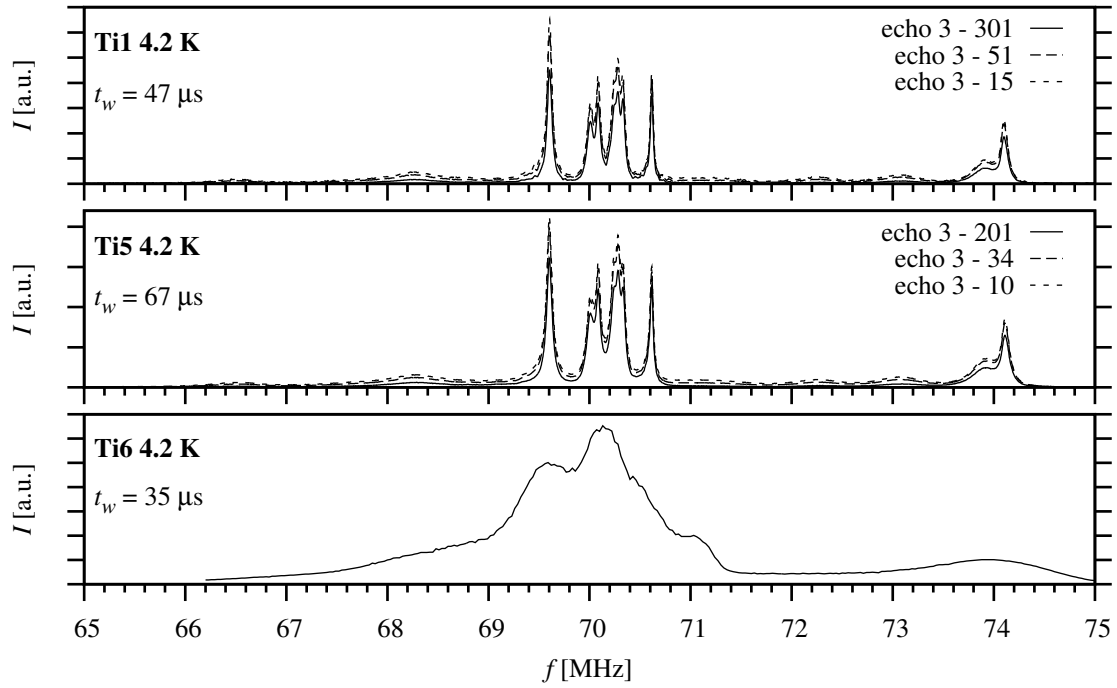

Figure 4.26: Comparison of NMR spectra of titanium substituted samples at 4.2 K in the range 65 – 75 MHz

4.4.2 Spectra above the Verwey Transition Temperature

NMR spectra of samples Ti1, Ti2, Ti3, Ti4 and Ti6 measured at temperatures of 144 K, 237 K and 273 K are compared in figures 4.27 to 4.32. Similarly to the spectra of the zinc substituted samples, the main spectral lines correspond to those in the spectrum of pure magnetite above the spin reorientation transition. In the spectra of the samples Ti1, Ti2, Ti3 and Ti4, satellite patterns were observed in the neighbourhood of the A lines, several satellite signals were resolved close to the B lines (except the sample Ti4 measured only at 144 K) and satellite lines were also evidenced in the region between the B and the A lines (this is also the case of the sample Ti6).

The spectra of the sample Ti6 are composed of relatively broad lines due to the high concentration of titanium substitution, whereas the spectral lines of the sample Ti4, which has the lowest titanium content, are the narrowest of all these samples. The widths of lines in the spectrum of the sample Ti2 are slightly higher than those of the sample Ti4 but still lower than those of the sample Ti1, thus suggesting that the actual substitution concentration is in the lower end of the claimed range. The line widths in the case of the sample Ti3 are apparently higher than those of the sample Ti1, so the titanium content at the higher end of the provided range of nominal substitution can be expected.

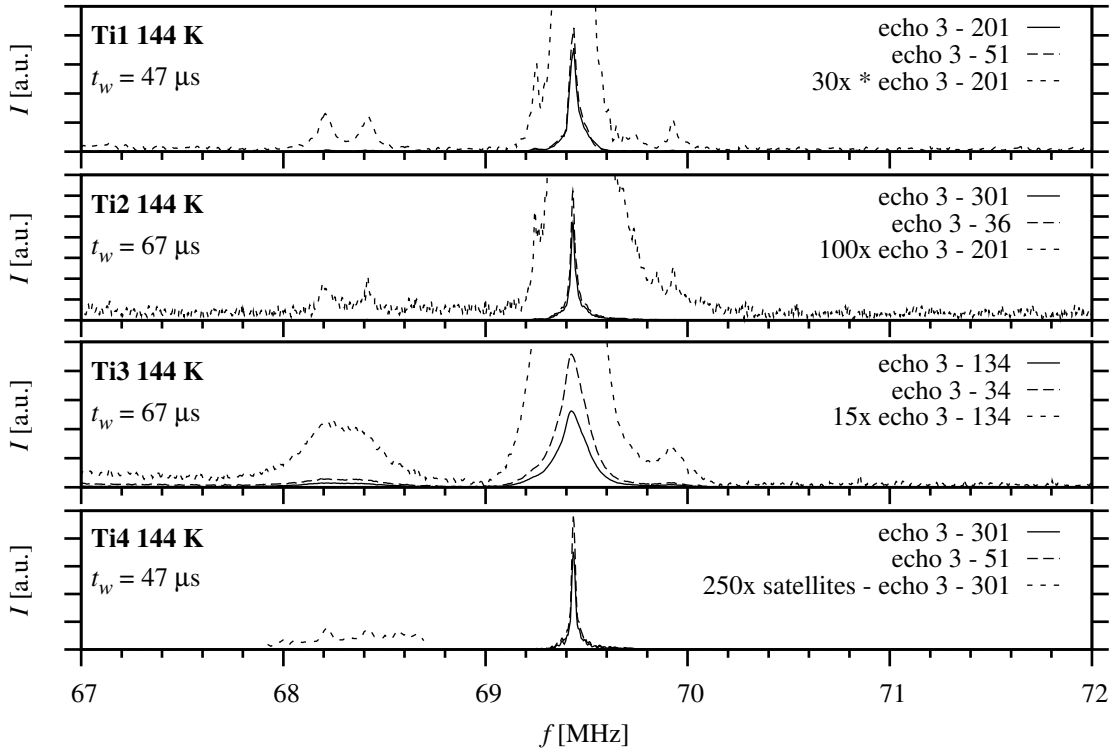

Figure 4.27: Comparison of NMR spectra of titanium substituted samples at 144 K – A lines

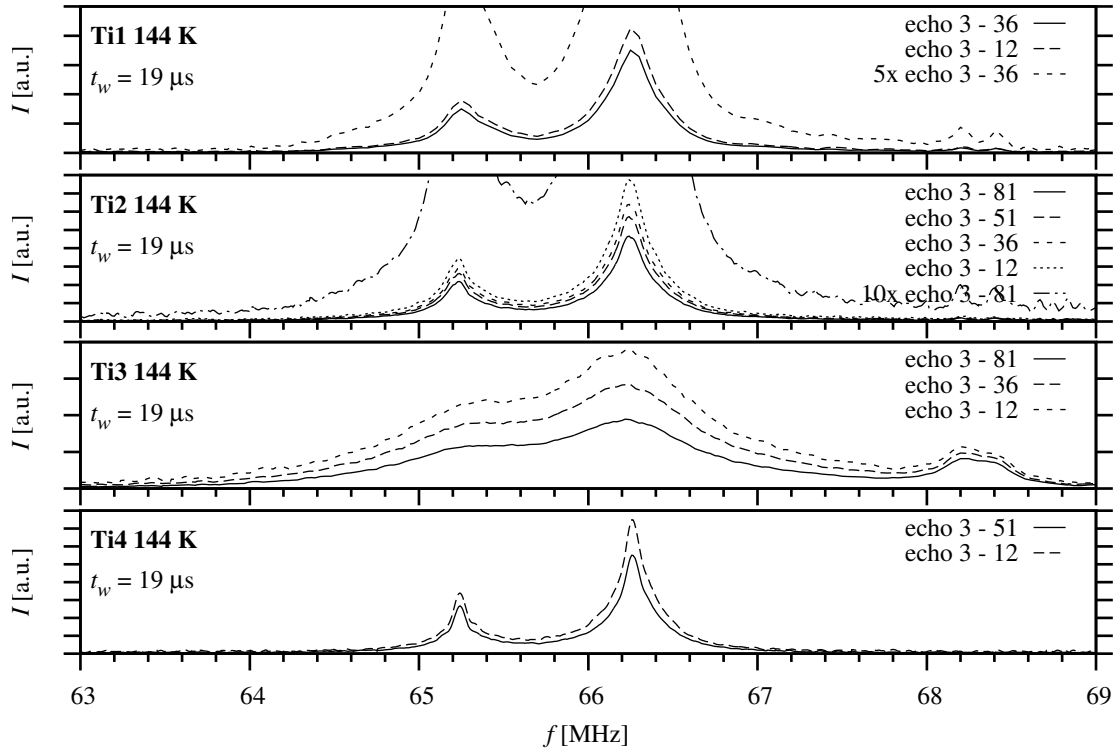

Figure 4.28: Comparison of NMR spectra of titanium substituted samples at 144 K – B lines

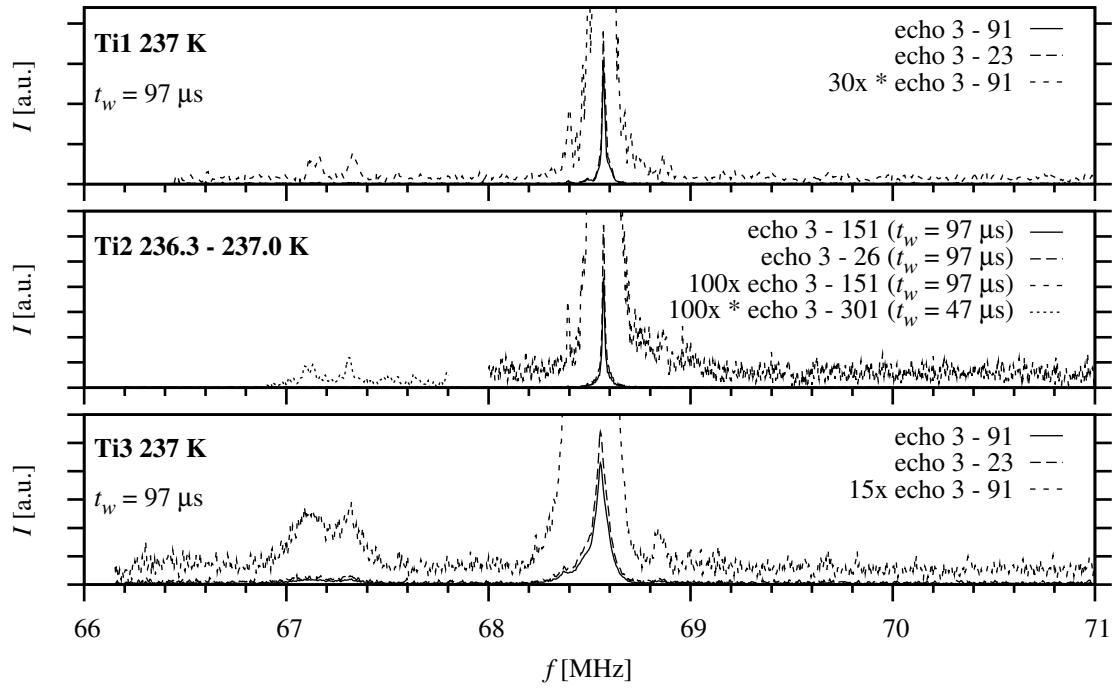

Figure 4.29: Comparison of NMR spectra of titanium substituted samples at 237 K – A lines

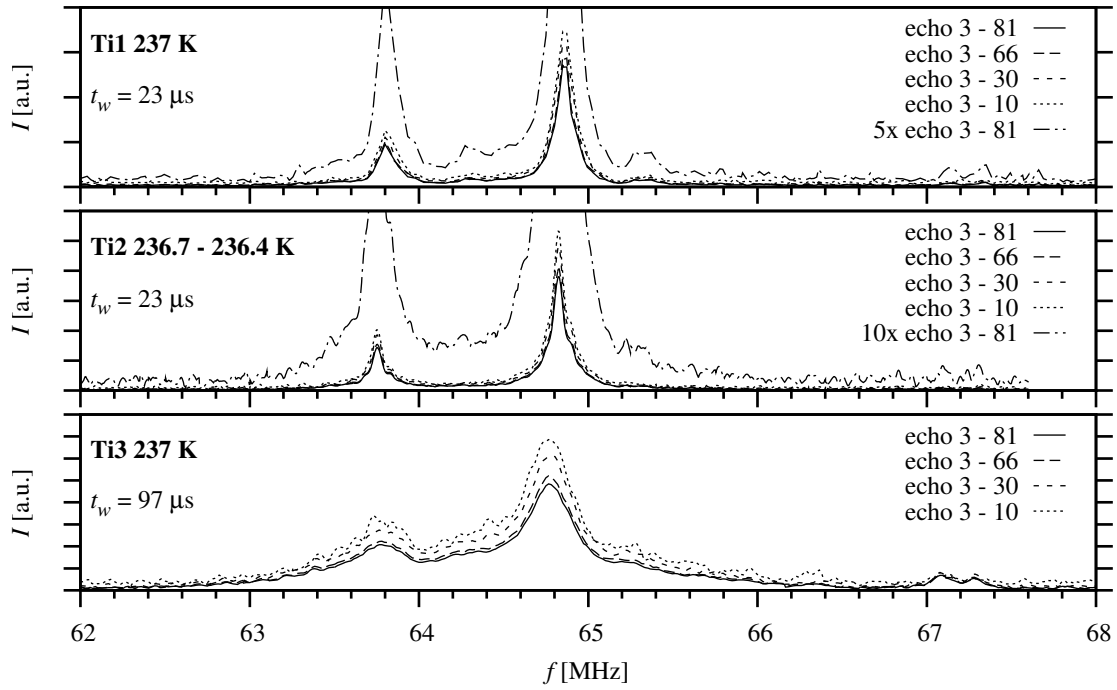

Figure 4.30: Comparison of NMR spectra of titanium substituted samples at 237 K – B lines

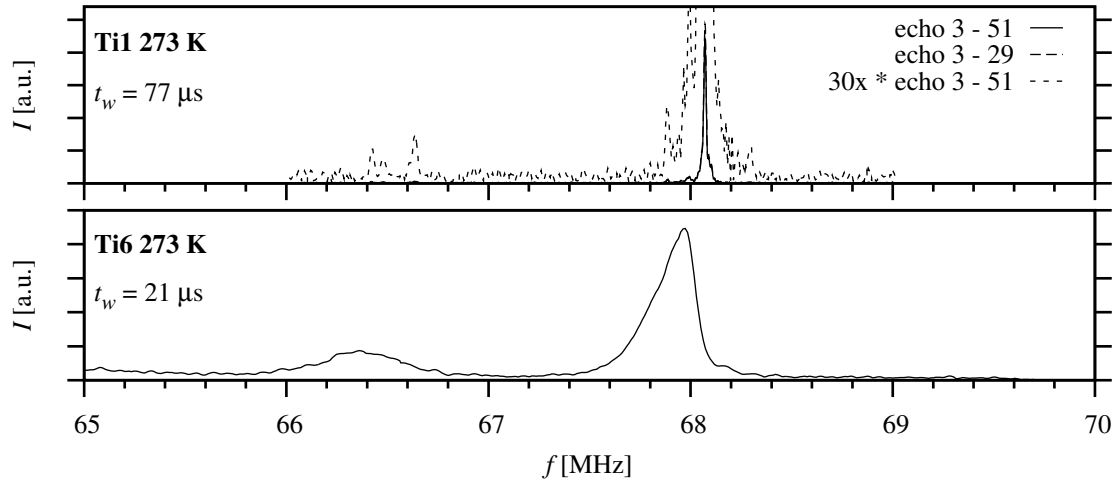

Figure 4.31: Comparison of NMR spectra of titanium substituted samples at 273 K – A lines

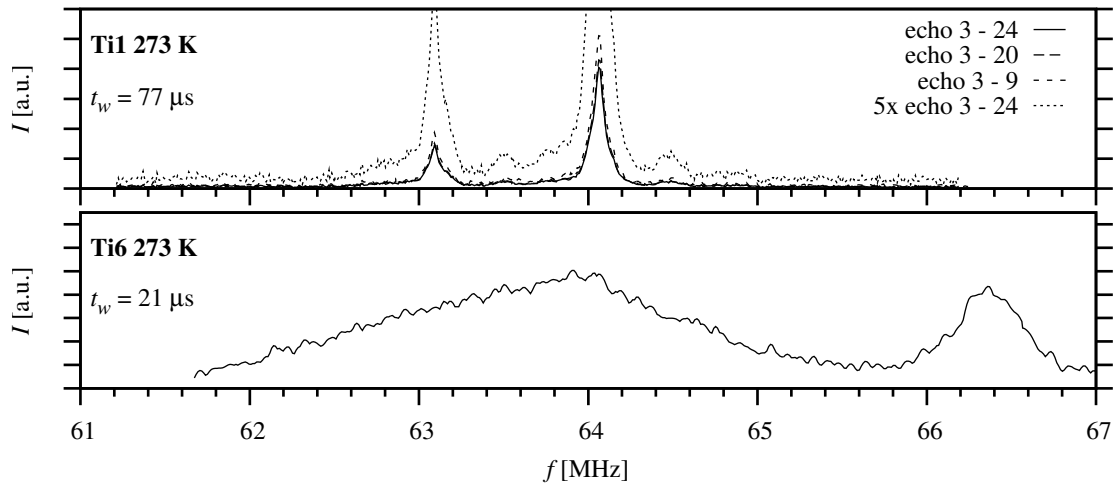

Figure 4.32: Comparison of NMR spectra of titanium substituted samples at 273 K – B lines

4.4.3 Temperature Dependences of Spectra above the Verwey Transition Temperature

Variation of NMR spectra of titanium substituted magnetite samples Ti1, Ti2 and Ti3 against the temperature were measured from temperatures near the Verwey transition up to 299 K. The obtained spectra are displayed in figures D.1 to D.9 in Appendix. In order to simplify a qualitative evaluation of the changes in the spectra with the varying temperature, the spectra were plotted relative to the most intensive line in the spectral range shown in figures 4.33 to 4.38. Graphs in the figures D.1 to D.9 which evidently belong to the temperatures when the samples were slightly below the Verwey transition are not given here. The most obvious effect in the spectra is presented by the spin reorientation transition. Furthermore, the narrowing of the main lines with the increasing temperature was observed. Just like in the case of the zinc substituted samples, particular care was taken to detect the satellite lines in the spectra to be able to track the dependences of their frequencies on the temperature.

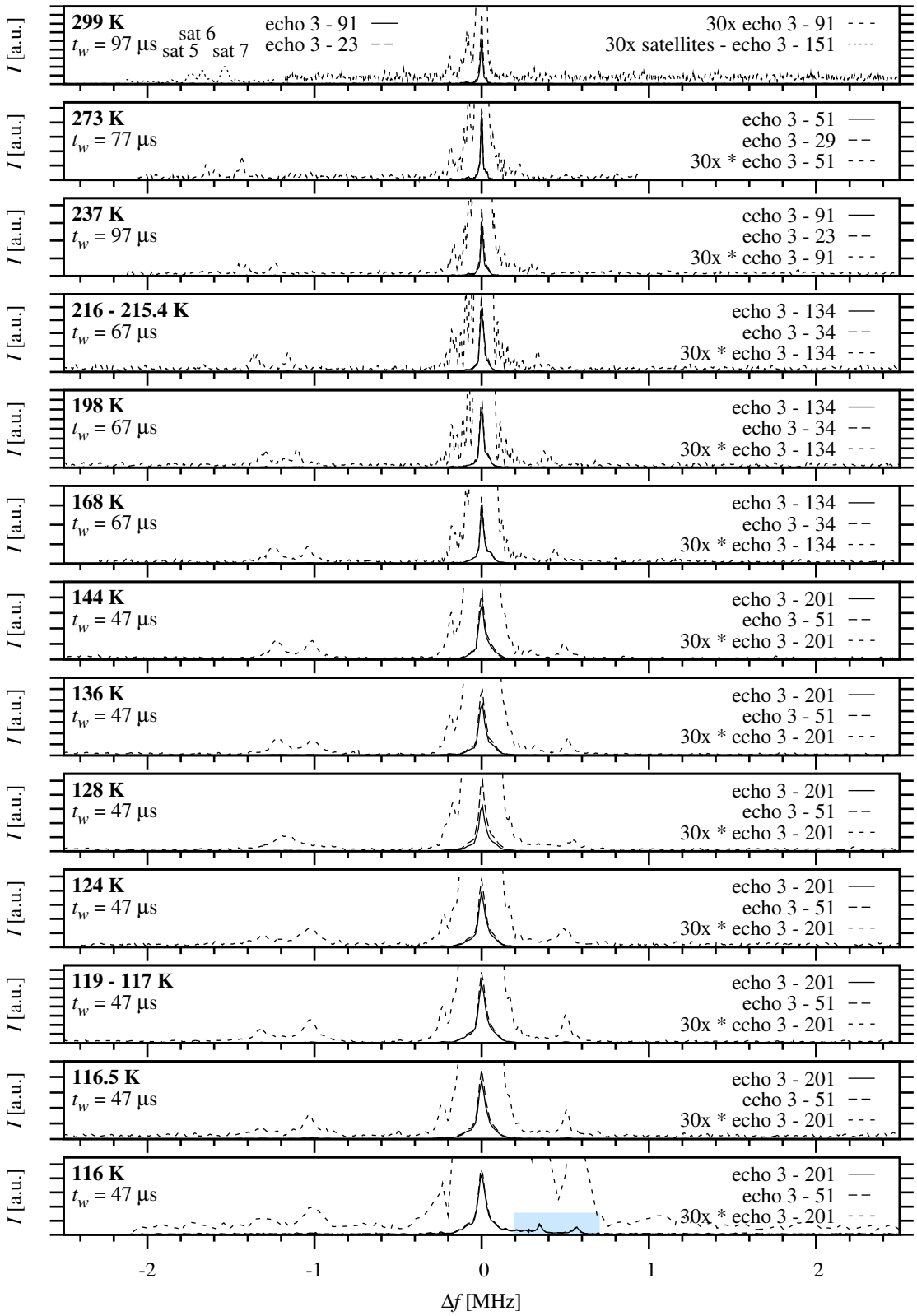

Figure 4.33: Temperature dependence of NMR spectra of sample Ti1 – spectra plotted relative to the A lines. The trace of low-temperature phase lines is visible in the spectrum at 116 K (marked by a light blue rectangle).

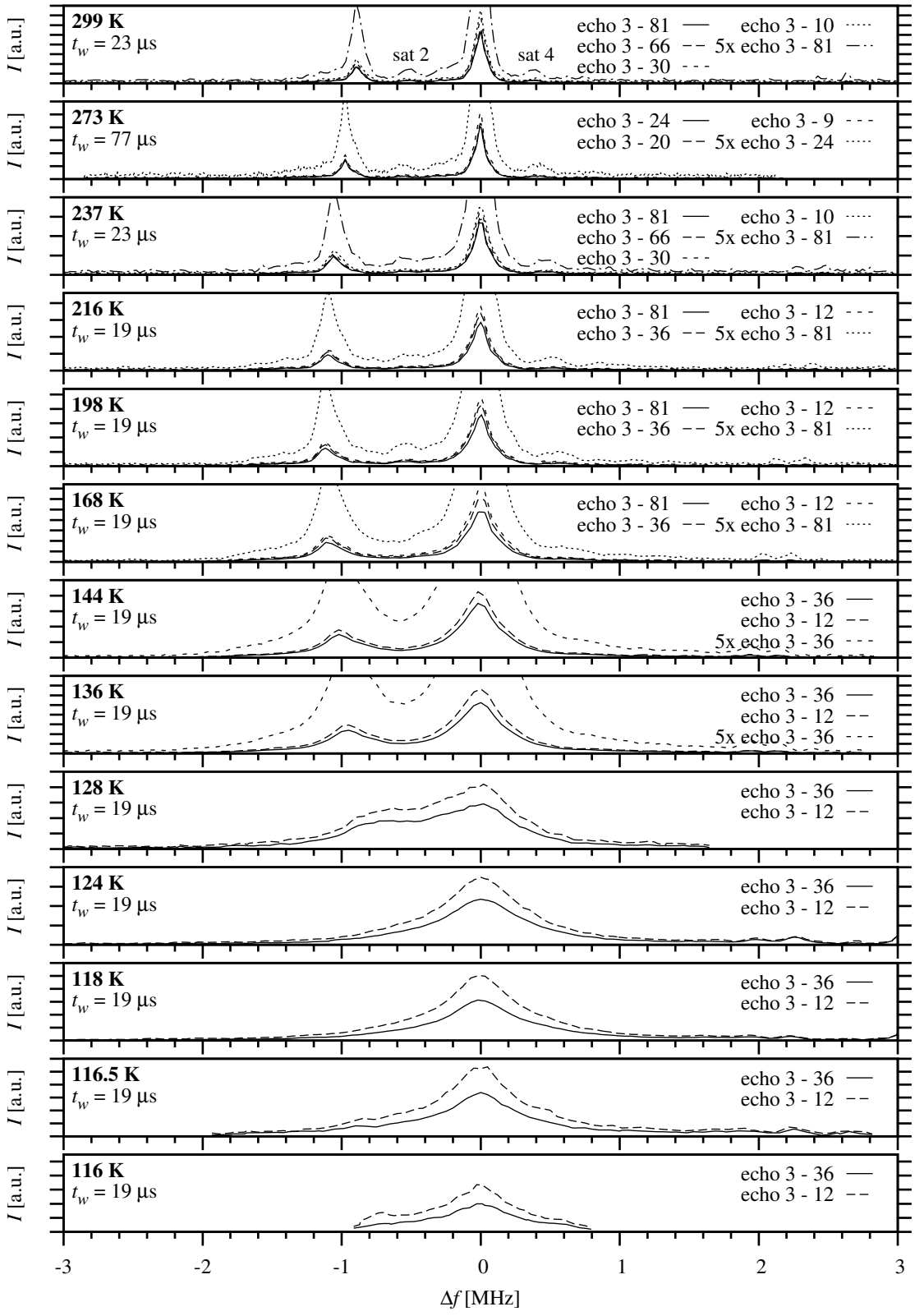

Figure 4.34: Temperature dependence of NMR spectra of sample Ti1 – spectra plotted relative to the B, B_2 lines

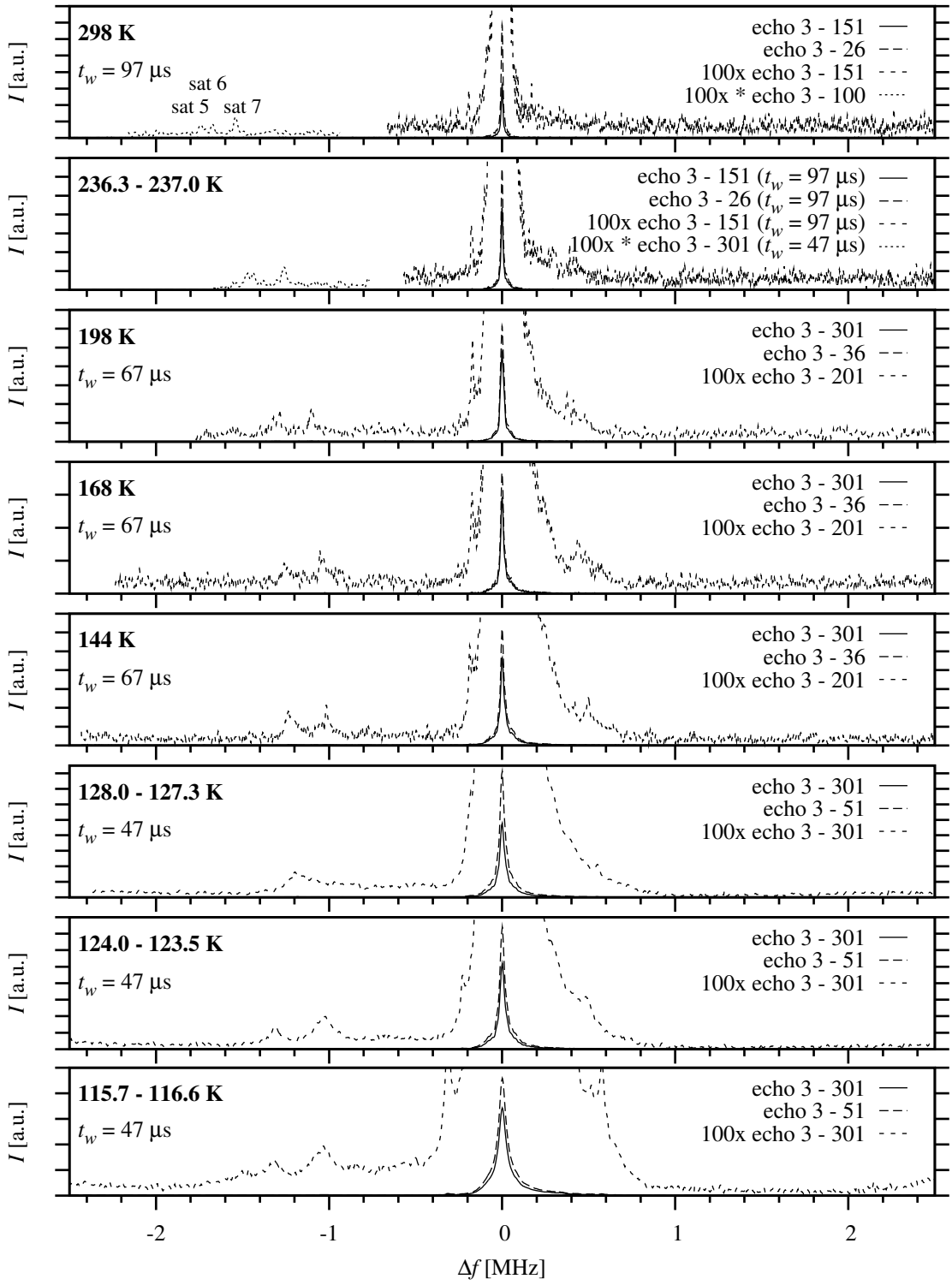

Figure 4.35: Temperature dependence of NMR spectra of sample Ti2 – spectra plotted relative to the A lines

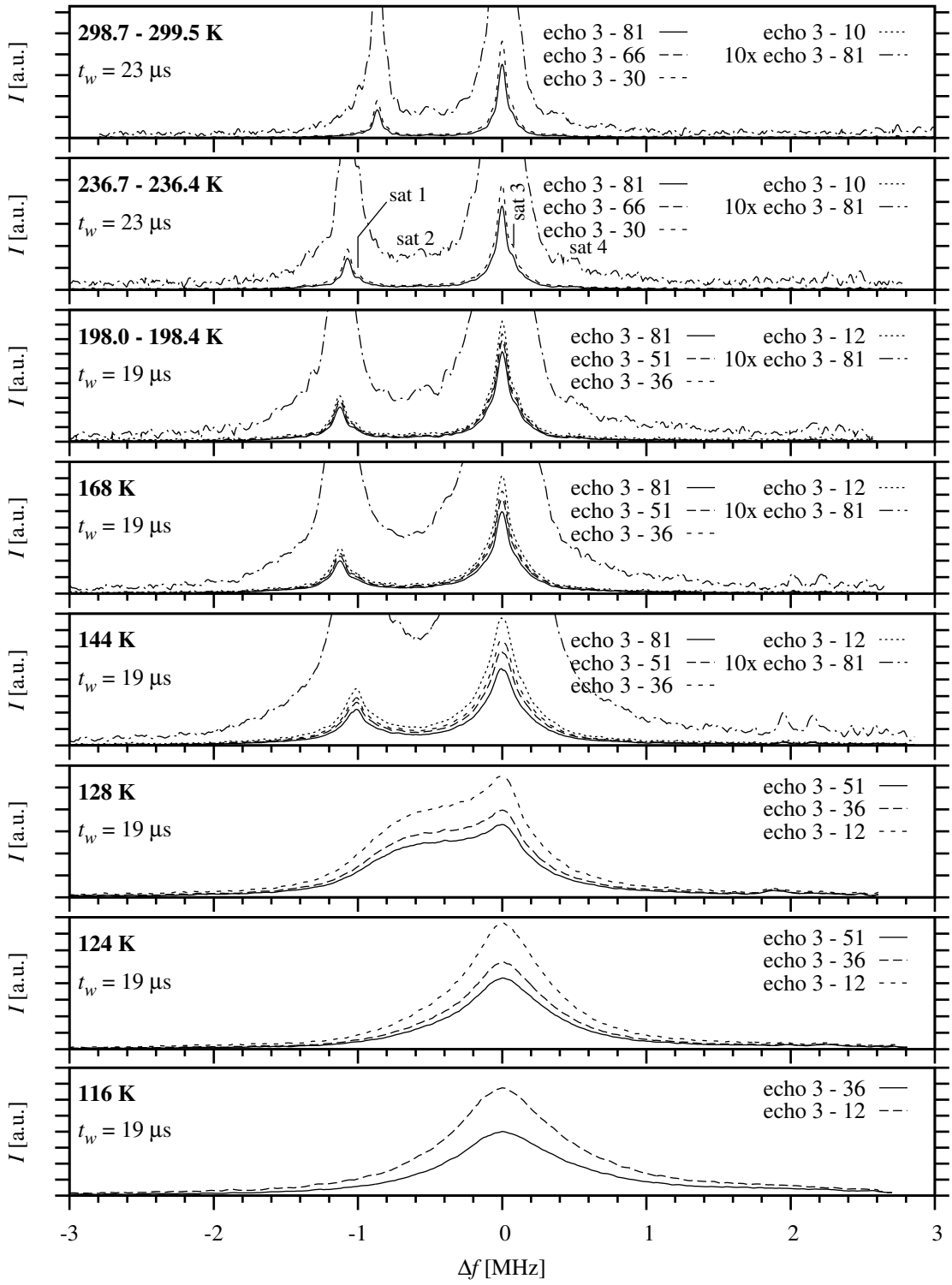

Figure 4.36: Temperature dependence of NMR spectra of sample Ti2 – spectra plotted relative to the B, B_2 lines

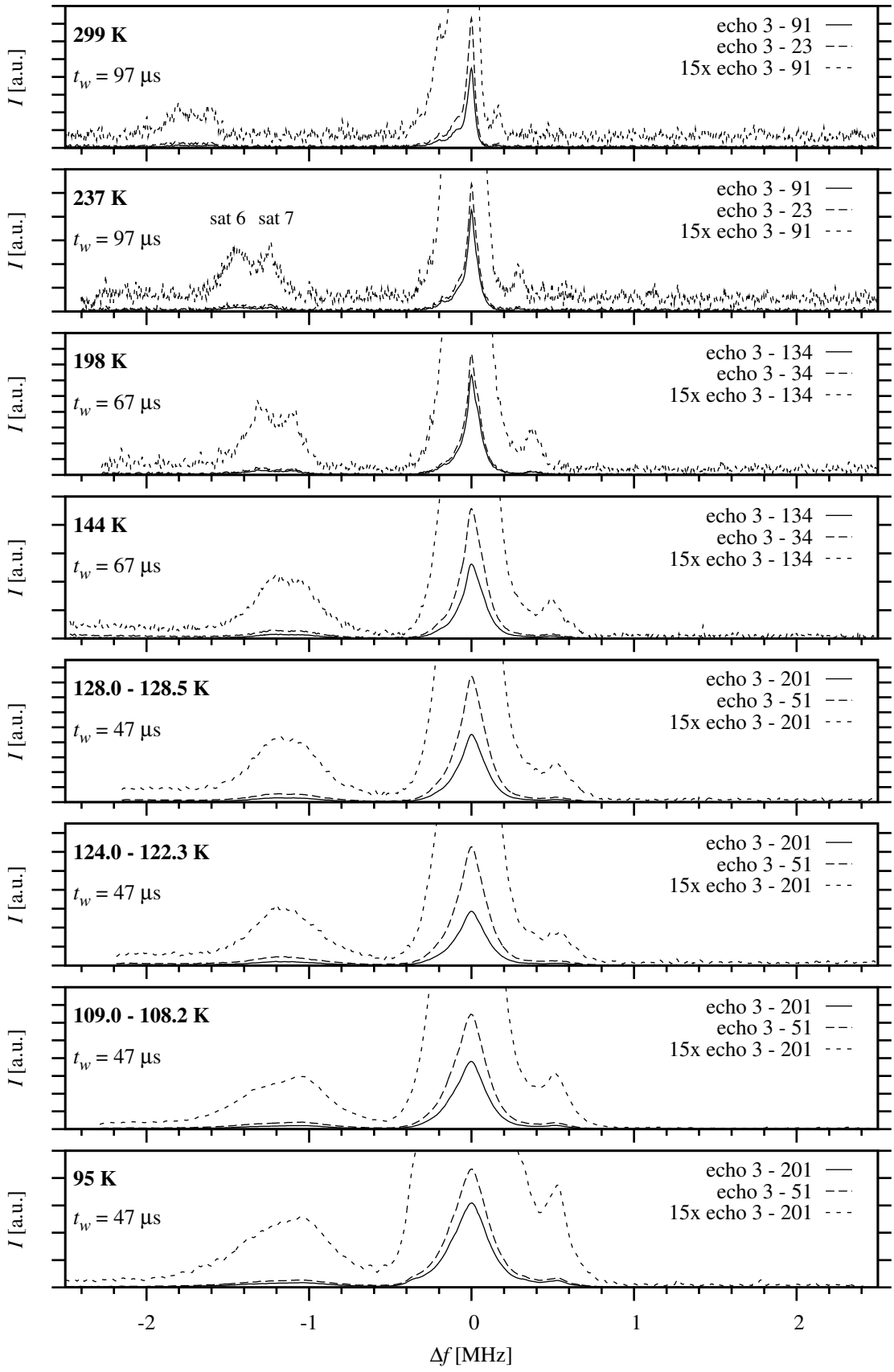

Figure 4.37: Temperature dependence of NMR spectra of sample Ti3 – spectra plotted relative to the A lines

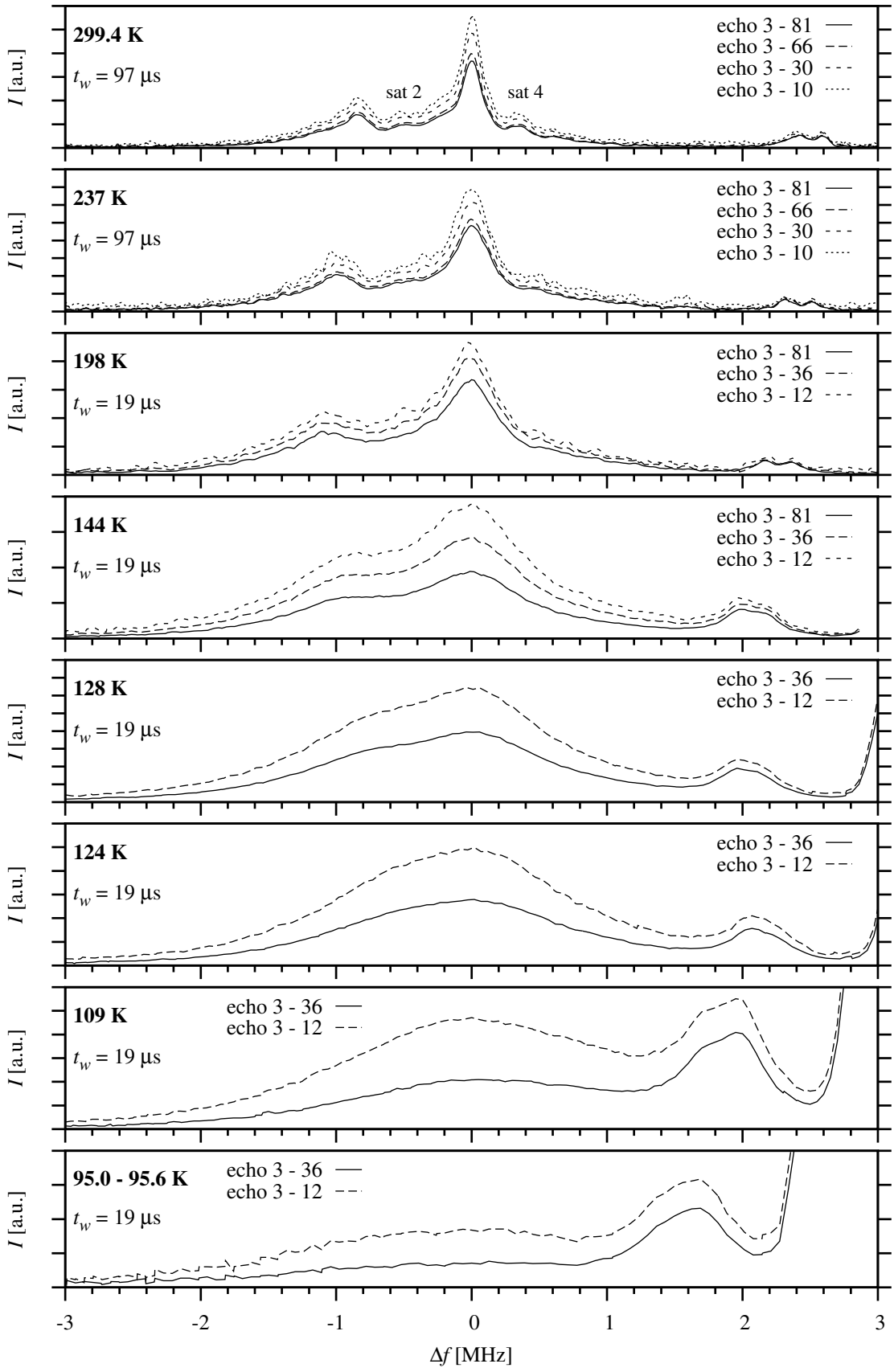

Figure 4.38: Temperature dependence of NMR spectra of sample Ti3 – spectra plotted relative to the B, B_2 lines

4.4.4 Temperature Dependences of Spectral Signal Frequencies

The frequencies of the main lines and of the satellite signals found in the temperature dependences of spectra are listed in tables E.1 to E.6 in Appendix and a graph of these temperature dependences is presented in figure 4.39. Satellite signals sat 5, sat 6 and sat 7 located in between the A line and the B lines originate from the presence of the titanium ion Ti^{4+} at the B site nearest to the resonating nuclei at the A sites, whereas the satellite pattern in the vicinity of the A line probably comes from the presence of the substitution at the B site in wider surroundings of the resonating nuclei at the A sites. Satellite lines sat 2 and sat 4 near the B lines arise from the resonating nuclei at the B sites with the substitution at the B site in the vicinity. The splitting between the B lines and these satellites is lower than that between the A line and the satellites sat 5, sat 6 and sat 7 due to higher distance between the nearest B sites than between the nearest A and B sites. Satellites sat 1 and sat 3 probably correspond to the presence of the titanium ion Ti^{4+} in a more distant neighbourhood of the resonating nuclei at the B sites.

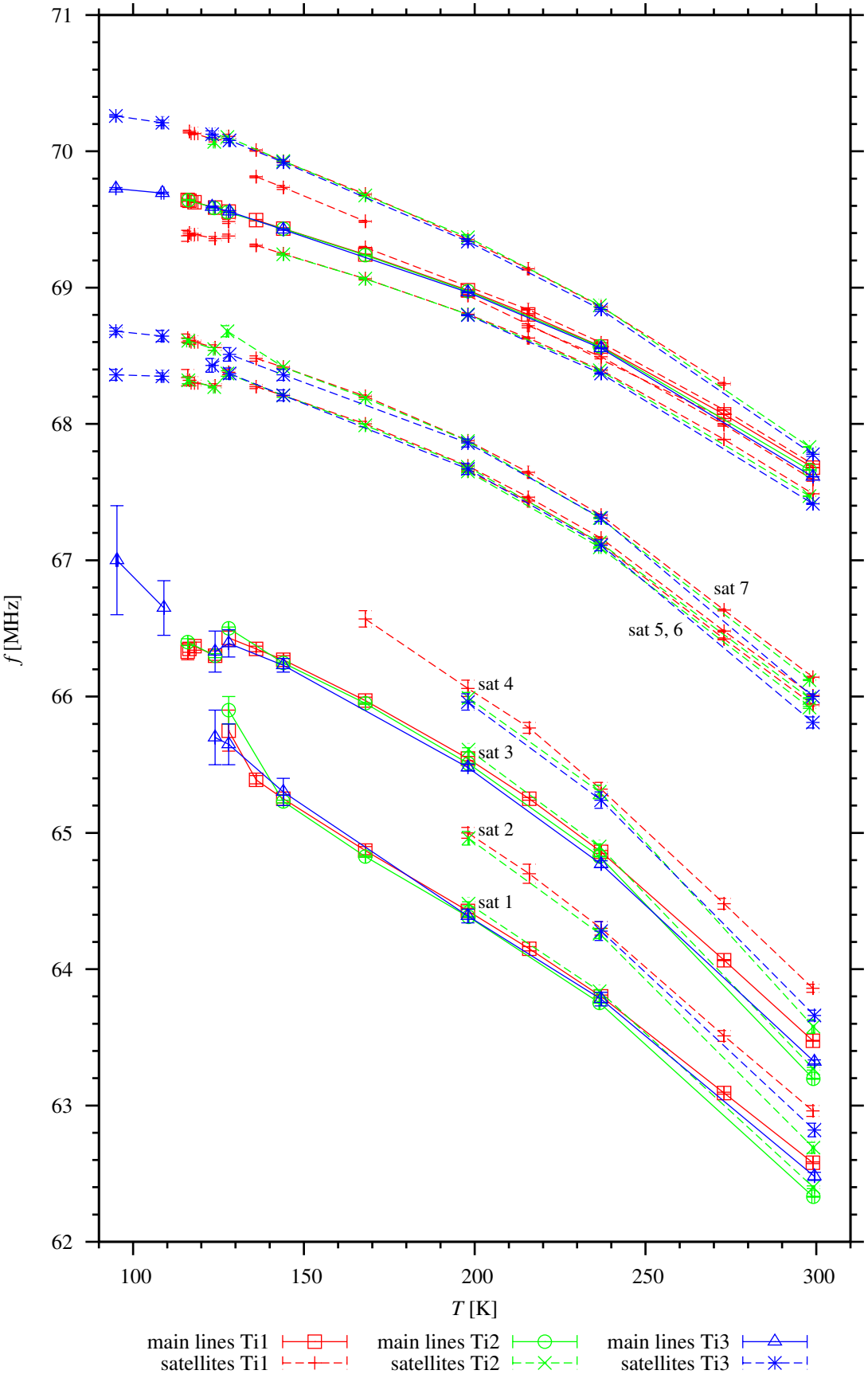

Figure 4.39: Temperature dependences of frequencies of the main lines and of the satellite signals in the spectra of the titanium substituted samples

4.4.5 Temperature Dependences of HWHM of the A Lines

The half widths of the A lines read out from the temperature dependences of the spectra of the samples Ti1, Ti2 and Ti3 are given in tables F.1 to F.3 in Appendix. Graphical representation of the variation of HWHM of the A lines against the temperature is provided in figure 4.40. The differences between curves are apparent, particularly interesting is the slightly faster decay of the dependence for the sample Ti2 than for the sample Ti1, supporting the suggestion of the actual concentration of the substitution in the sample Ti2 being near the lower end of the claimed range.

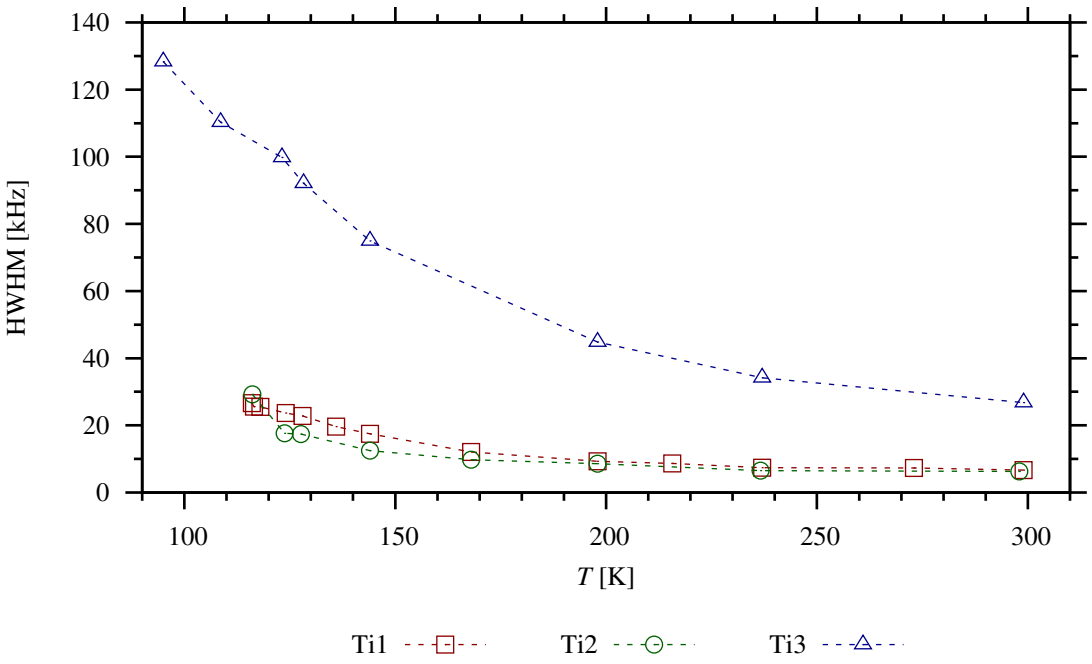

Figure 4.40: Temperature dependences of half width at half maximum of the A lines in the spectra of the titanium substituted samples

4.5 Discussion

Analysis of the acquired NMR spectra of the zinc and titanium substituted magnetite is based on an interpretation of spectra of pure magnetite at the corresponding temperature. In addition to giving rise to satellite signals, the presence of the substitution causes broadening of lines in the spectra.

Experiments at 4.2 K were performed on samples with relatively low substitution concentration except the sample Ti6, thus it is possible to distinguish most of the spectral lines despite their broadening. Frequencies of the spectral lines are the same as those of the lines in the spectra of pure magnetite. However, as already stated, the satellite pattern could not be observed due to being overlaid by the dense structure of the broadened main lines. In case of the sample Ti6, the lines in the spectra are so broad that it is impossible to resolve particular lines.

The structure of the main lines in the spectra acquired at the temperatures above the Verwey transition is relatively simple and the frequencies of the main

lines correspond to those of the lines in the spectra of pure magnetite – see figure 4.41. The most apparent effect in the spectra is the spin reorientation transition manifesting itself by the splitting of the B line into the B_1 and B_2 lines. The spectra corresponding to a cubic phase were observed to lower temperatures compared to pure magnetite because the Verwey transition temperatures of the investigated samples are lower due to the presence of the substitution. The spectrum of the sample Ti6 at 273 K differs from the spectra of the other titanium substituted samples by significantly broader lines making the B lines merge into a wide band, by the lower frequency of the A line and by a high intensity of the satellite signal between the A and B lines due to relatively high substitution concentration.

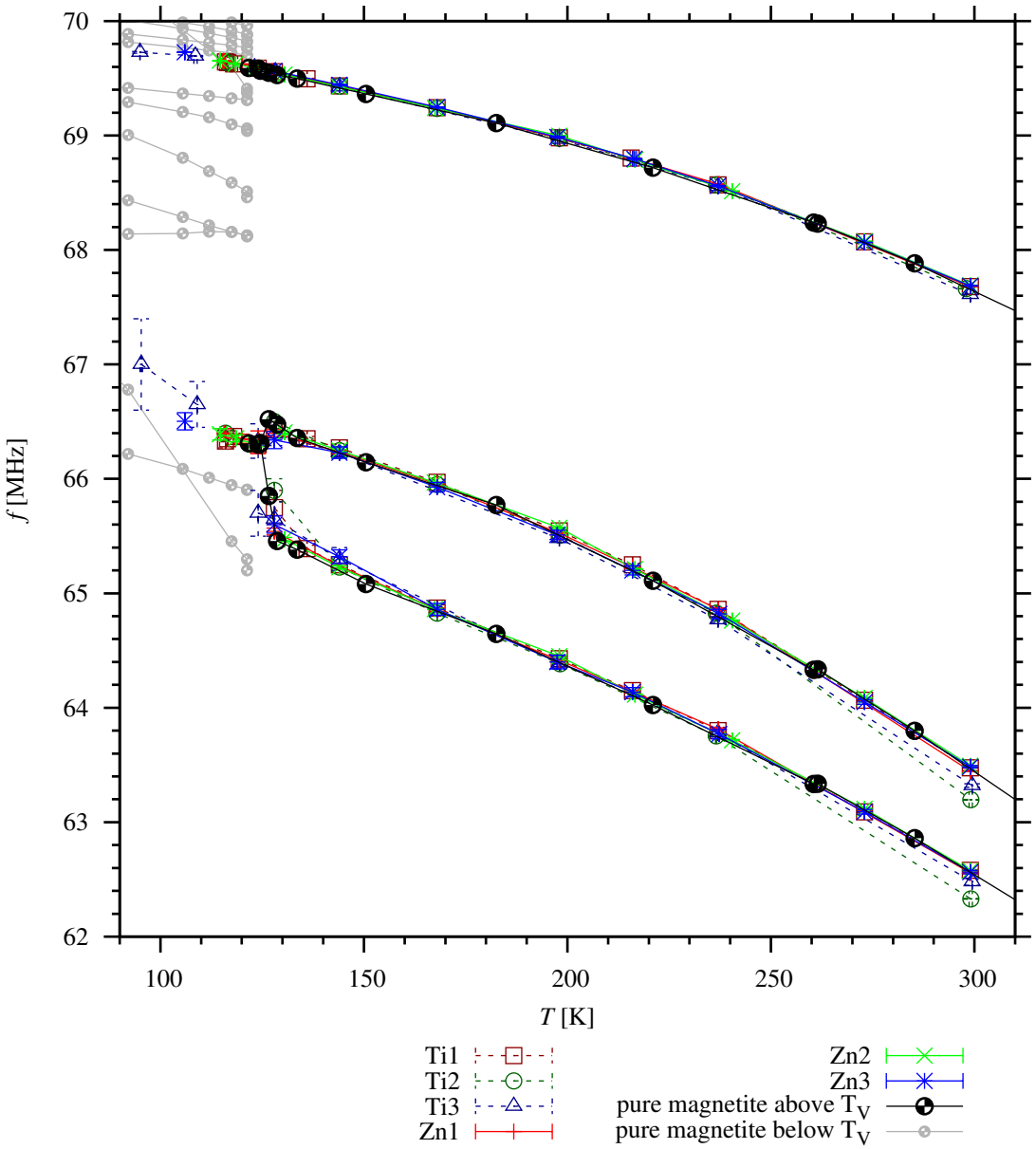

Figure 4.41: Temperature dependences of frequencies of the main lines in the spectra of the zinc and titanium substituted samples and of pure magnetite [26], [3]

Satellite signal patterns were observed in the spectra measured above the Verwey transition frequency and the temperature dependences of their frequencies were constructed. The limitation factors of resolving the satellite signals were the signal-to-noise ratio and the overlaying of the satellites by the broadened main spectral lines in case of the satellite lines that were located close to the main lines.

In case of the zinc substituted samples, there are numerous satellite lines close to the A line, forming a complex structure arising from the presence of zinc ion Zn^{2+} in a wider surrounding of the resonating nuclei at the A site. There were also several satellite lines resolved in the vicinity of the B lines. Satellite sat 1 and most likely also satellites sat 3 and sat 5 originate from the presence of the substitution in the A position nearest to the resonating nuclei at the B sites, whereas in case of the satellite signals sat 2 and sat 4, we cannot avoid the possibility that these signals are caused be the zinc ion Zn^{2+} located at the A site in a more distant surrounding of the resonating nuclei at the B positions. Temperature dependences of frequencies of the satellite lines plotted relative to the main lines are presented in figures 4.42 and 4.43. Satellite line sat 1, which is of a particular interest due to the highest splitting between this line and the B lines, was compared in figure 4.44 to the satellite observed below the B lines in the spectra of gallium substituted magnetite [30]. Temperature dependences of frequencies of the satellite signal sat1 and of the B_2 line normalized to their frequencies at 299 K are shown in figure 4.45 and a similar plot in figure 4.46 provides the comparison with the abovementioned satellite found in the spectra of gallium substituted magnetite. As evidenced, a decrease of the frequency with increasing temperature of the satellite sat 1 is much slower than in case of the referred satellite line in the spectra of gallium substituted magnetite. Another signal deserving a special mention is marked as sat 20. Origin of this relatively broad line, which was observed only at the lower end of the temperature dependences, is not clear – it may be a satellite signal from resonating iron nuclei at the A sites but it can also be caused by the resonance of the oxygen nuclei ^{17}O reported in [31] at about 80 MHz for the (Zn-Mn-Fe)O_4 compound at the temperature of 4 K. Satellite signals observed in the spectra of the sample Zn2 which are marked in table B.4 by an asterisk originate from the presence of a low concentration of vacancies in the sample, as was clearly demonstrated in figure 4.23.

The most interesting satellite signals found in the spectra of the titanium substituted samples, marked sat 5, sat 6 and sat 7, are in between the A line and the B lines. At higher temperatures, these signals can be resolved as three distinct lines with intensity ratio of 1:1:2 (see table 3.3). These satellite lines arise from the presence of the substitution at the B site nearest to the resonating nuclei at the A sites. The satellite lines near the A line probably originate from the presence of the titanium ion Ti^{4+} at B site in wider neighbourhood of the resonating nuclei at the A sites. Satellite lines in the vicinity of the B lines can be divided into two groups. The first group consisting of the satellites sat 2 and sat 4 arise from the presence of the substitution at the B site nearest to the resonating nuclei at the B sites. The second group is formed by the satellite signals sat 1 and sat 3 induced probably by the substitution ion located in a wider surroundings of the resonating nuclei at the B sites. Temperature dependences of frequencies of the satellite lines plotted relative to the main lines are provided in figures 4.47 and 4.48. Temperature dependences of frequencies of the satellite signals sat 5, sat 6

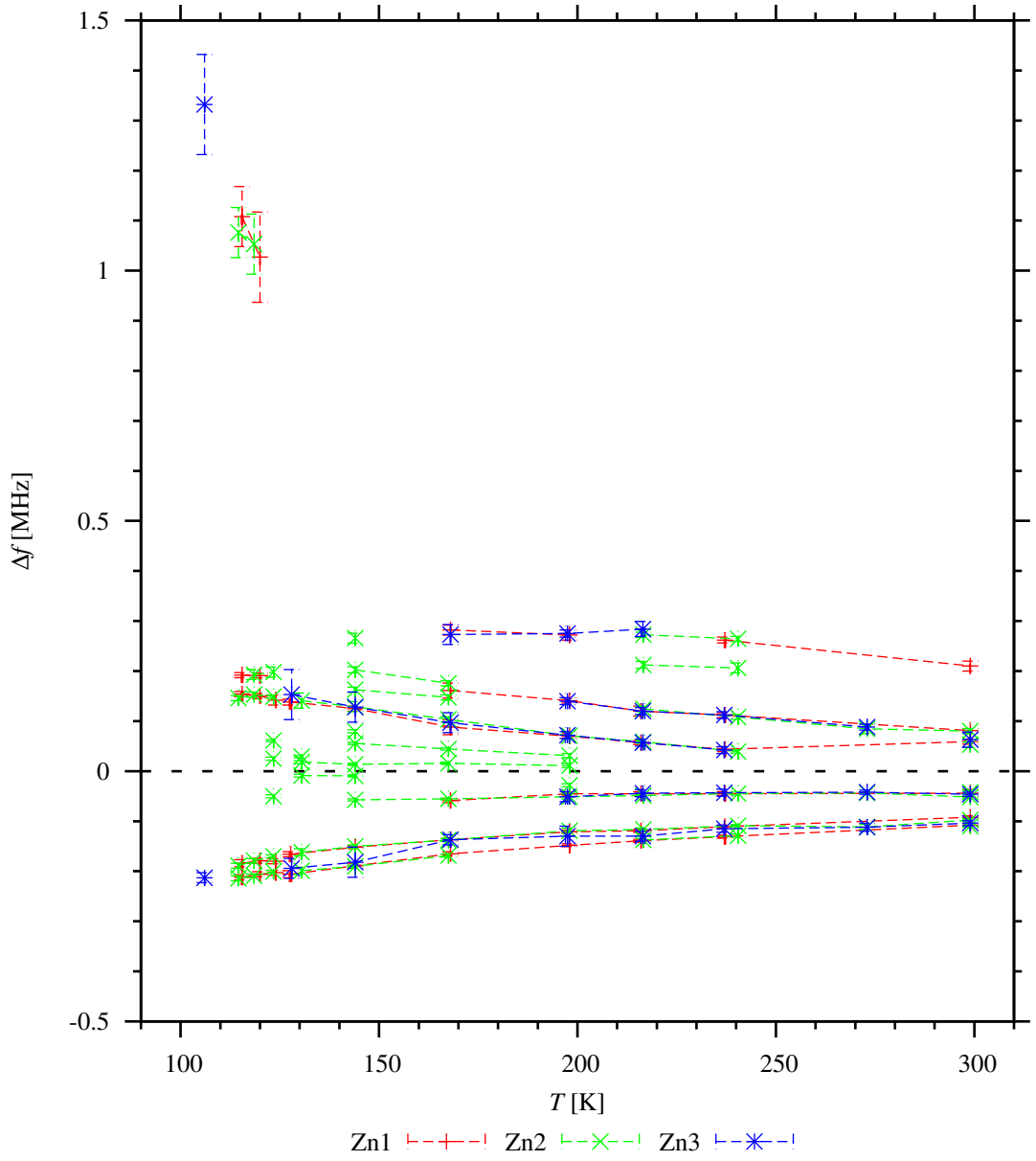

Figure 4.42: Temperature dependences of frequencies of the satellite signals near the A line in the spectra of the zinc substituted samples plotted relative to the A line

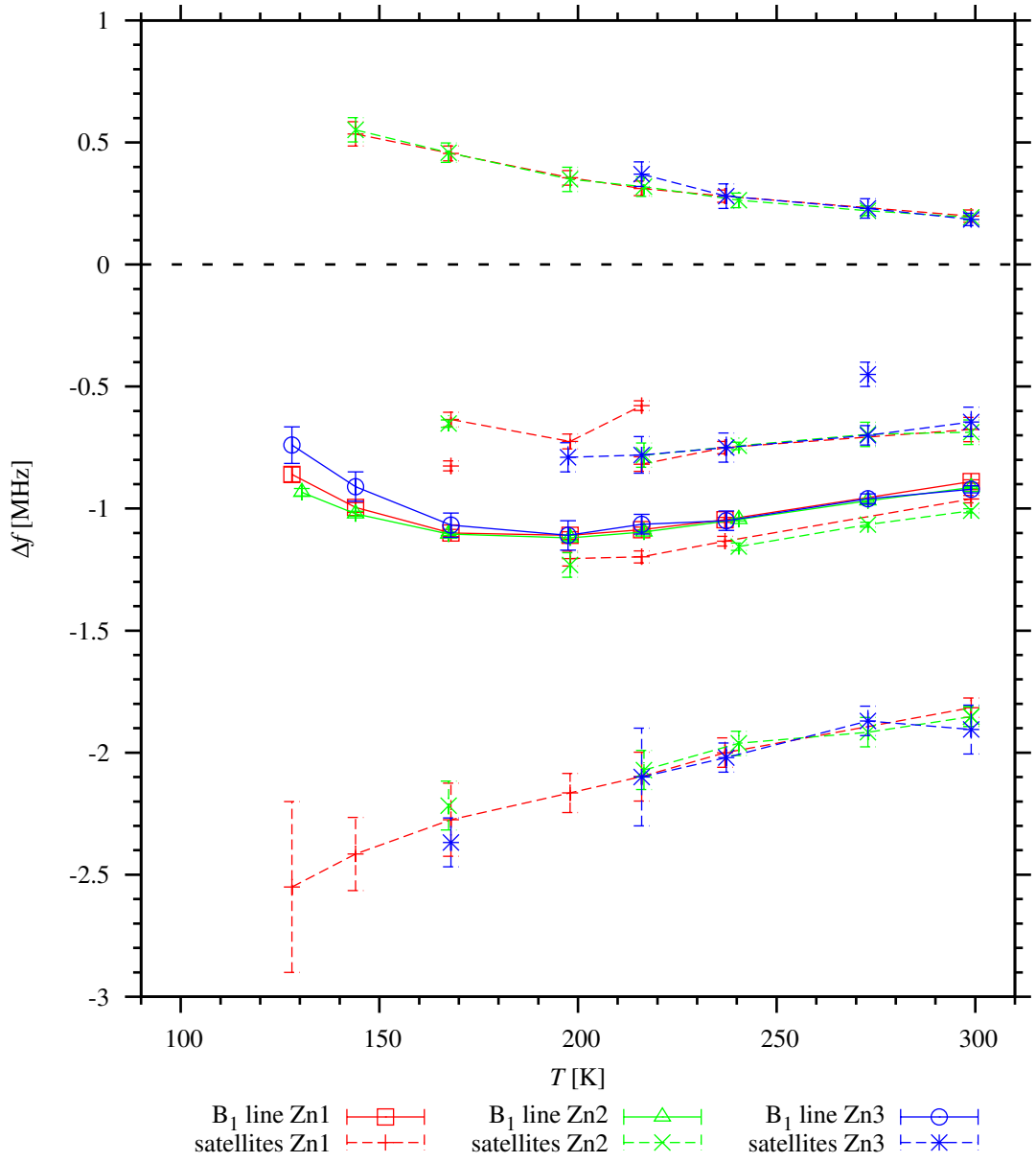

Figure 4.43: Temperature dependences of frequencies of the B_1 line and the satellite signals near the B lines in the spectra of the zinc substituted samples plotted relative to the B_2 line

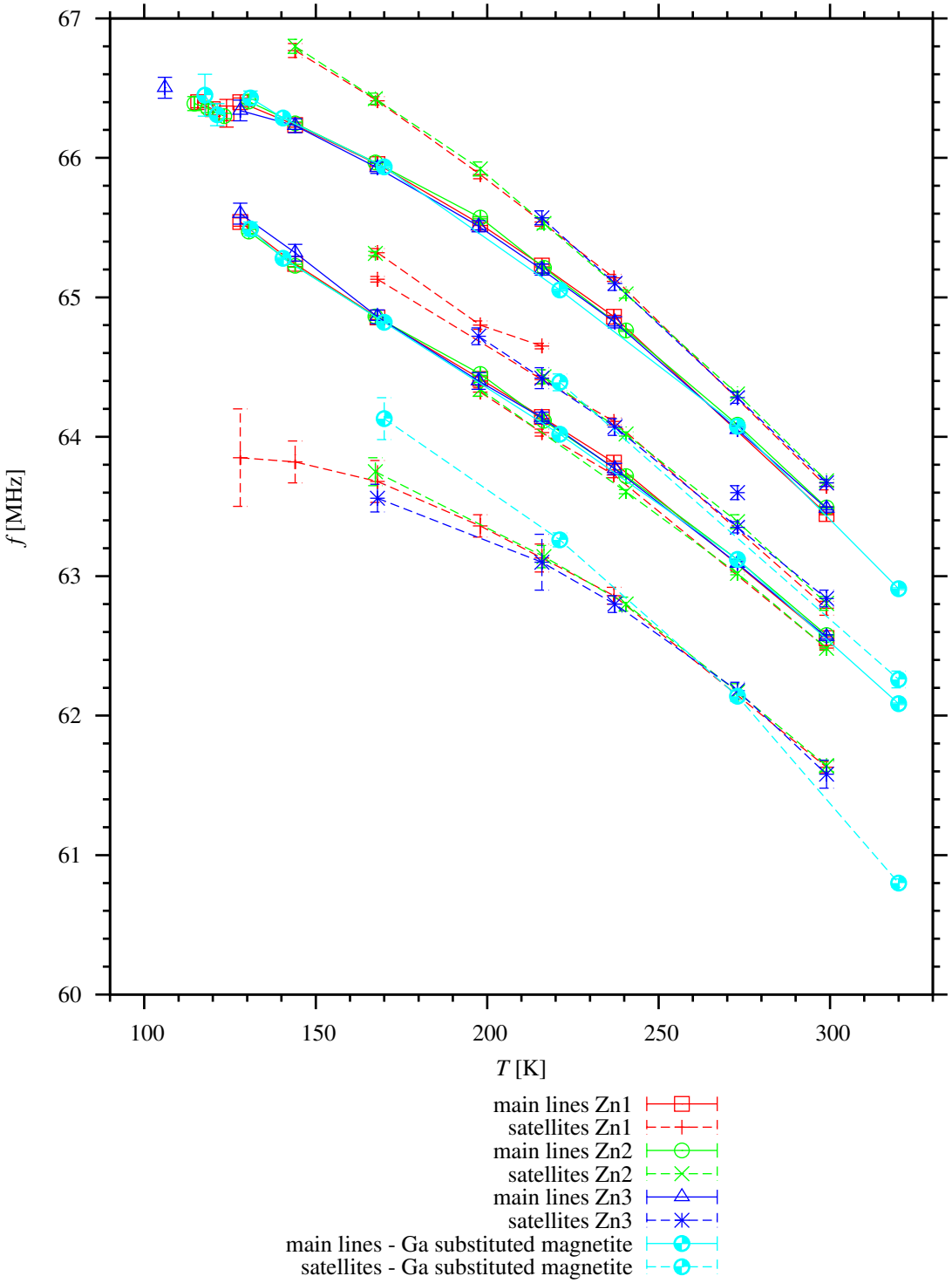

Figure 4.44: Comparison of the temperature dependences of frequencies of the B lines and of the satellite signals near them in the spectra of the zinc substituted samples with the data for gallium substituted magnetite $Fe_{2.95}Ga_{0.05}O_4$ [30]

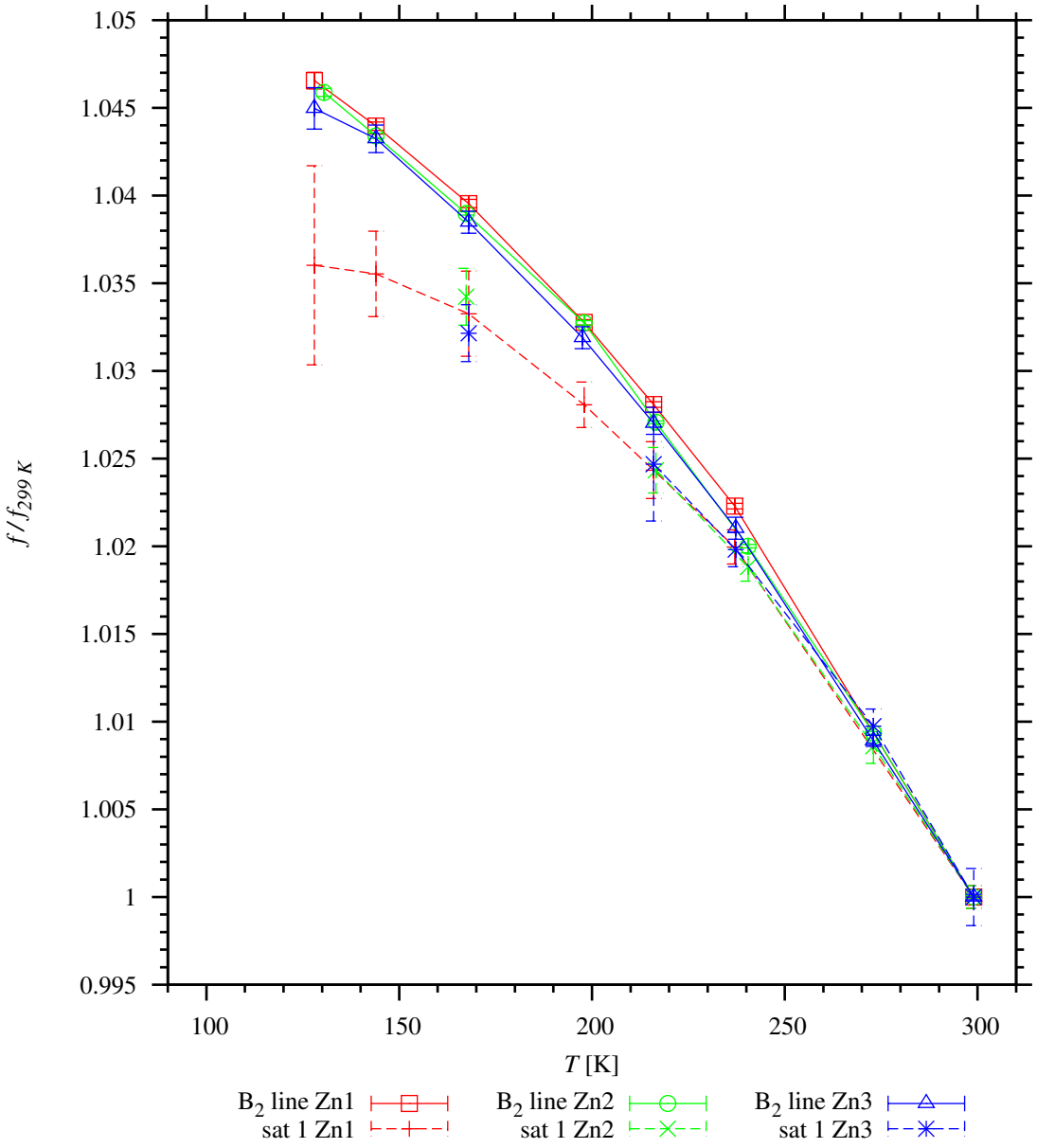

Figure 4.45: Temperature dependences of frequencies of the B_2 line and of the satellite signal sat1 in the spectra of the zinc substituted samples normalized to their frequencies at 299 K

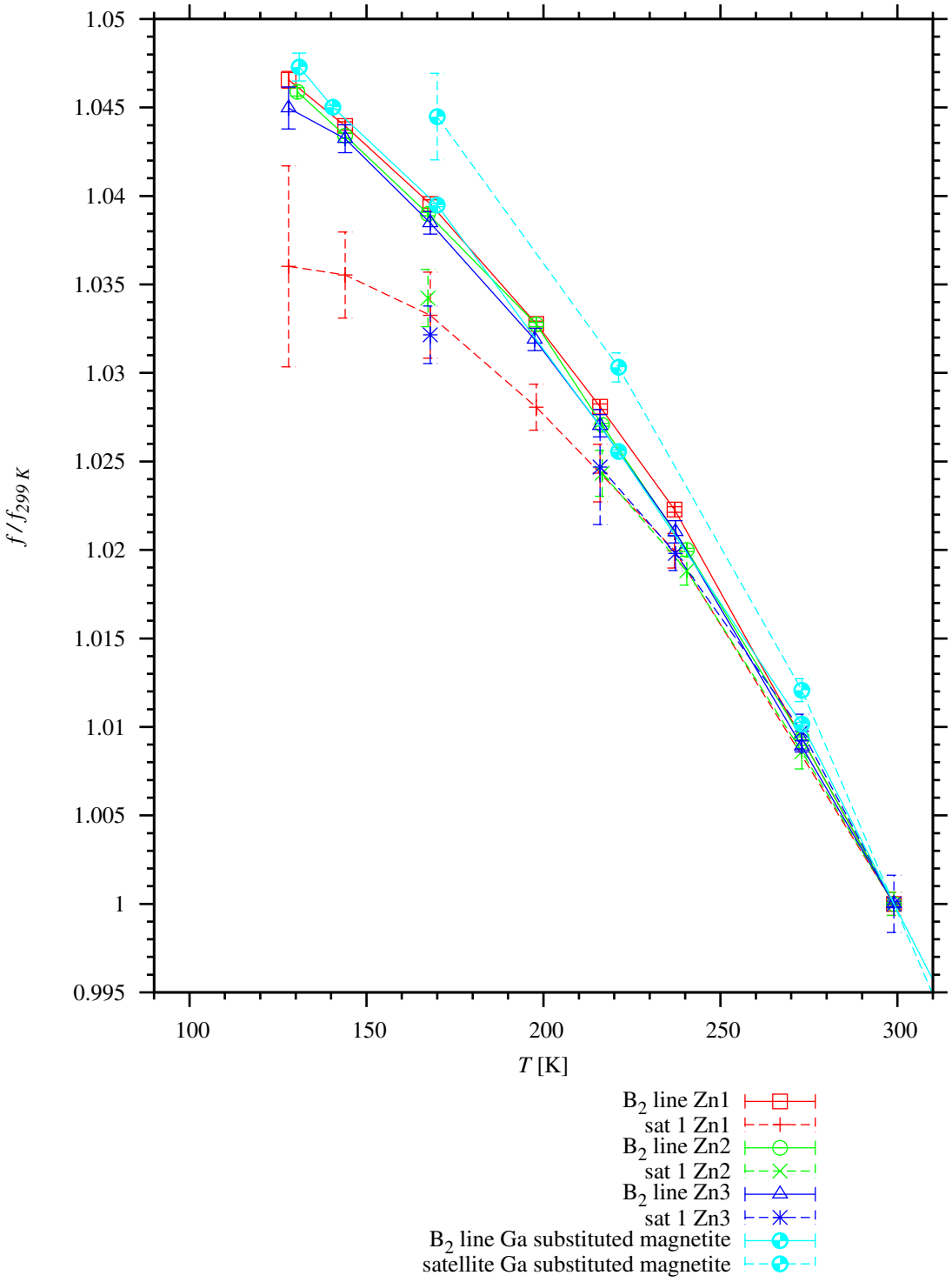

Figure 4.46: Comparison of the temperature dependences of frequencies of the B_2 line and of the satellite signal sat1 in the spectra of the zinc substituted samples normalized to their frequencies at 299 K with the data for gallium substituted magnetite $Fe_{2.95}Ga_{0.05}O_4$ [30]

and sat 7 and of the A line normalized to their frequencies at 144 K is presented in figure 4.49 and the comparison with the satellite signal in the spectra of aluminium substituted magnetite [3] and of non-stoichiometric magnetite [22] is provided in figure 4.50. A decrease of the frequency with increasing temperature of the satellite signals sat 5, sat 6 and sat 7 is slower than in case of the satellites in the spectra of non-stoichiometric magnetite but it is faster than in case of satellite lines in the spectra of aluminium substituted magnetite. However, all displayed satellite lines have faster decrease of the frequency with increasing temperature than the main A line due to a perturbed A-B exchange interaction.

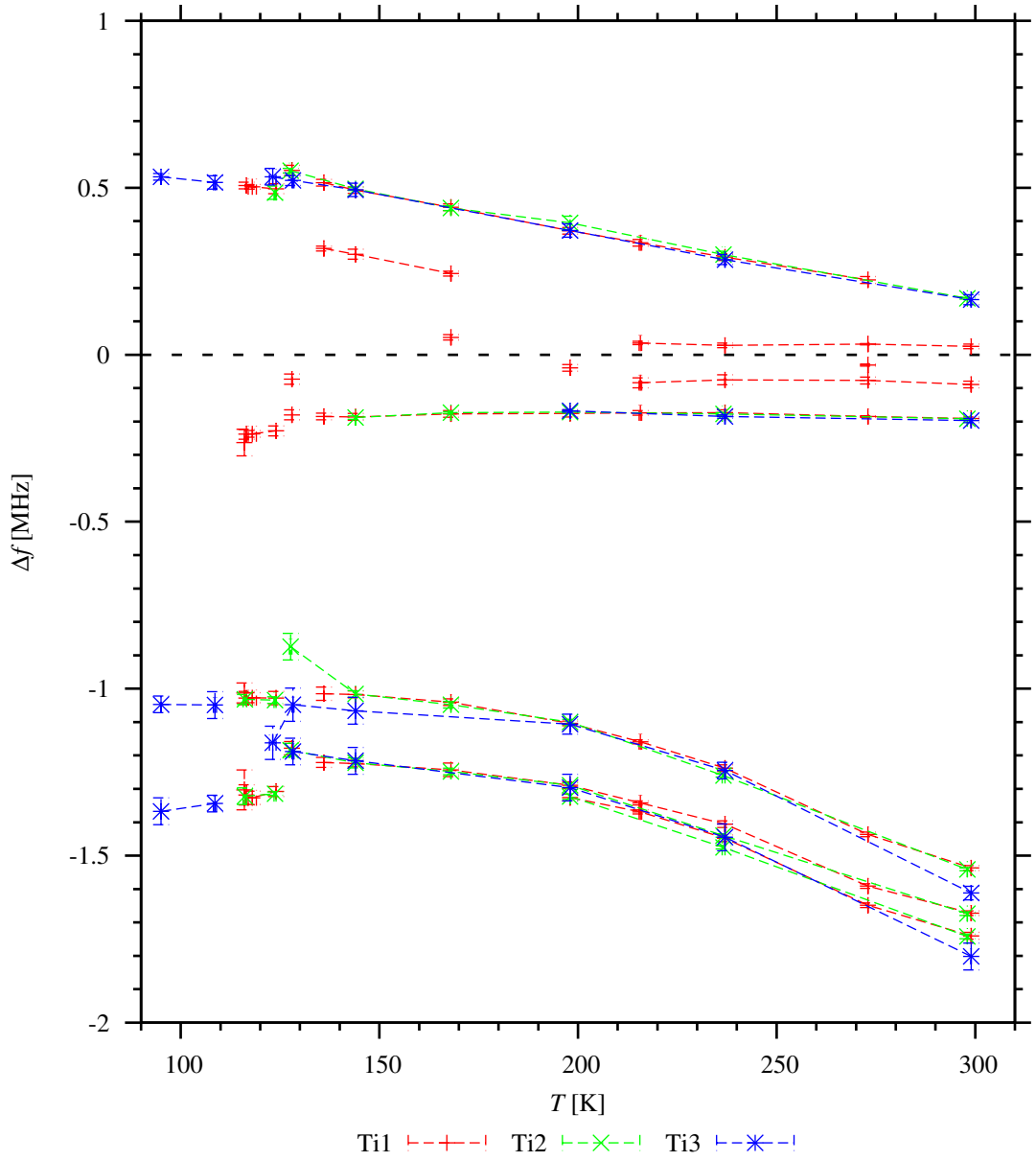

Figure 4.47: Temperature dependences of frequencies of the satellite signals near the A line in the spectra of the titanium substituted samples plotted relative to the A line

Temperature dependences of the widths of the A lines in the acquired spectra above the Verwey transition exhibit very interesting behaviour. Typically in

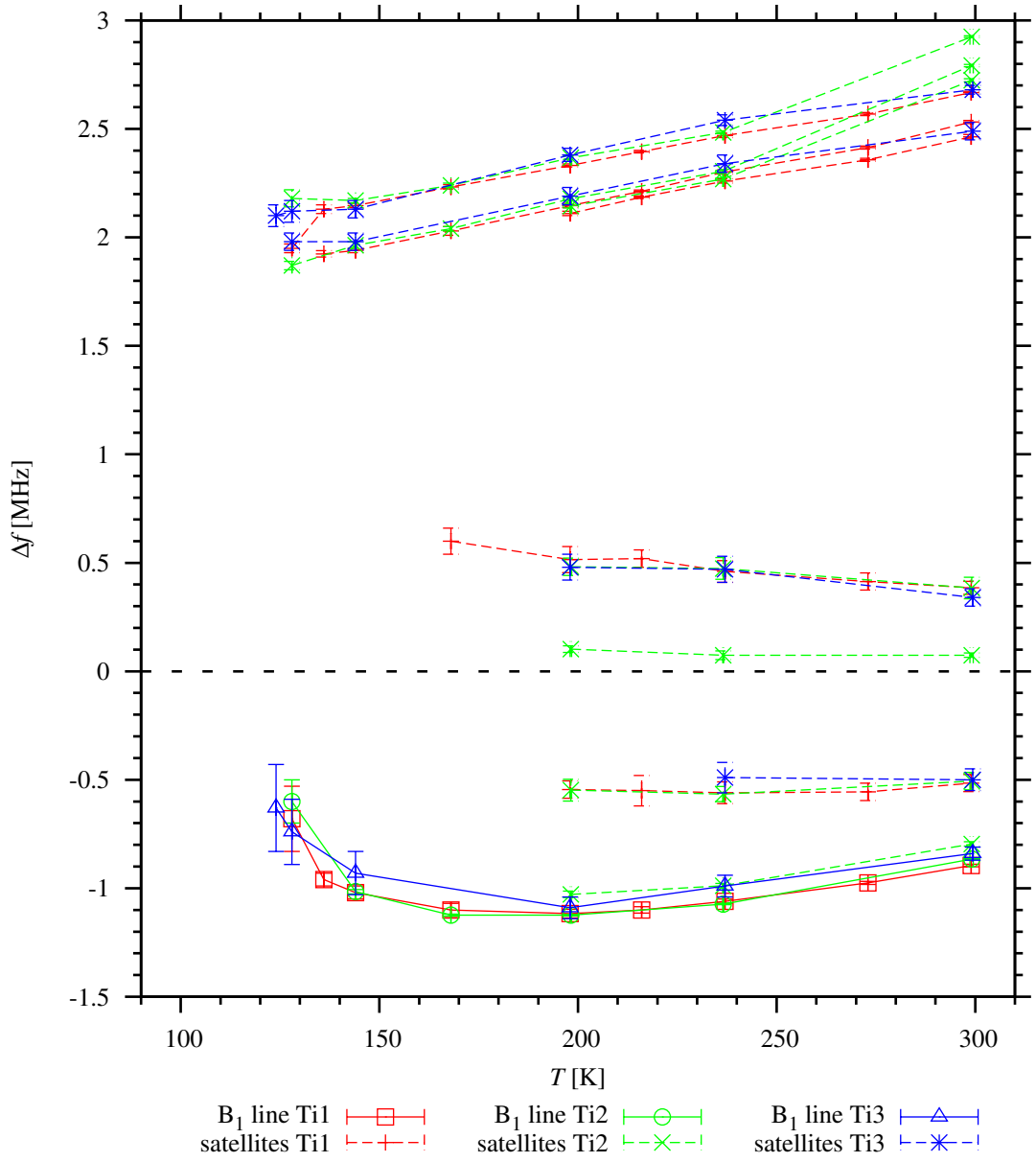

Figure 4.48: Temperature dependences of frequencies of the B_1 line and the satellite signals near the B lines in the spectra of the titanium substituted samples plotted relative to the B_2 line

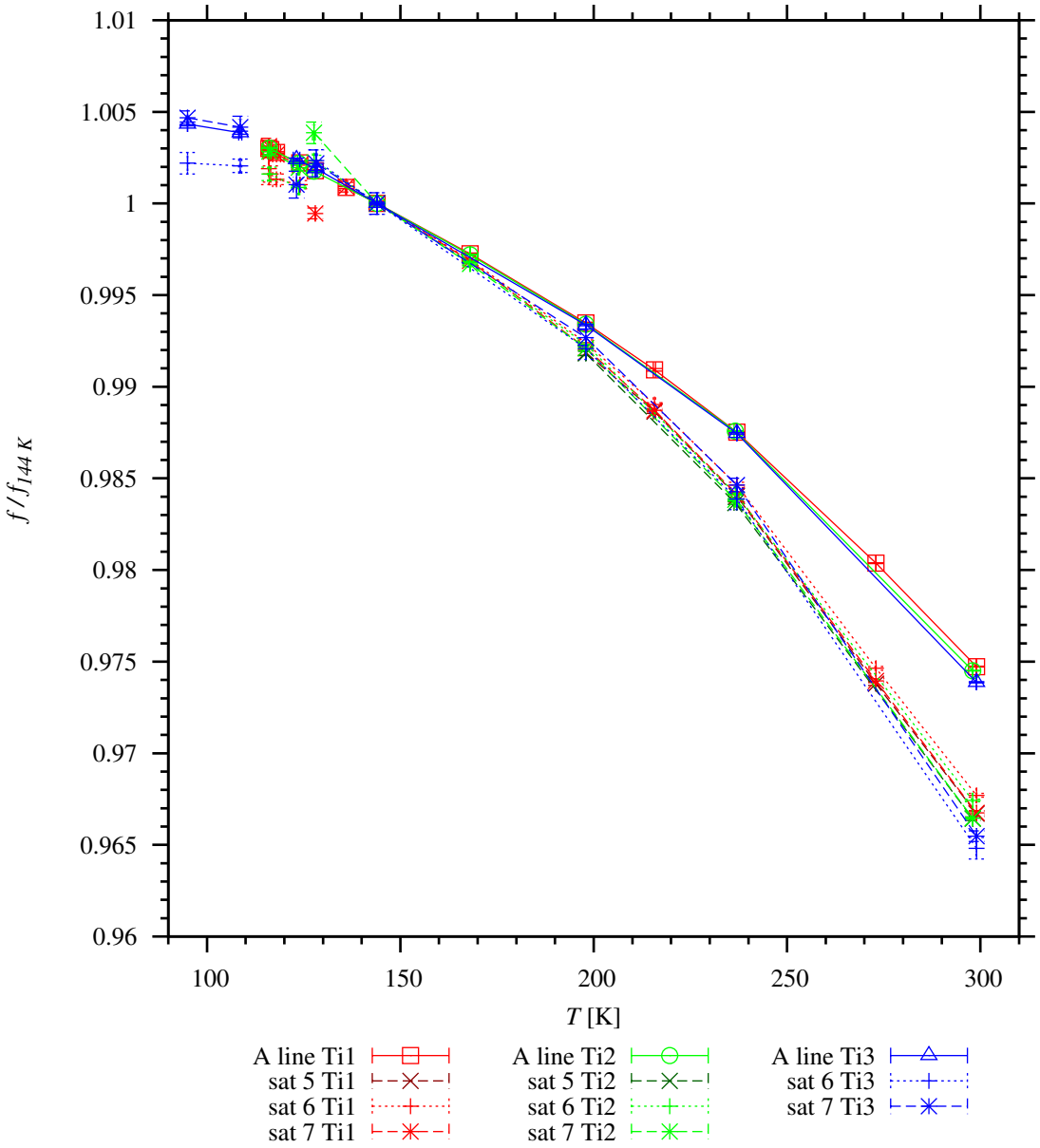

Figure 4.49: Temperature dependences of frequencies of the A line and of the satellite signals sat 5, sat 6 and sat 7 in the spectra of the titanium substituted samples normalized to their frequencies at 144 K

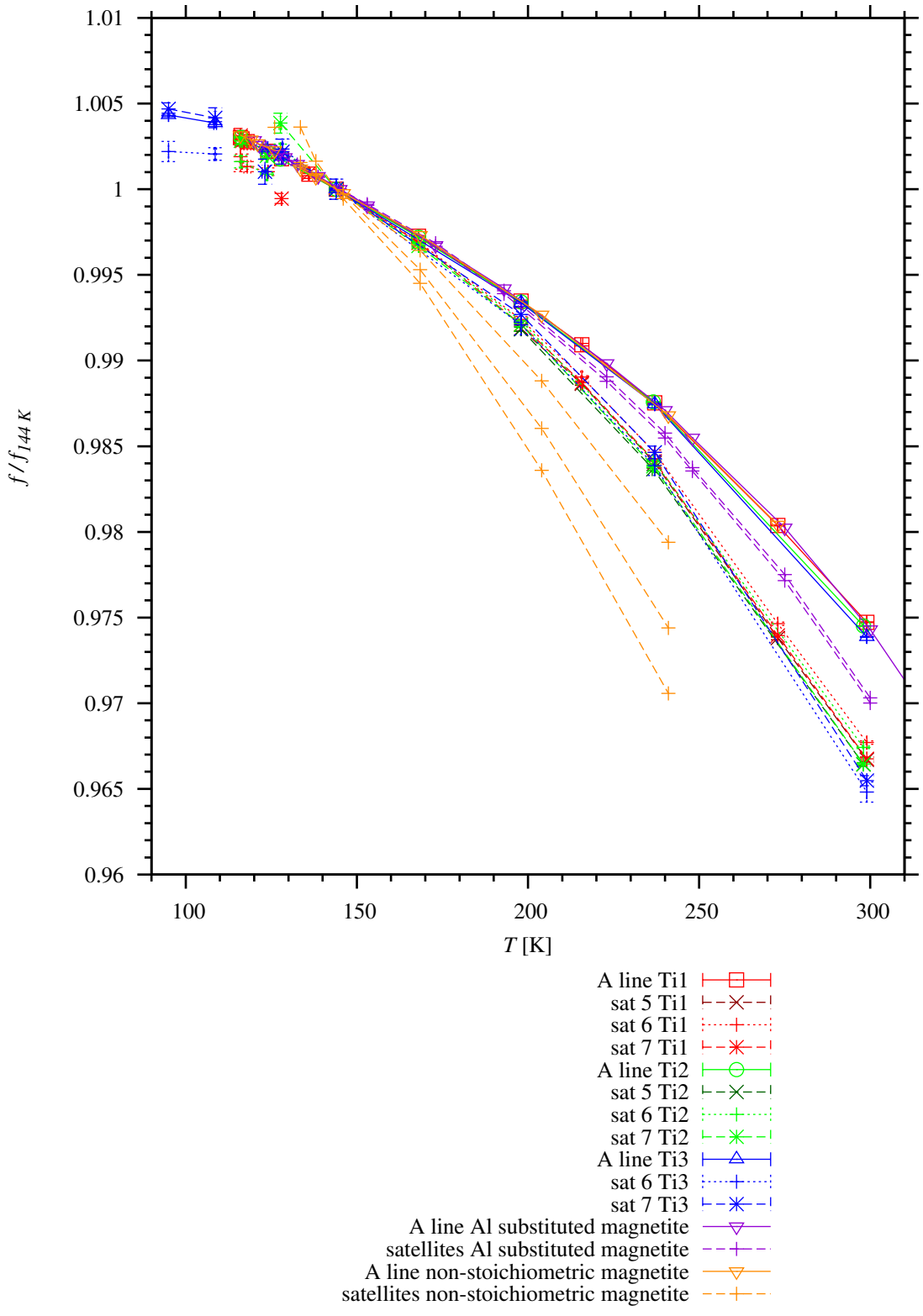

Figure 4.50: Comparison of the temperature dependences of frequencies of the A line and of the satellite signal sat1 in the spectra of the titanium substituted samples normalized to their frequencies at 144 K with the data for aluminium substituted magnetite $Fe_{2.995}Al_{0.005}O_4$ [3] and for non-stoichiometric magnetite $Fe_{3(1-0.0025)}O_4$ [22]

magnetic iron oxides, the line widths increase with increasing temperature due to the increasing fluctuations of the hyperfine magnetic field – a model case is represented by the spectral lines of YIG (see [32]). However, as shown in [23], the A line in the spectra of pure magnetite is broadened at temperatures near the spin reorientation transition and quickly decreases with the increasing temperature up to approximately 260 K and then increases at higher temperatures. The presence of the substitution or vacancies in the sample broadens the widths of the spectral lines and emphasizes the effect of the decrease in the A line width with increasing temperature. Comparison of the temperature dependences of widths of the A lines obtained from the measured temperature dependences of the spectra of the zinc and titanium samples with the data for pure magnetite [3], [23] and the magnetite samples with aluminium substitution [3] and with vacancies [22] is provided in figure 4.51. The A line width in the spectra of the sample Zn2 above the spin reorientation transition is relatively close to the width of the A line of pure magnetite. However, the line width sharply increases when the temperature decreases toward the Verwey transition, which might be explained by the increasing disorder in the electron system enhanced by the presence of the zinc substitution. All the remaining dependences presented in figure 4.51 exhibit A line widths significantly higher than those in the spectra of pure magnetite, and although the ratio of the line width near the Verwey transition and that at the ambient temperature is higher than in case of pure magnetite, the decrease of the line width with increasing temperature is considerably slower than in case of the sample Zn2. Moreover, the decay of the A line width in these cases does not seem to be tightly connected with the spin reorientation transition. A possible explanation can be found in an idea that with decreasing temperature the presence of the substitution or vacancies in the sample increasingly affects electron dynamics in the sample thus producing inhomogeneities of the electron density, resulting in a broader hyperfine field distribution.

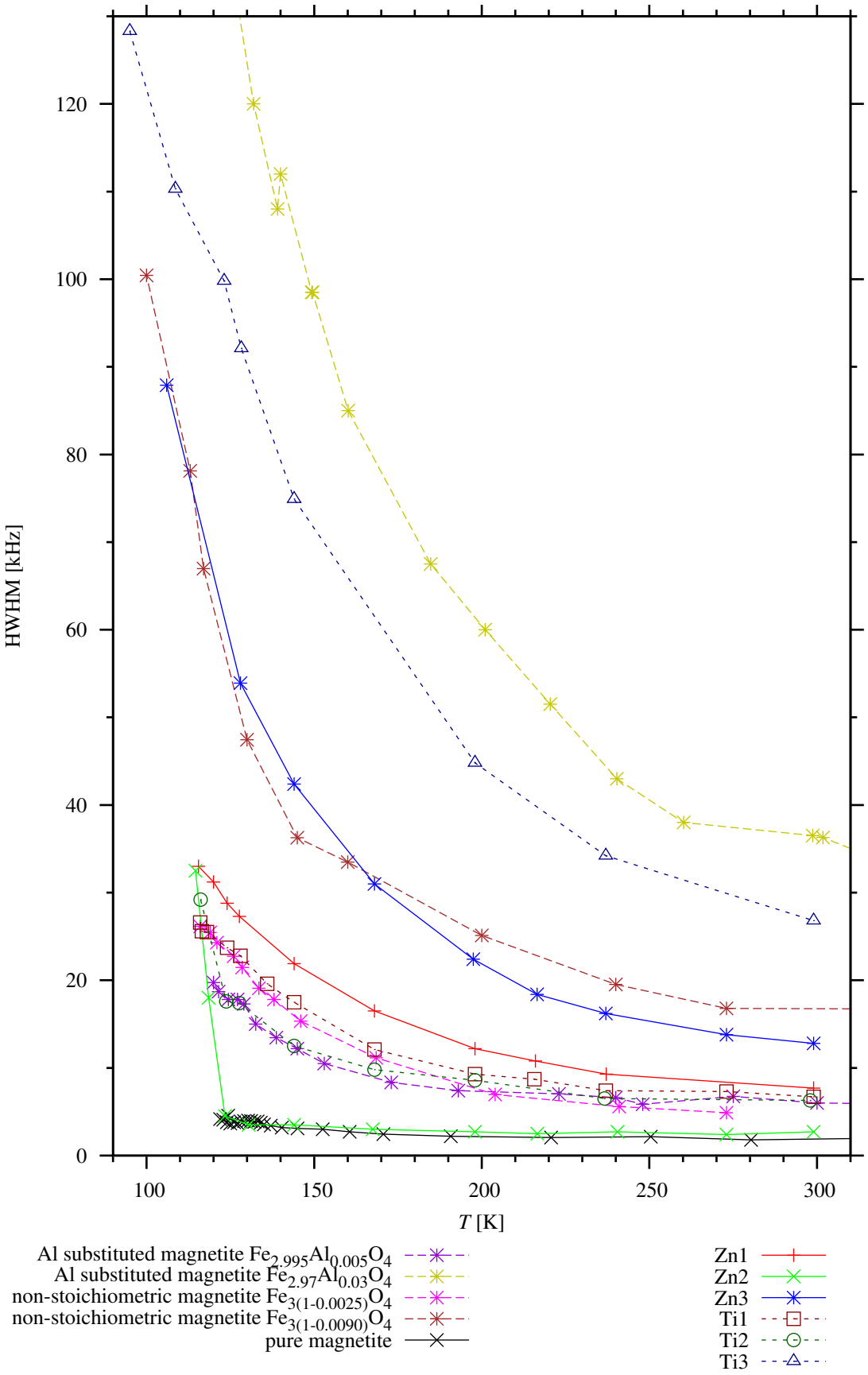

Figure 4.51: Comparison of the temperature dependences of half width at half maximum of the A lines in the spectra of aluminium substituted samples [3], non-stoichiometric magnetite [22], pure magnetite [3], [23] and the zinc and titanium substituted samples

Chapter 5

Conclusion

The subject matter of the presented work was an experimental study of zinc and titanium substituted magnetite by means of the nuclear magnetic resonance spectroscopy. The goal was to extend the knowledge about the impact of cationic substitutions on the NMR spectra by performing a series of experiments on sets of single crystal samples while focusing on the temperature dependences of the spectra above the Verwey transition. This work shows the particular suitability of the NMR method and of the zinc and titanium substitution for the investigation of electronic structure of magnetite. Moreover, the results of this study contribute to the set of information about magnetite that has been systematically collected by NMR and many other methods for a long period of time.

The temperature dependences of the spectra were measured from the temperatures near the Verwey transition up to the ambient temperature. In addition, NMR spectra were acquired also below the Verwey transition at the temperature of 4.2 K. Frequencies of the main spectral lines correspond to those in the spectra of pure magnetite. The broadening of the spectral lines due to the presence of the substitution was stated. In case of a high substitution concentration, the spectra lose resolution as the lines in the spectra merge together. The structures of satellite signals induced by the substitution presence were observed in the spectra of both the zinc and the titanium substituted samples acquired above the Verwey transition temperature.

Frequencies of both the main lines and the satellite signals in the spectra above the Verwey transition were found and their temperature dependences were constructed. Satellite lines of particular interest were identified in the spectra of both zinc and titanium substituted magnetite and the temperature dependences of their frequencies were compared to those of the satellites found in the spectra of magnetite with other substitutions and of non-stoichiometric magnetite.

Temperature dependences of the widths of the A lines in the acquired spectra above the Verwey transition were constructed. These dependences exhibit narrowing of the A lines with increasing temperature, which represents a very unusual behaviour among the magnetically ordered iron oxides. A comparison with the data for pure magnetite, aluminium substituted magnetite and non-stoichiometric magnetite was performed and the emphasizing of the effect by the presence of the substitution or vacancies was stated.

In the scope of further study, NMR experiments on the investigated samples should be performed at higher temperatures in order to track the behaviour of

both the main lines and the satellite signals, while taking special care to observe the changes of the width of the A lines and the satellite shifts with increasing temperature. Detailed information about the origin of the satellite signals in the spectra could be provided by measuring angular dependences of the spectra in an external magnetic field. This type of experiment could be also beneficial in the interpretation of the narrowing of the A lines with increasing temperature. Last but not least, employment of ab-initio calculations for further interpretation of the experimental results will be considered.

Appendix A

Temperature Dependences of NMR Spectra of Zinc Substituted Magnetite Samples

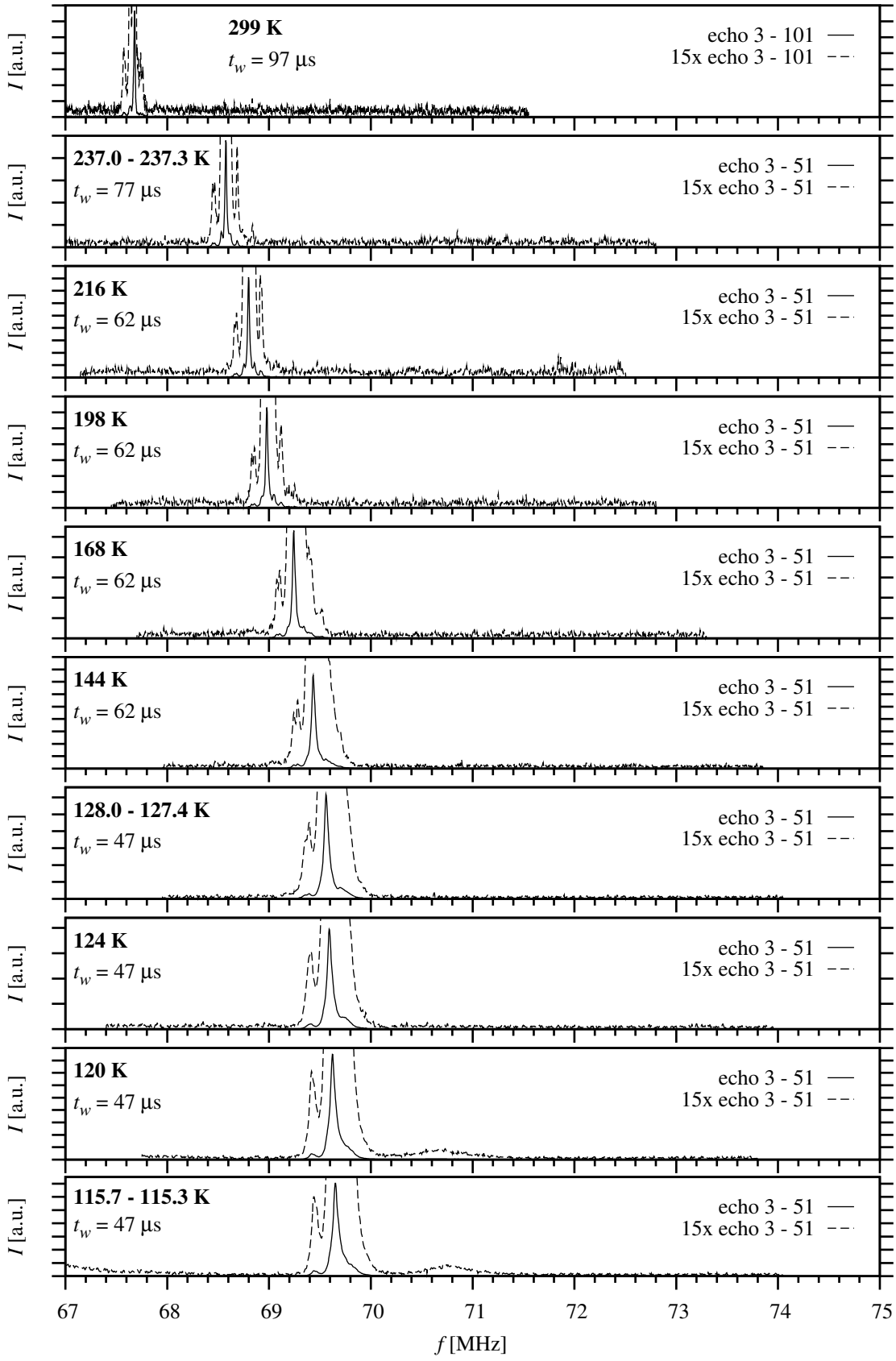

Figure A.1: Temperature dependence of NMR spectra of sample Zn1 in the range 67 – 75 MHz

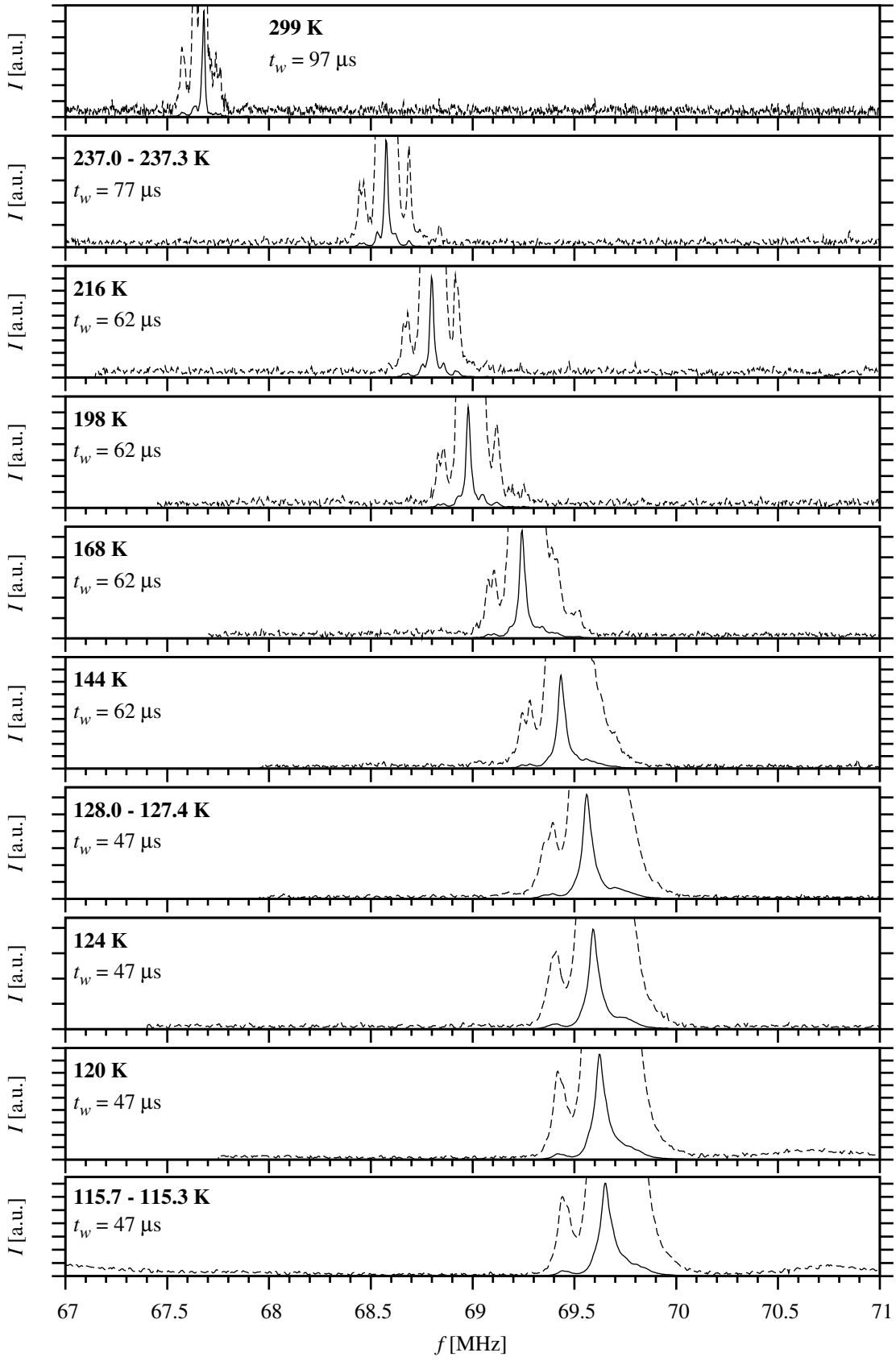

Figure A.2: Temperature dependence of NMR spectra of sample Zn1 in the range 67 – 71 MHz (detail of fig. A.1; see fig. A.1 for key)

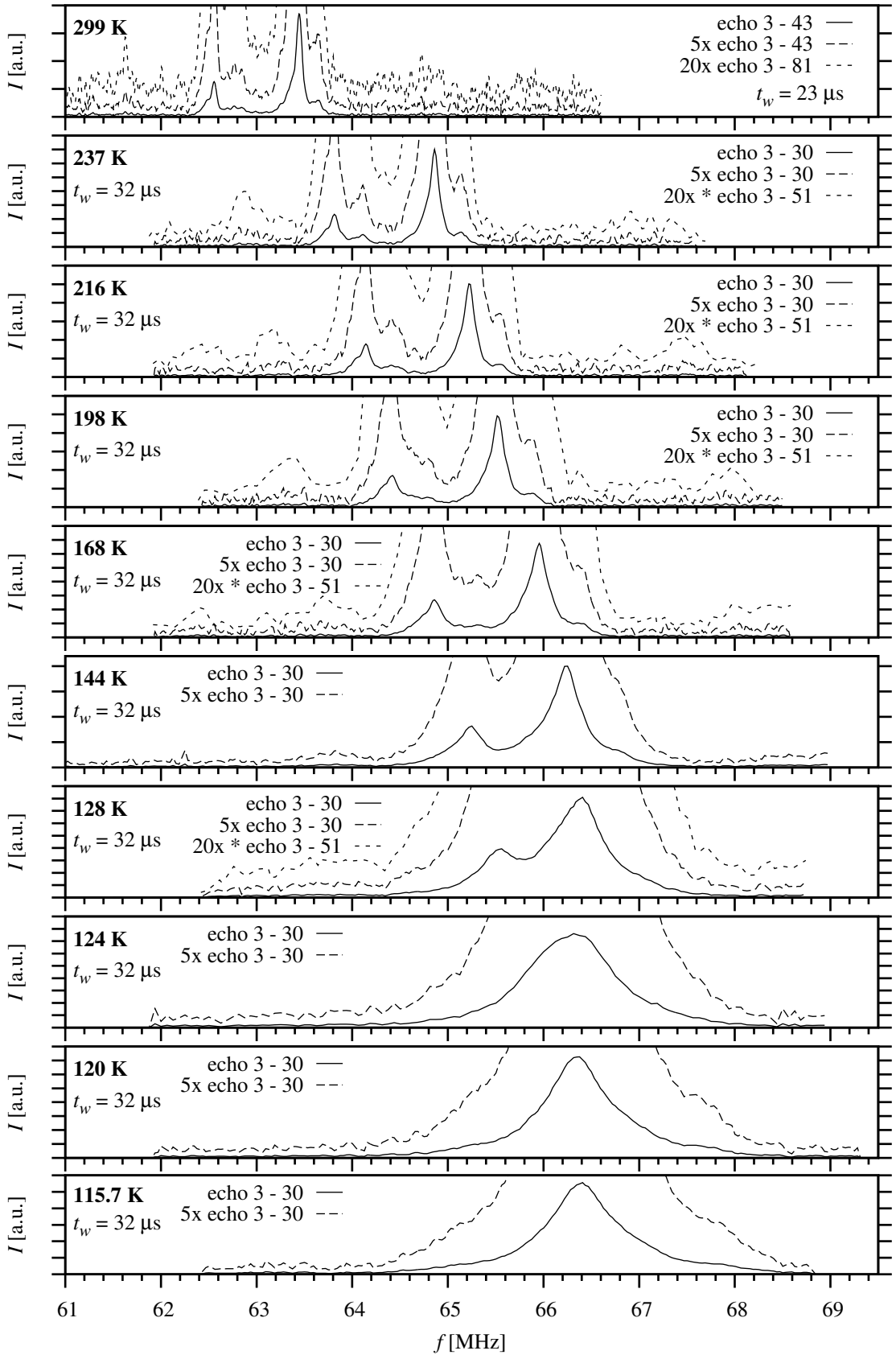

Figure A.3: Temperature dependence of NMR spectra of sample Zn1 in the range 61 – 69.5 MHz

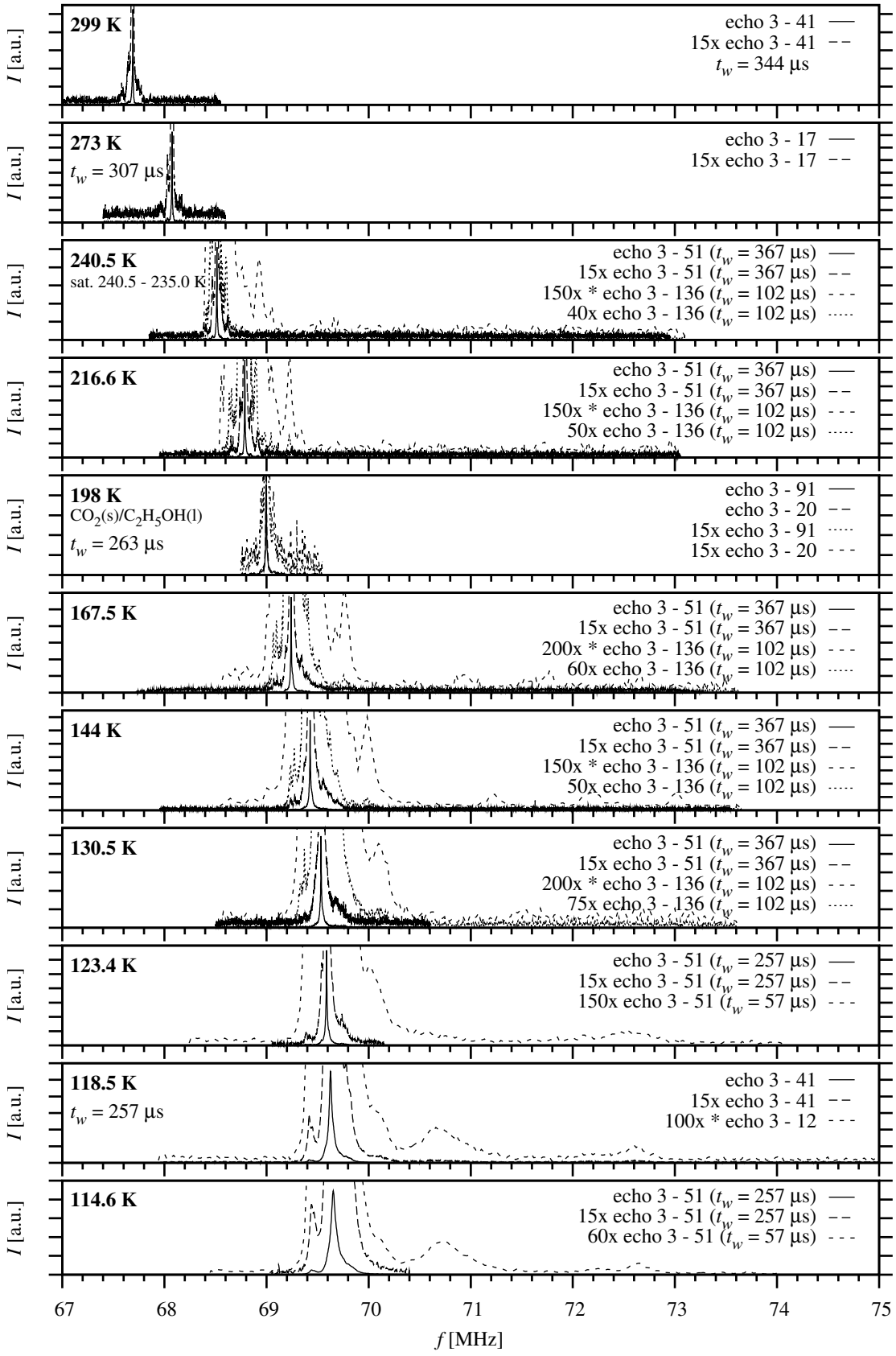

Figure A.4: Temperature dependence of NMR spectra of sample Zn2 in the range 67 – 75 MHz

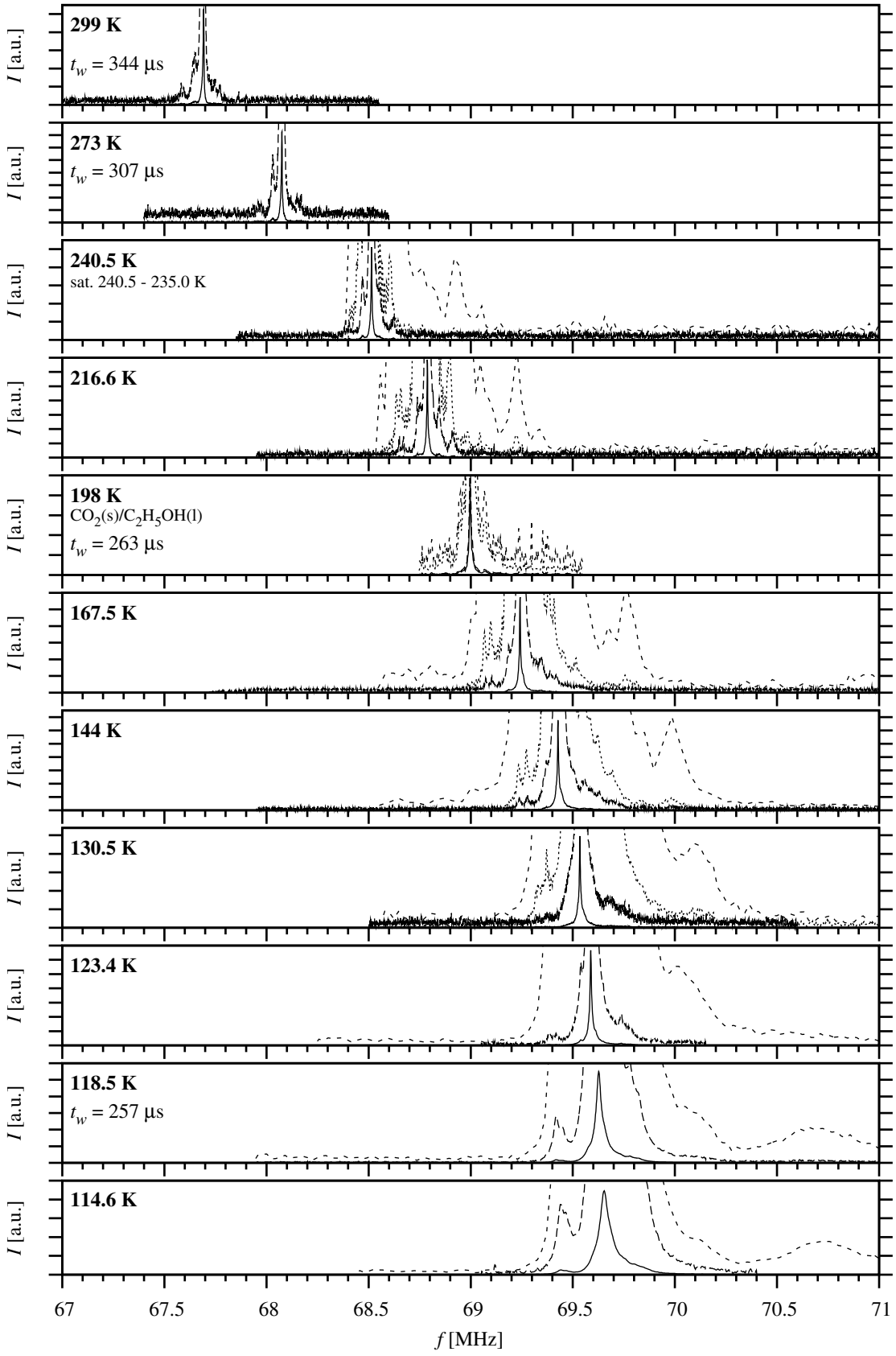

Figure A.5: Temperature dependence of NMR spectra of sample Zn2 in the range 67 – 71 MHz (detail of fig. A.4; see fig. A.4 for key)

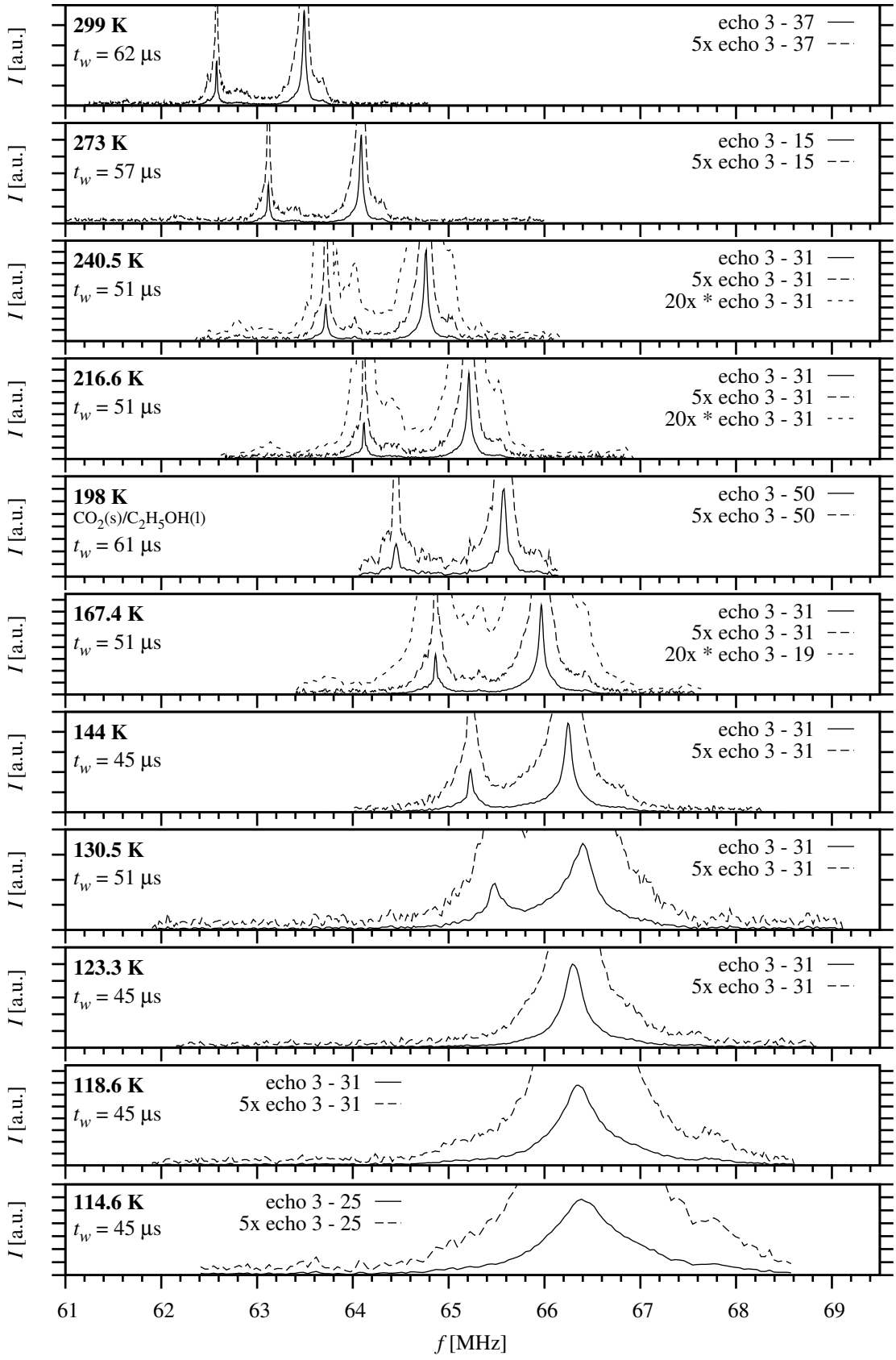

Figure A.6: Temperature dependence of NMR spectra of sample Zn2 in the range 61 – 69.5 MHz

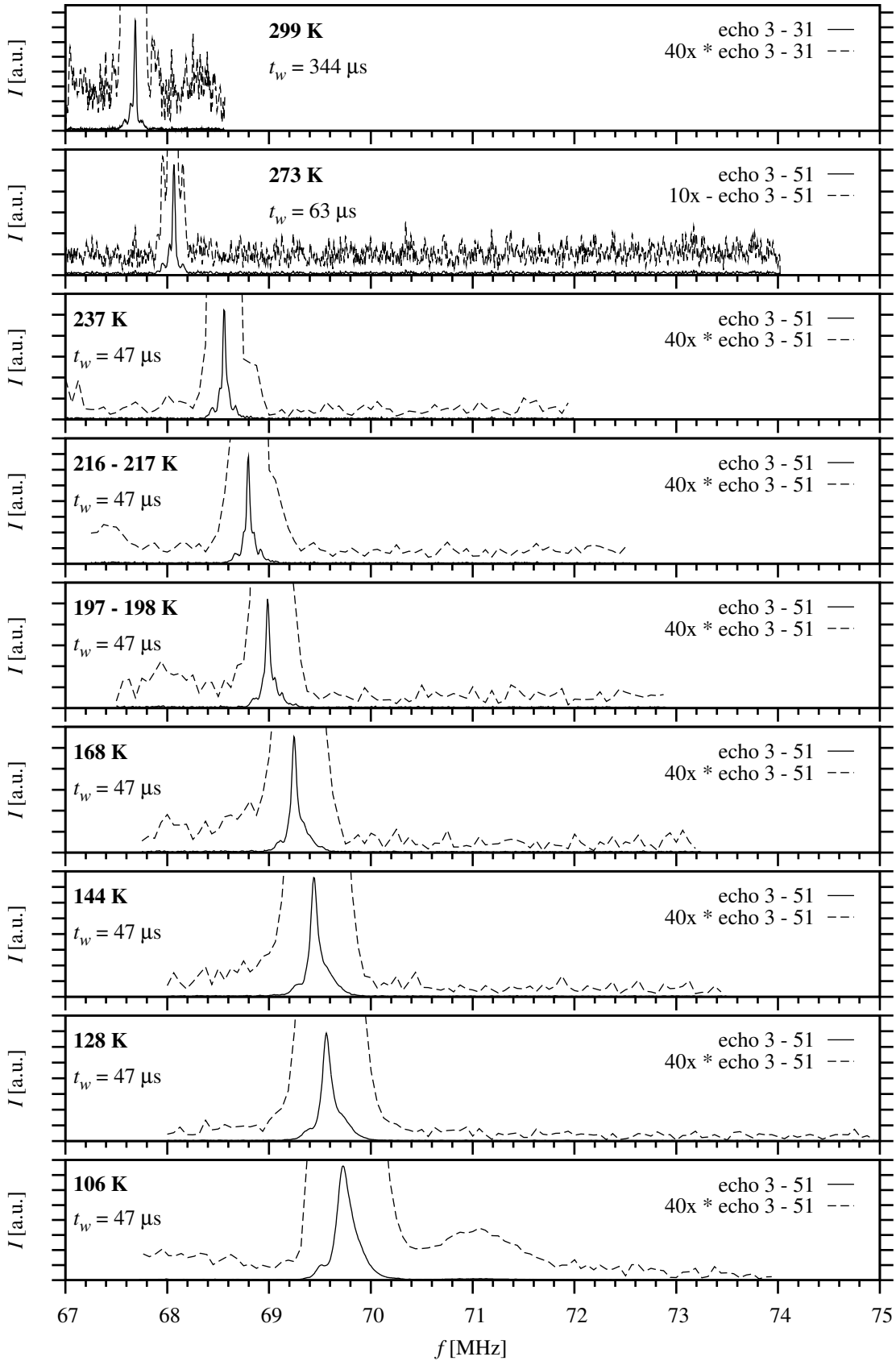

Figure A.7: Temperature dependence of NMR spectra of sample Zn3 in the range 67 – 75 MHz

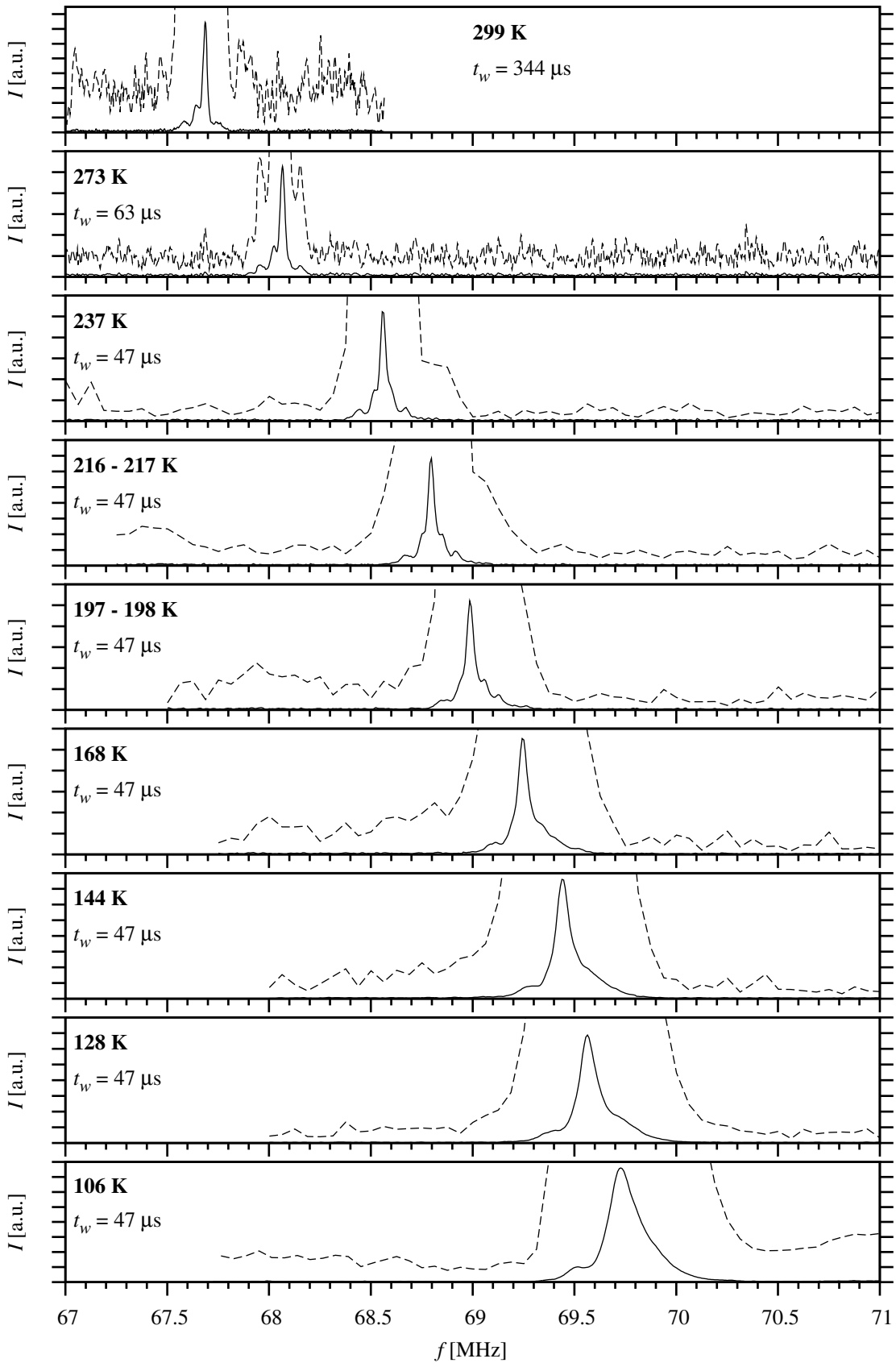

Figure A.8: Temperature dependence of NMR spectra of sample Zn3 in the range 67 – 71 MHz (detail of fig. A.7; see fig. A.7 for key)

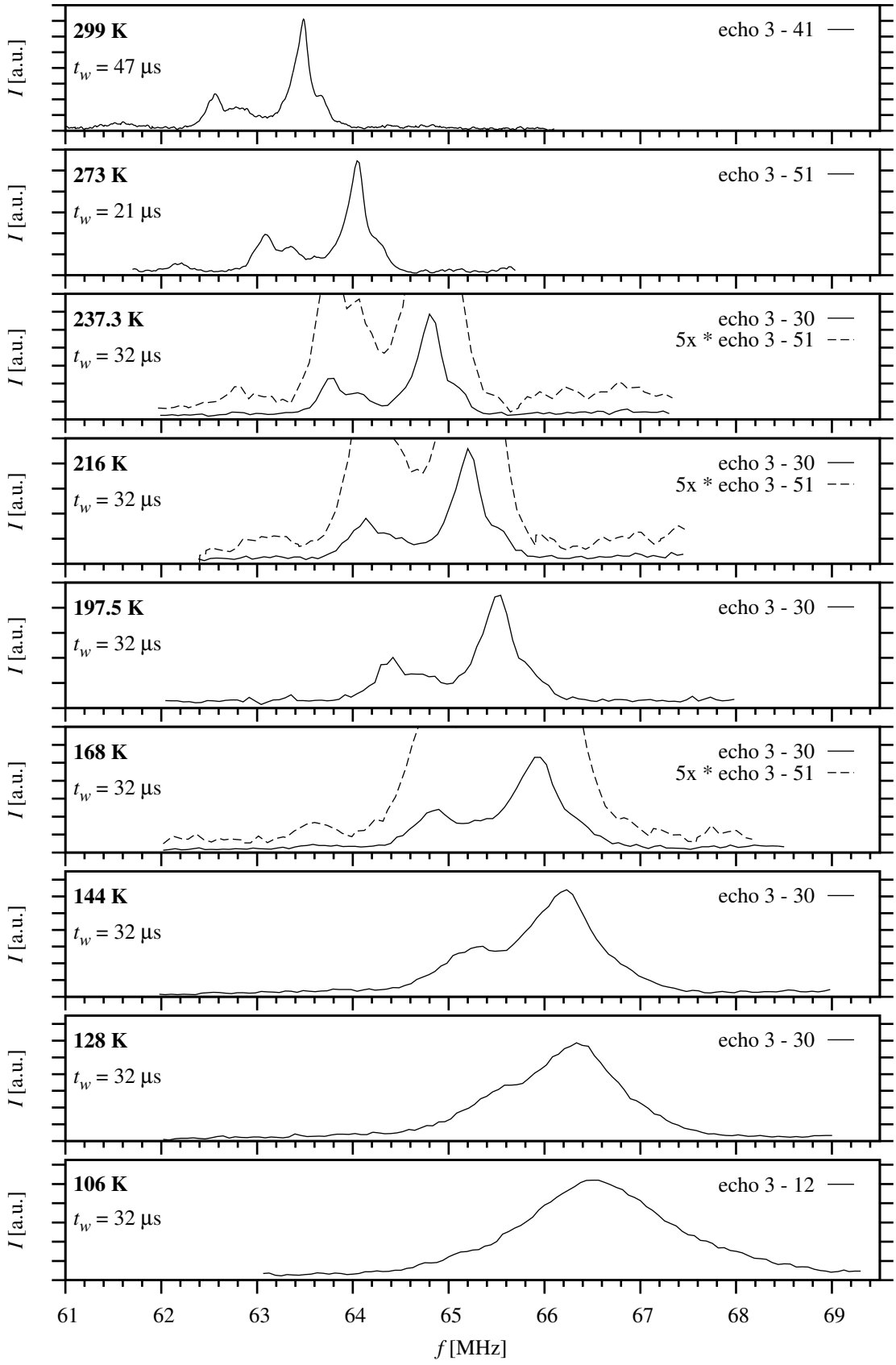

Figure A.9: Temperature dependence of NMR spectra of sample Zn3 in the range 61 – 69.5 MHz

Appendix B

Temperature Dependences of Spectral Signal Frequencies of Zinc Substituted Magnetite Samples - Tables

Table B.1: Temperature dependences of spectral signal frequencies of the sample Zn1 - part 1

Temperature	**Frequency** f [MHz]									
T [K] ± 0.5	sat 1	sat 2	**B$_1$**	sat 3	sat 4	**B**	**B$_2$**	sat 5	sat 6	sat 7
115.7						66.40 ± 0.04			67.84 ± 0.06	
120.0						66.35 ± 0.04			67.64 ± 0.10	
124.0						66.32 ± 0.10				
128.0	63.85 ± 0.35		65.540 ± 0.030				66.400 ± 0.030			
144.0	63.82 ± 0.15		65.240 ± 0.020				66.235 ± 0.015	66.770 ± 0.050		
168.0	63.68 ± 0.15		64.855 ± 0.015	65.130 ± 0.020	65.320 ± 0.030		65.955 ± 0.015	66.410 ± 0.030		68.30 ± 0.30
198.0	63.36 ± 0.08	64.320 ± 0.030	64.415 ± 0.015		64.800 ± 0.030		65.525 ± 0.010	65.880 ± 0.030		67.94 ± 0.12
216.0	63.13 ± 0.10	64.030 ± 0.025	64.142 ± 0.010	64.410 ± 0.030	64.650 ± 0.020		65.228 ± 0.010	65.540 ± 0.030		67.46 ± 0.15
237.0	62.86 ± 0.06	63.726 ± 0.020	63.814 ± 0.010	64.110 ± 0.025			64.860 ± 0.010	65.140 ± 0.025		
299.0	61.63 ± 0.04	62.485 ± 0.015	62.557 ± 0.007	62.770 ± 0.050			63.446 ± 0.005	63.644 ± 0.025		

Table B.2: Temperature dependences of spectral signal frequencies of the sample Zn1 - part 2

Temperature	**Frequency** f [MHz]							
T [K] ± 0.5	sat 8	sat 9	sat 10	**A**	sat 15	sat 16	sat 18	sat 20
115.5	69.440 ± 0.005	69.468 ± 0.007		69.652 ± 0.003	69.806 ± 0.005	69.844 ± 0.005		70.760 ± 0.060
120.0	69.417 ± 0.005	69.444 ± 0.005		69.623 ± 0.003	69.773 ± 0.005	69.814 ± 0.005		70.650 ± 0.090
124.0	69.390 ± 0.005	69.413 ± 0.005		69.593 ± 0.003	69.735 ± 0.010			
127.7	69.355 ± 0.007	69.395 ± 0.005		69.561 ± 0.002	69.699 ± 0.006			
144.0	69.244 ± 0.005	69.281 ± 0.003		69.433 ± 0.002	69.558 ± 0.005			
168.0	69.077 ± 0.004	69.105 ± 0.003	69.183 ± 0.004	69.242 ± 0.003	69.330 ± 0.015	69.403 ± 0.015	69.524 ± 0.010	
198.0	68.830 ± 0.003	68.857 ± 0.003	68.933 ± 0.003	68.978 ± 0.003	69.048 ± 0.005	69.119 ± 0.005	69.250 ± 0.010	
216.0	68.661 ± 0.003	68.681 ± 0.003	68.755 ± 0.004	68.800 ± 0.003	68.857 ± 0.004	68.920 ± 0.010		
237.2	68.445 ± 0.003	68.465 ± 0.003	68.531 ± 0.004	68.576 ± 0.002	68.620 ± 0.005	68.688 ± 0.005	68.838 ± 0.006	
299.0	67.572 ± 0.003	67.588 ± 0.003	67.636 ± 0.007	67.680 ± 0.002	67.739 ± 0.005	67.761 ± 0.004	67.890 ± 0.010	

Table B.3: Temperature dependences of spectral signal frequencies of the sample Zn2 - part 1

Temperature	**Frequency** f [MHz]								
T [K] ± 0.5	sat 1	sat 2	**B**$_1$	sat 3	sat 4	**B**	**B**$_2$	sat 5	sat 6
114.6						66.390 ± 0.050			67.78 ± 0.10
118.6						66.354 ± 0.030			67.70 ± 0.10
123.3						66.300 ± 0.020			67.58 ± 0.10
130.5			65.472 ± 0.015				66.405 ± 0.015		
144.0			65.227 ± 0.010				66.248 ± 0.010	66.800 ± 0.050	
167.4	63.75 ± 0.10		64.863 ± 0.006		65.315 ± 0.015		65.967 ± 0.006	66.425 ± 0.040	
198.0		64.340 ± 0.050	64.451 ± 0.010				65.571 ± 0.008	65.920 ± 0.050	
216.6	63.14 ± 0.08		64.115 ± 0.005	64.430 ± 0.050			65.211 ± 0.005	65.530 ± 0.040	
240.5	62.80 ± 0.05	63.606 ± 0.015	63.717 ± 0.006	64.019 ± 0.015			64.762 ± 0.006	65.025 ± 0.030	
273.0	62.17 ± 0.06	63.020 ± 0.010	63.118 ± 0.006	63.390 ± 0.050			64.086 ± 0.005	64.306 ± 0.020	
299.0	61.64 ± 0.04	62.483 ± 0.008	62.578 ± 0.004	62.805 ± 0.050			63.492 ± 0.004	63.685 ± 0.010	

Table B.4: Temperature dependences of spectral signal frequencies of the sample Zn2 - part 2 (satellites marked by an asterisk ("*") arise from the presence of vacancies – see the text)

Temperature	**Frequency** f [MHz]									
T [K] ± 0.5	sat 8	sat 9	sat 10	sat 11	**A**	sat 12	sat 13	sat 14	sat 15	sat 16
114.6	69.440 ± 0.005	69.465 ± 0.005			69.654 ± 0.004				69.800 ± 0.005	
118.5	69.418 ± 0.003	69.448 ± 0.004			69.627 ± 0.002				69.780 ± 0.005	
123.4	69.387 ± 0.003	69.418 ± 0.003	69.538 ± 0.003		69.588 ± 0.002	69.613 ± 0.003	69.649 ± 0.002		69.737 ± 0.003	
130.5	69.335 ± 0.007	69.372 ± 0.007		69.525 ± 0.003	69.534 ± 0.001	69.552 ± 0.003		69.563 ± 0.002	69.675 ± 0.015	
144.0	69.237 ± 0.003	69.277 ± 0.003	69.370 ± 0.002	69.418 ± 0.002	69.4273 ± 0.0010	69.441 ± 0.002	69.483 ± 0.002	69.507 ± 0.003	69.556 ± 0.010	69.590 ± 0.005
167.5	69.073 ± 0.003	69.104 ± 0.003	69.186 ± 0.002		69.2415 ± 0.0010	69.257 ± 0.002	69.286 ± 0.002		69.345 ± 0.005	69.389 ± 0.005
198.0		68.878 ± 0.005	68.946 ± 0.005	68.969 ± 0.003	68.997 ± 0.003	69.008 ± 0.004	69.028 ± 0.004		69.068 ± 0.007	
216.6	68.650 ± 0.003	68.671 ± 0.003	68.739 ± 0.002		68.7876 ± 0.0010				68.846 ± 0.003	68.912 ± 0.005
240.5	68.386 ± 0.003	68.406 ± 0.002	68.470 ± 0.003		68.5147 ± 0.0005				68.554 ± 0.003	68.623 ± 0.005
273.0		67.964 ± 0.005	68.032 ± 0.001		68.0753 ± 0.0003					68.160 ± 0.010
299.0	67.582 ± 0.002	67.594 ± 0.003	67.640 ± 0.002	67.650 ± 0.003	67.6919 ± 0.0003				67.745 ± 0.005	67.772 ± 0.005
Temperature	**Frequency** f [MHz]									
T [K] ± 0.5	sat 17	sat 18	sat 19 *	sat 20	sat 21 *	sat 22 *	sat 23 *	sat 24 *	sat 25 *	
114.6				70.720 ± 0.050	72.220 ± 0.050	72.630 ± 0.050				
118.5	69.820 ± 0.010		70.110 ± 0.060	70.680 ± 0.060	72.160 ± 0.100	72.620 ± 0.040				
123.4	69.786 ± 0.010					72.560 ± 0.030				
130.5			70.110 ± 0.040							
144.0	69.630 ± 0.006	69.693 ± 0.010	69.990 ± 0.025				71.220 ± 0.030	72.170 ± 0.080	73.010 ± 0.040	
167.5	69.417 ± 0.005		69.770 ± 0.030				70.940 ± 0.040	71.780 ± 0.030	72.660 ± 0.030	
198.0										
216.6	68.985 ± 0.007	69.045 ± 0.005	69.225 ± 0.015							
240.5	68.704 ± 0.010	68.762 ± 0.005	68.920 ± 0.010							
273.0										
299.0										

Table B.5: Temperature dependences of spectral signal frequencies of the sample Zn3 - part 1

Temperature	**Frequency** f [MHz]						
T [K] ± 0.5	sat 1	**B**$_1$	sat 3	sat 4	**B**	**B**$_2$	sat 5
106.0					66.503 ± 0.075		
128.0		65.600 ± 0.075				66.340 ± 0.075	
144.0		65.320 ± 0.060				66.230 ± 0.050	
168.0	63.56 ± 0.10	64.860 ± 0.050				65.928 ± 0.040	
197.5		64.400 ± 0.060	64.720 ± 0.060			65.510 ± 0.040	
216.0	63.10 ± 0.20	64.136 ± 0.040	64.420 ± 0.075			65.200 ± 0.040	65.570 ± 0.050
237.3	62.80 ± 0.06	63.770 ± 0.040	64.070 ± 0.060			64.820 ± 0.040	65.100 ± 0.050
273.0	62.18 ± 0.06	63.090 ± 0.020	63.350 ± 0.040	63.600 ± 0.050		64.050 ± 0.020	64.280 ± 0.040
299.0	61.58 ± 0.10	62.564 ± 0.015	62.840 ± 0.060			63.485 ± 0.010	63.670 ± 0.025

Table B.6: Temperature dependences of spectral signal frequencies of the sample Zn3 - part 2

Temperature	**Frequency** f [MHz]							
T [K] ± 0.5	sat 7	sat 9	sat 10	**A**	sat 15	sat 16	sat 18	sat 20
106.0		69.515 ± 0.010		69.728 ± 0.003				71.06 ± 0.10
128.0		69.370 ± 0.020		69.564 ± 0.004	69.717 ± 0.050			
144.0		69.260 ± 0.030		69.442 ± 0.004	69.570 ± 0.030			
168.0		69.110 ± 0.010		69.247 ± 0.004	69.344 ± 0.020		69.520 ± 0.020	
197.5	67.94 ± 0.15	68.858 ± 0.020	68.937 ± 0.010	68.988 ± 0.005	69.060 ± 0.007	69.128 ± 0.007	69.263 ± 0.007	
216.5	67.43 ± 0.08	68.666 ± 0.010	68.752 ± 0.007	68.796 ± 0.005	68.853 ± 0.007	68.916 ± 0.007	69.080 ± 0.015	
237.0		68.445 ± 0.007	68.517 ± 0.007	68.560 ± 0.004	68.602 ± 0.007	68.672 ± 0.007		
273.0		67.954 ± 0.008	68.024 ± 0.004	68.066 ± 0.002		68.154 ± 0.006		
299.0		67.583 ± 0.005	67.641 ± 0.004	67.687 ± 0.002	67.750 ± 0.015			

Appendix C

Temperature Dependences of HWHM of the A Lines of Zinc Substituted Magnetite Samples - Tables

Table C.1: Temperature dependence of half width at half maximum of the A line of the sample Zn1

Temperature T [K] ±0.5	**A HWHM** [kHz] ±0.20
115.5	32.95
120.0	31.15
124.0	28.80
127.7	27.30
144.0	21.90
168.0	16.50
198.0	12.20
216.0	10.80
237.2	9.25
299.0	7.70

Table C.2: Temperature dependence of half width at half maximum of the A line of the sample Zn2

Temperature T [K] ±0.5	**A HWHM** [kHz] ±0.20
114.6	32.50
118.5	18.00
123.4	4.50
130.5	3.50
144.0	3.50
167.5	2.95
198.0	2.65
216.6	2.50
240.5	2.65
273.0	2.40
299.0	2.65

Table C.3: Temperature dependence of half width at half maximum of the A line of the sample Zn3

Temperature T [K] ±0.5	**A HWHM** [kHz] ±0.20
106.0	87.90
128.0	53.85
144.0	42.35
168.0	30.95
197.5	22.35
216.5	18.35
237.0	16.15
273.0	13.80
299.0	12.75

Appendix D

Temperature Dependences of NMR Spectra of Titanium Substituted Magnetite Samples

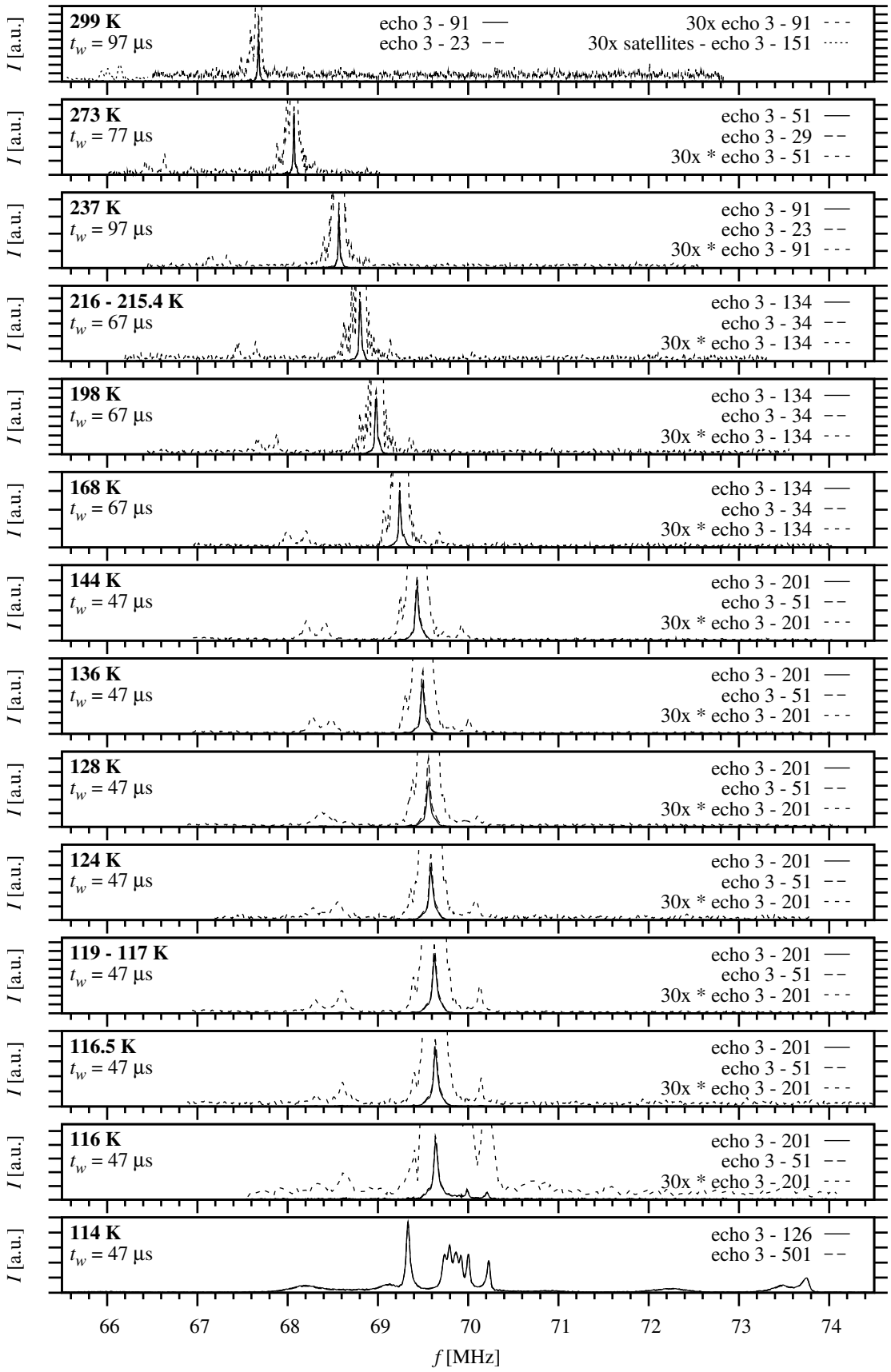

Figure D.1: Temperature dependence of NMR spectra of sample Ti1 in the range 65.5 – 74.5 MHz

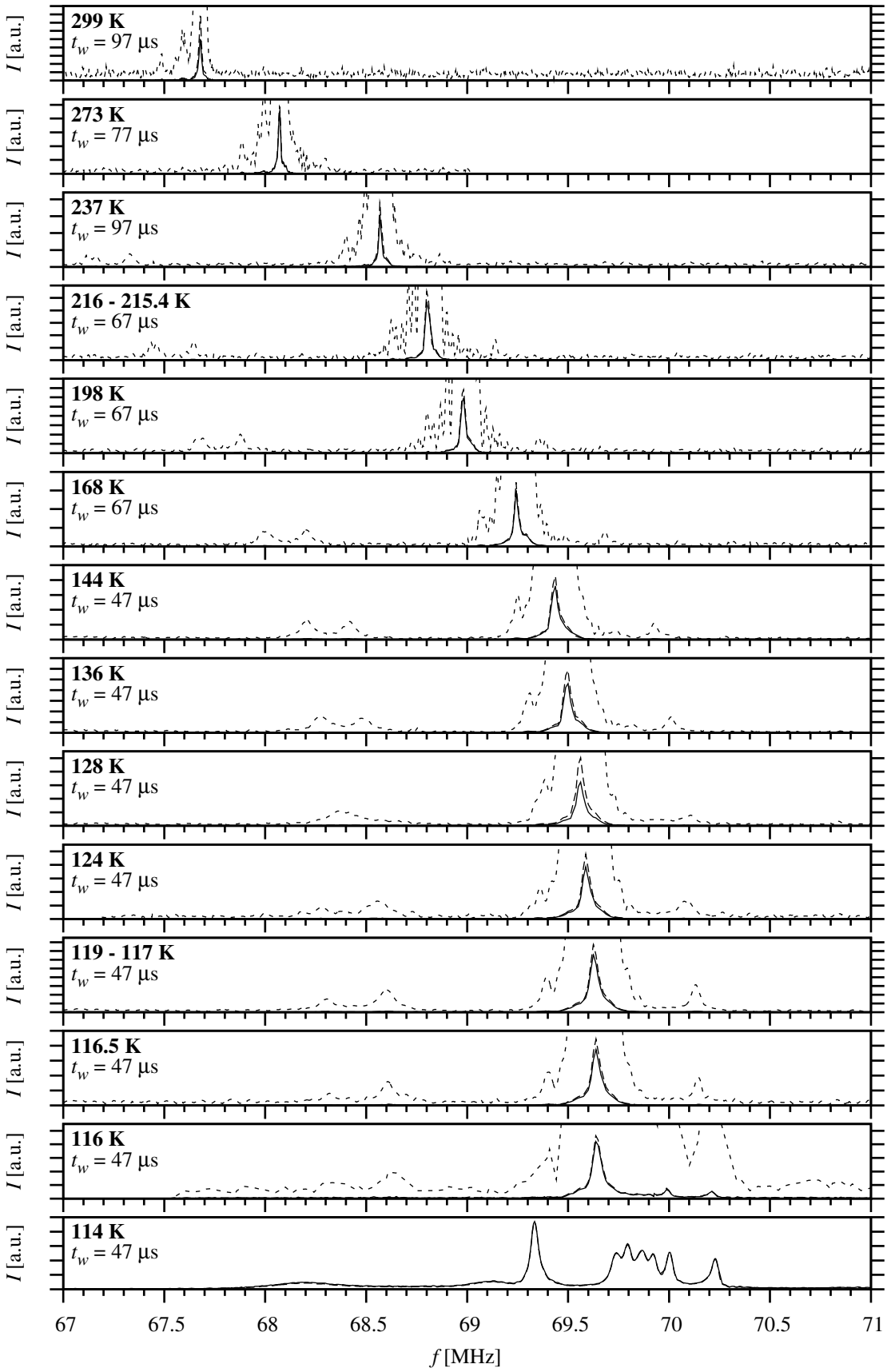

Figure D.2: Temperature dependence of NMR spectra of sample Ti1 in the range 67 – 71 MHz (detail of fig. D.1; see fig. D.1 for key)

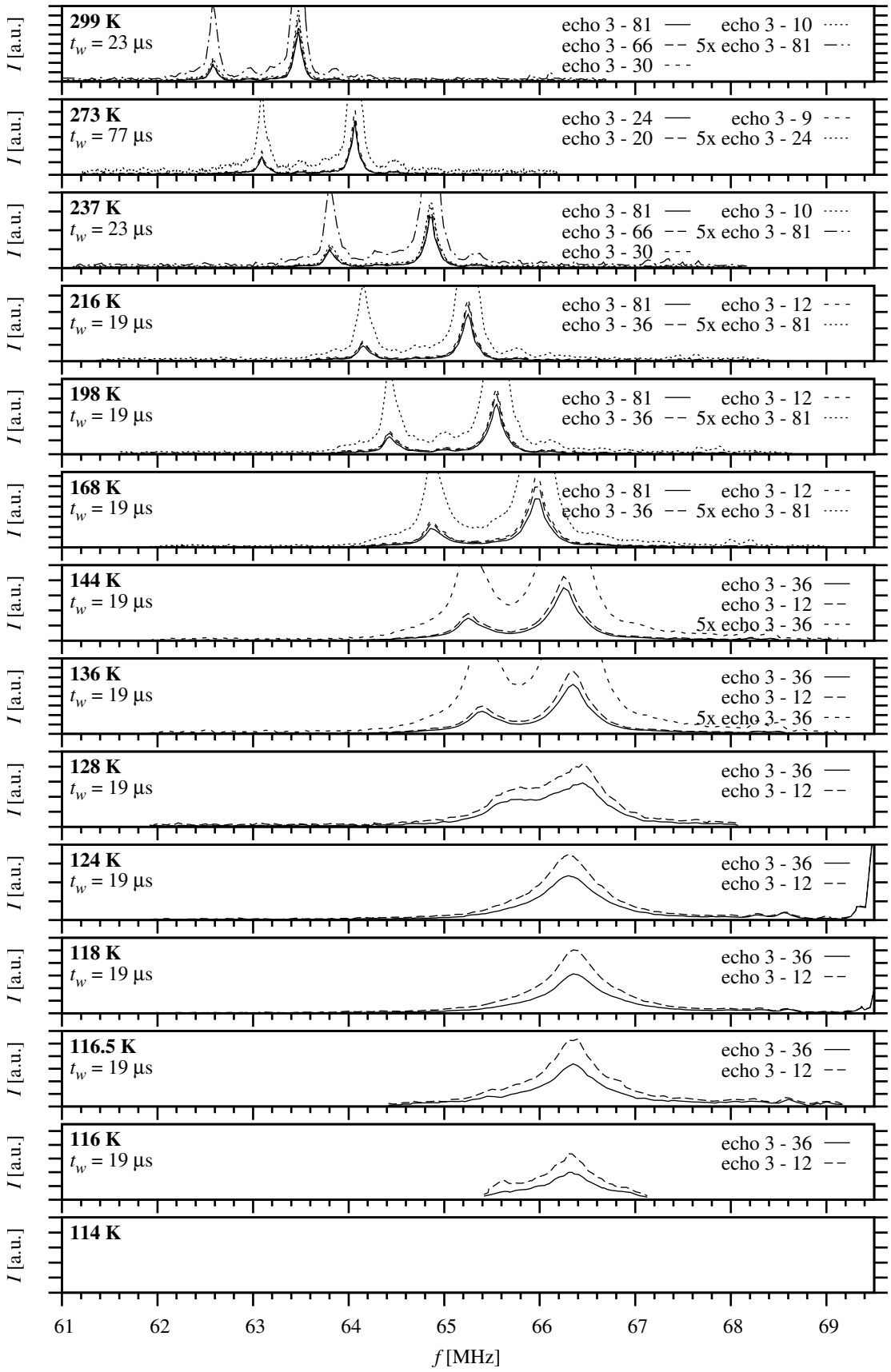

Figure D.3: Temperature dependence of NMR spectra of sample Ti1 in the range 61 – 69.5 MHz

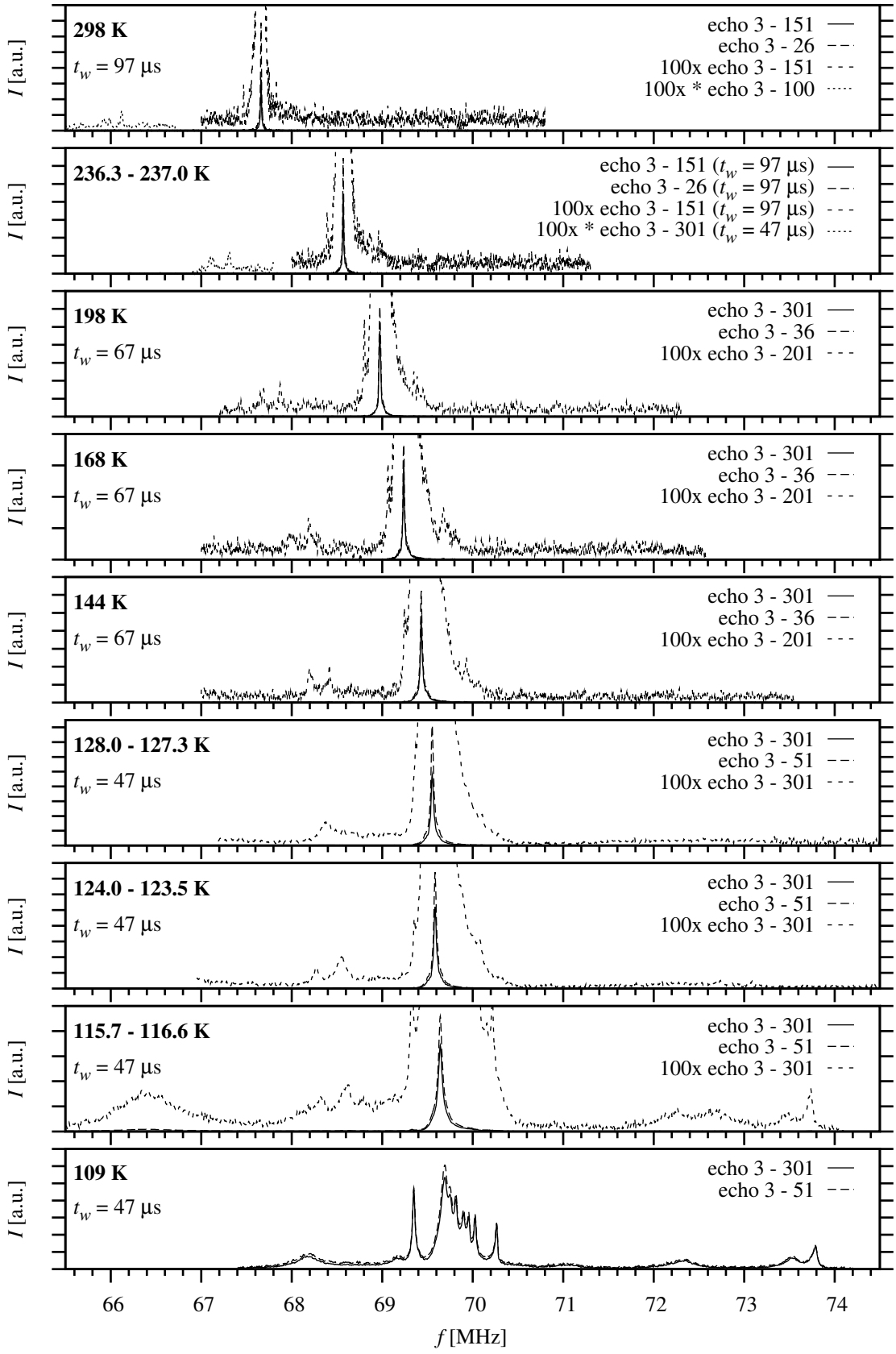

Figure D.4: Temperature dependence of NMR spectra of sample Ti2 in the range 65.5 – 74.5 MHz

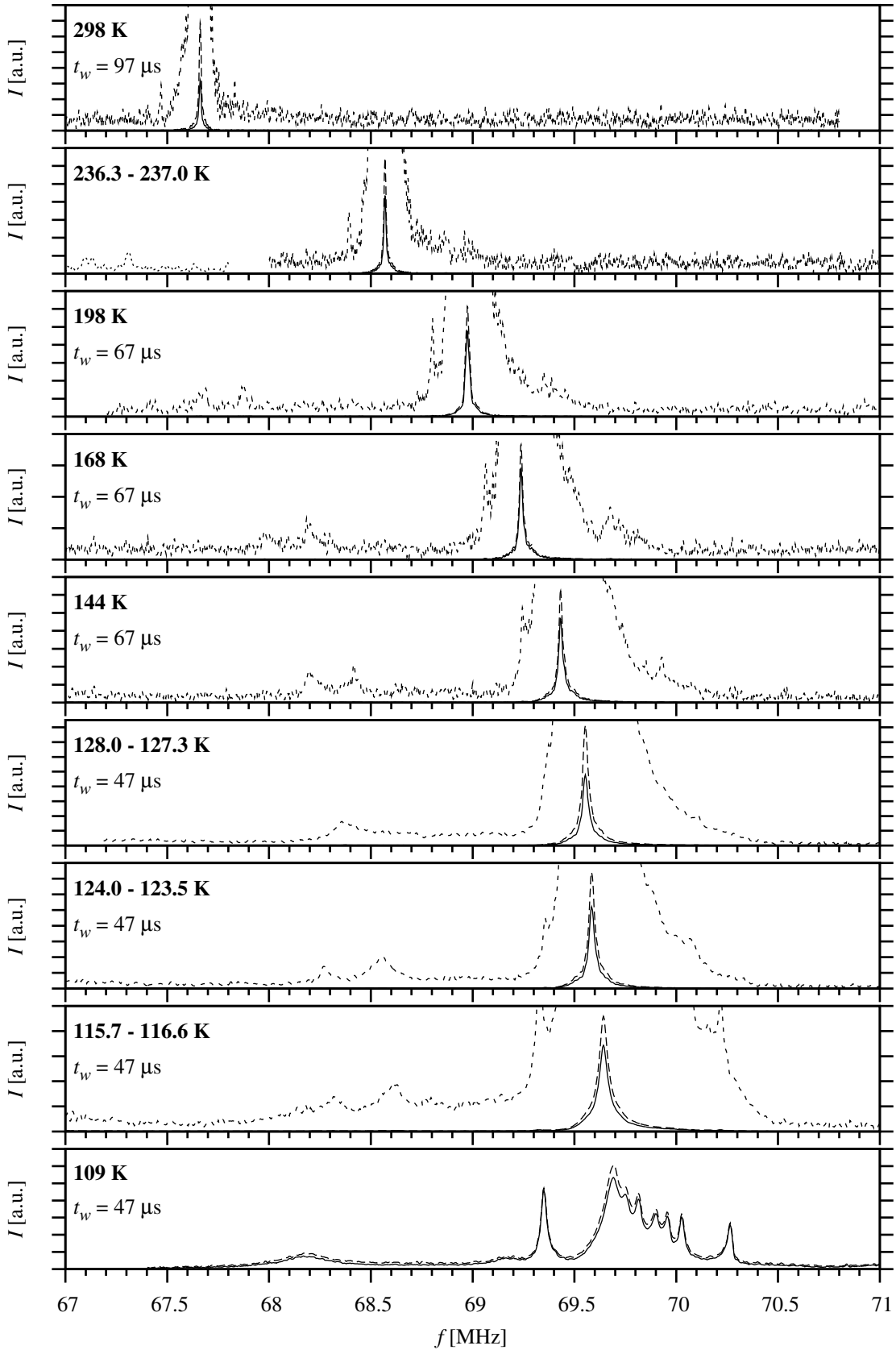

Figure D.5: Temperature dependence of NMR spectra of sample Ti2 in the range 67 – 71 MHz (detail of fig. D.4; see fig. D.4 for key)

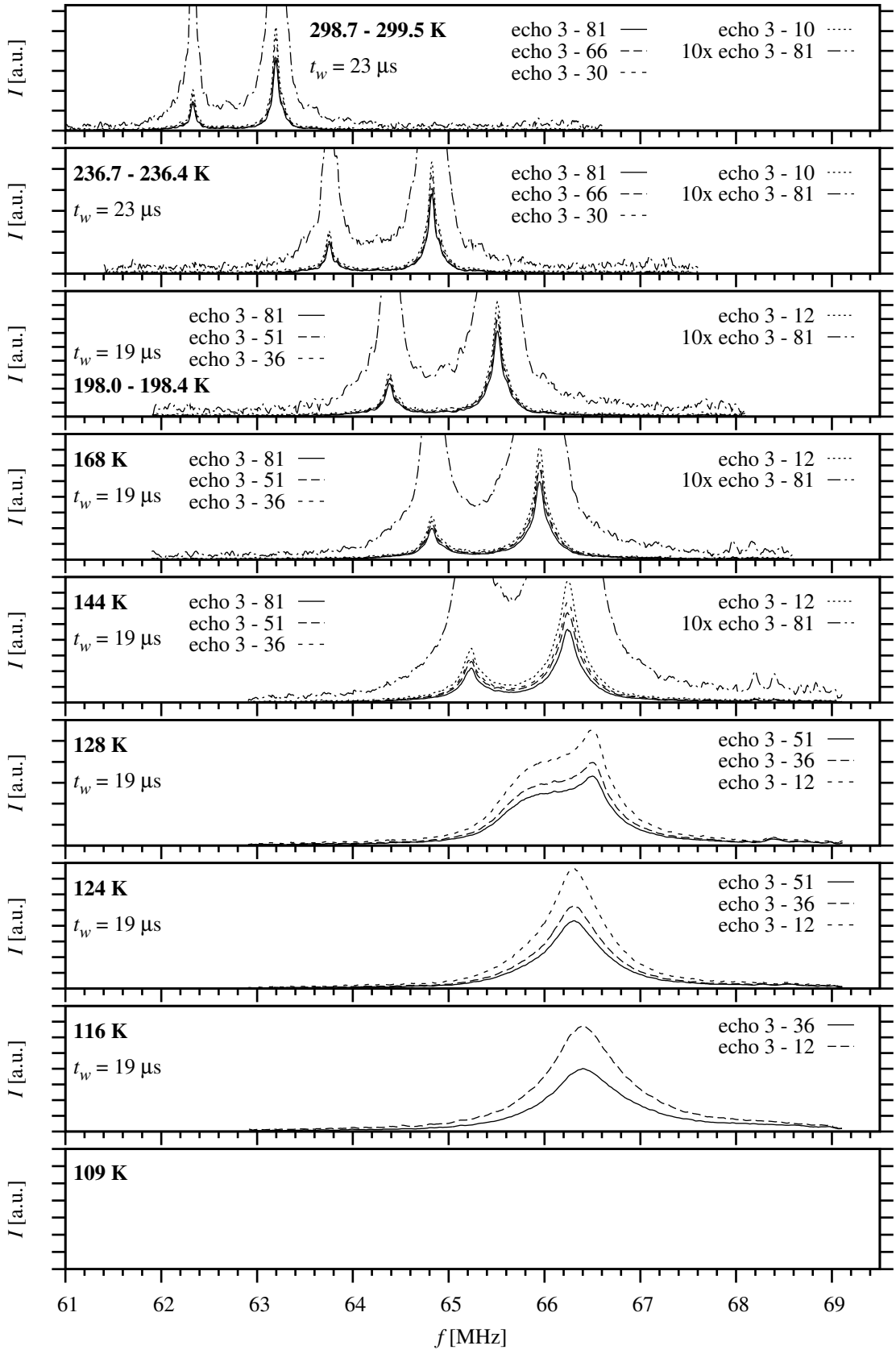

Figure D.6: Temperature dependence of NMR spectra of sample Ti2 in the range 61 – 69.5 MHz

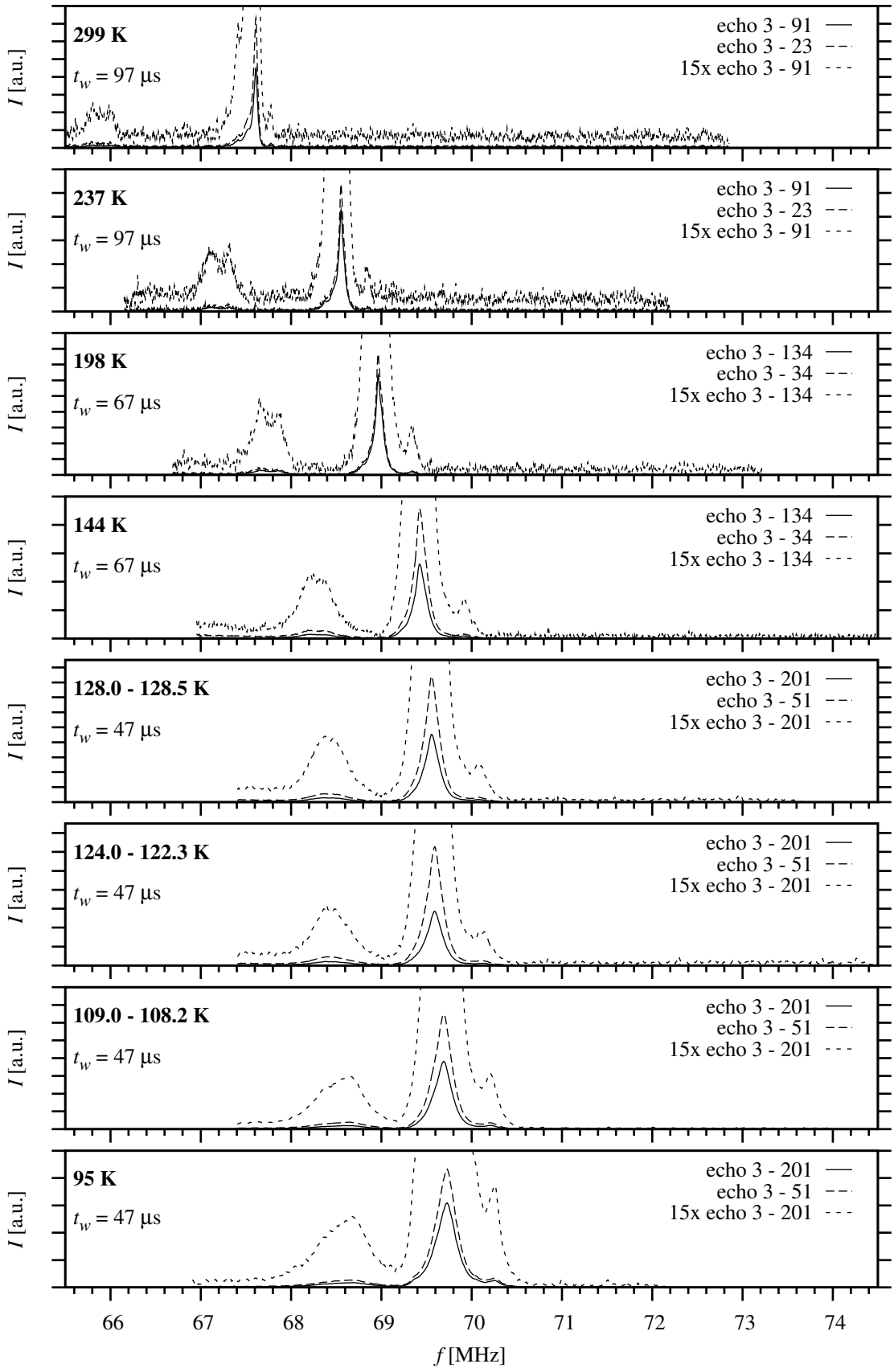

Figure D.7: Temperature dependence of NMR spectra of sample Ti3 in the range 65.5 – 74.5 MHz

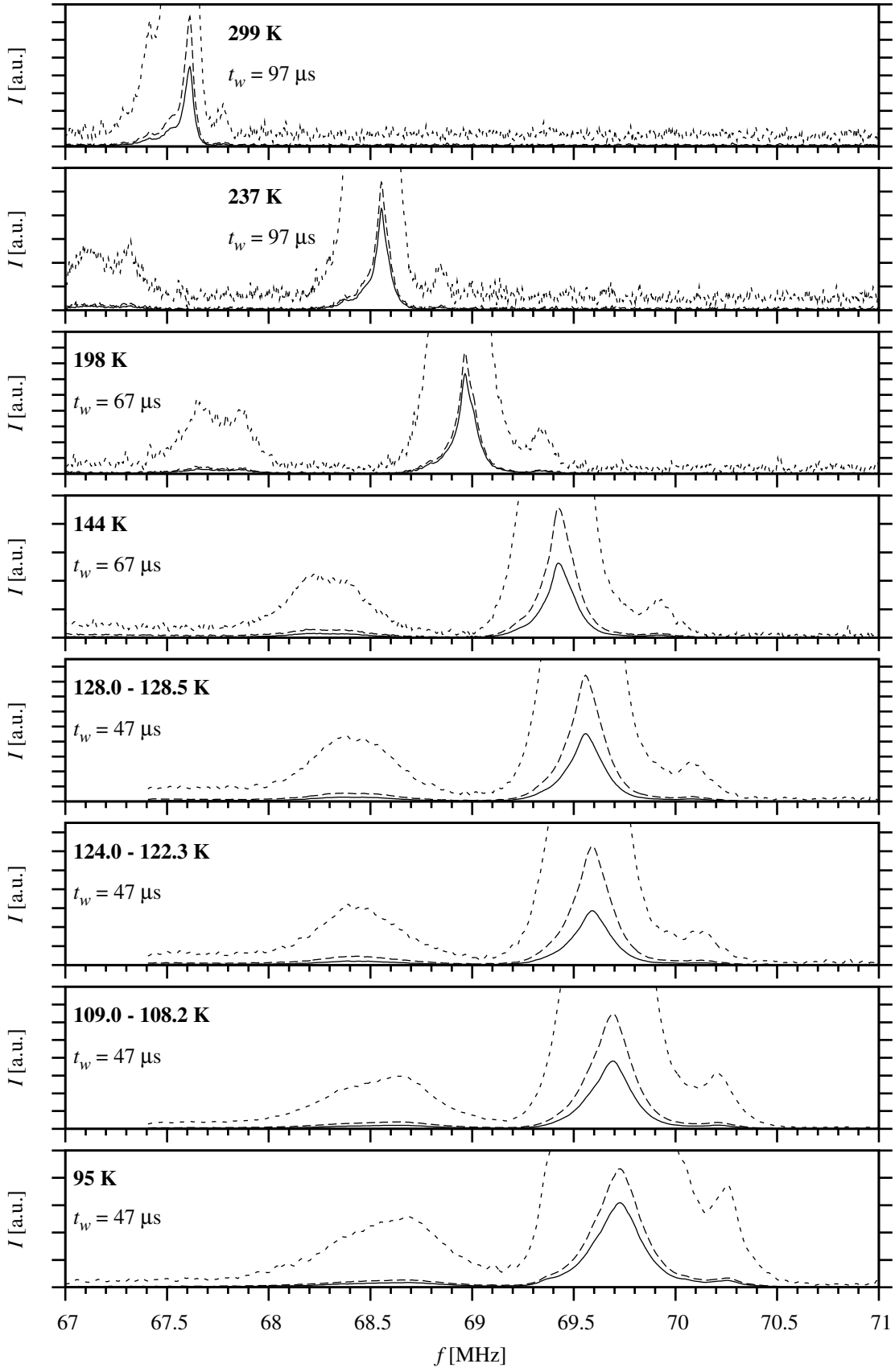

Figure D.8: Temperature dependence of NMR spectra of sample Ti3 in the range 67 – 71 MHz (detail of fig. D.7; see fig. D.7 for key)

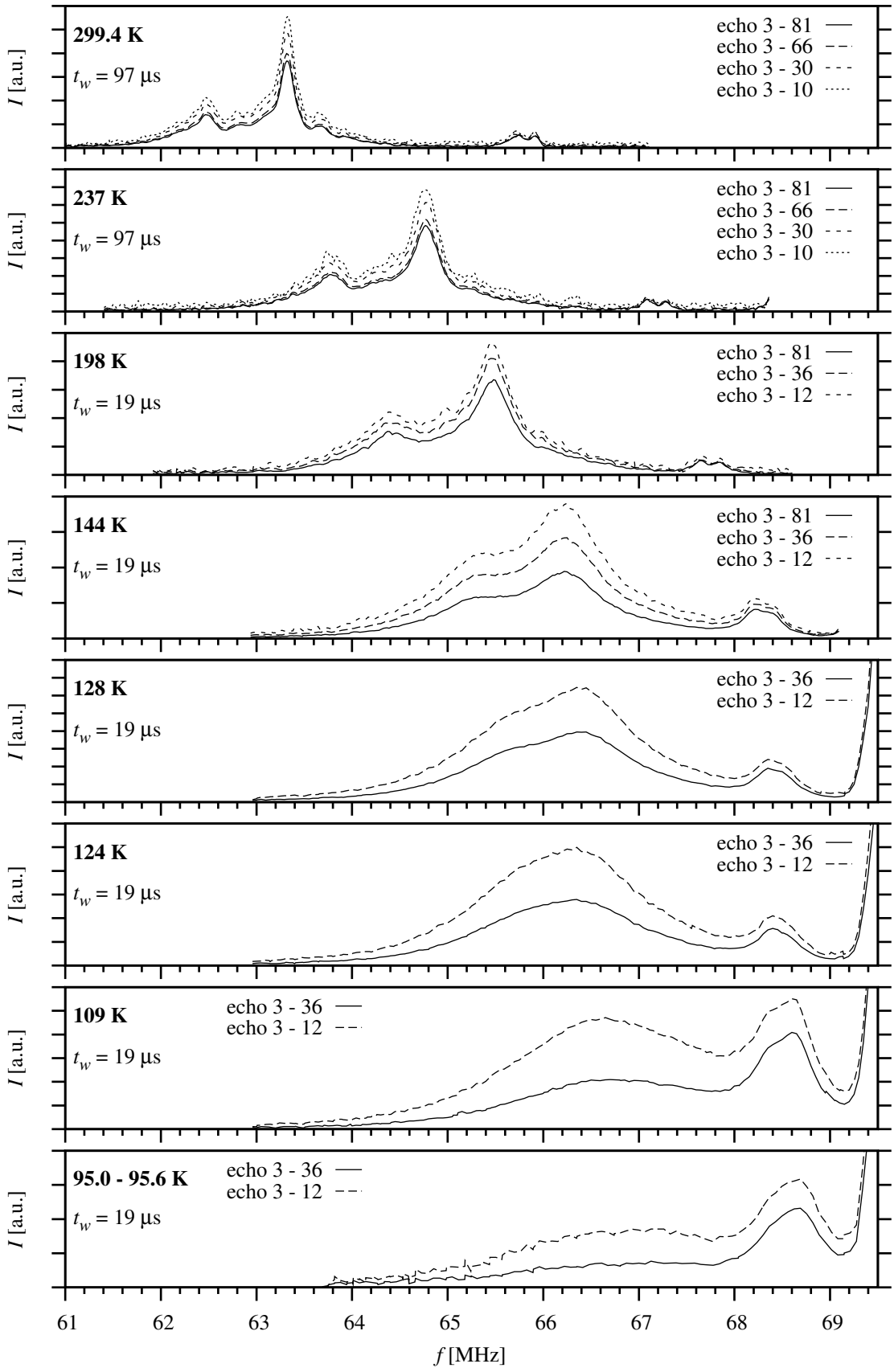

Figure D.9: Temperature dependence of NMR spectra of sample Ti3 in the range 61 – 69.5 MHz

Appendix E

Temperature Dependences of Spectral Signal Frequencies of Titanium Substituted Magnetite Samples - Tables

Table E.1: Temperature dependences of spectral signal frequencies of the sample Ti1 - part 1

Temperature	**Frequency** f [MHz]				
T [K] ± 0.5	$\mathbf{B_1}$	sat 2	**B**	$\mathbf{B_2}$	sat 4
116.0			66.330 ± 0.060		
116.5			66.350 ± 0.025		
118.0			66.370 ± 0.030		
124.0			66.300 ± 0.035		
128.0	65.75 ± 0.15			66.430 ± 0.060	
136.0	65.390 ± 0.030			66.350 ± 0.020	
144.0	65.250 ± 0.030			66.270 ± 0.030	
168.0	64.870 ± 0.030			65.970 ± 0.025	66.570 ± 0.060
198.0	64.428 ± 0.020	65.000 ± 0.040		65.545 ± 0.015	66.060 ± 0.060
216.0	64.150 ± 0.015	64.700 ± 0.070		65.250 ± 0.010	65.770 ± 0.040
237.0	63.800 ± 0.010	64.300 ± 0.050		64.860 ± 0.010	65.320 ± 0.050
273.0	63.091 ± 0.007	63.510 ± 0.040		64.066 ± 0.004	64.480 ± 0.040
299.0	62.580 ± 0.006	62.960 ± 0.040		63.475 ± 0.003	63.860 ± 0.030

Table E.2: Temperature dependences of spectral signal frequencies of the sample Ti1 - part 2

Temperature	**Frequency** f [MHz]									
T [K] ± 0.5	sat 5	sat 6	sat 7	sat 8	sat 9	sat 10	**A**	sat 11	sat 12	sat 13
116.0		68.340 ± 0.060	68.630 ± 0.030	69.380 ± 0.040			69.643 ± 0.006			
116.5		68.320 ± 0.030	68.610 ± 0.020	69.400 ± 0.015			69.638 ± 0.003			70.145 ± 0.010
118.0 ± 1.0		68.300 ± 0.020	68.600 ± 0.015	69.390 ± 0.010			69.627 ± 0.003			70.130 ± 0.007
124.0		68.280 ± 0.015	68.560 ± 0.020	69.360 ± 0.015			69.588 ± 0.003			70.085 ± 0.015
128.0			68.380 ± 0.020	69.378 ± 0.015		69.485 ± 0.015	69.558 ± 0.004			70.110 ± 0.015
136.0		68.274 ± 0.015	68.480 ± 0.020	69.310 ± 0.010			69.495 ± 0.005		69.813 ± 0.007	70.010 ± 0.010
144.0		68.210 ± 0.010	68.417 ± 0.010	69.248 ± 0.010			69.434 ± 0.005		69.735 ± 0.015	69.927 ± 0.010
168.0		68.000 ± 0.020	68.203 ± 0.010	69.066 ± 0.010			69.243 ± 0.003	69.295 ± 0.008	69.486 ± 0.007	69.685 ± 0.010
198.0	67.655 ± 0.010	67.692 ± 0.010	67.877 ± 0.007	68.805 ± 0.010		68.942 ± 0.010	68.981 ± 0.003			69.352 ± 0.010
215.7	67.435 ± 0.006	67.462 ± 0.006	67.645 ± 0.006	68.630 ± 0.007	68.720 ± 0.015		68.804 ± 0.005	68.839 ± 0.005		69.139 ± 0.010
237.0	67.120 ± 0.010	67.162 ± 0.010	67.330 ± 0.010	68.395 ± 0.008	68.493 ± 0.015		68.568 ± 0.002	68.596 ± 0.007		68.860 ± 0.010
273.0	66.423 ± 0.007	66.480 ± 0.007	66.635 ± 0.007	67.886 ± 0.003	67.994 ± 0.010	68.040 ± 0.003	68.0712 ± 0.0015	68.103 ± 0.002		68.295 ± 0.010
299.0	65.939 ± 0.010	66.007 ± 0.007	66.142 ± 0.007	67.488 ± 0.005	67.590 ± 0.010		67.6790 ± 0.0015	67.704 ± 0.007		

Table E.3: Temperature dependences of spectral signal frequencies of the sample Ti2 - part 1

Temperature	**Frequency** f [MHz]						
T [K] ± 0.5	$\mathbf{B_1}$	sat 1	sat 2	**B**	$\mathbf{B_2}$	sat 3	sat 4
116.0				66.400 ± 0.025			
124.0				66.300 ± 0.015			
128.0	65.90 ± 0.10				66.500 ± 0.010		
144.0	65.230 ± 0.010				66.246 ± 0.007		
168.0	64.826 ± 0.005				65.950 ± 0.005		
198.2	64.384 ± 0.004	64.480 ± 0.015	64.960 ± 0.050		65.508 ± 0.003	65.610 ± 0.015	65.990 ± 0.040
236.6	63.753 ± 0.003	63.838 ± 0.010	64.260 ± 0.035		64.826 ± 0.003	64.900 ± 0.020	65.300 ± 0.050
299.1	62.330 ± 0.003	62.400 ± 0.010	62.690 ± 0.040		63.196 ± 0.003	63.270 ± 0.010	63.580 ± 0.050

Table E.4: Temperature dependences of spectral signal frequencies of the sample Ti2 - part 2

Temperature	**Frequency** f [MHz]					
T [K] ± 0.5	sat 5	sat 6	sat 7	sat 8	**A**	sat 13
116.2		68.320 ± 0.025	68.610 ± 0.015		69.642 ± 0.002	
123.8		68.270 ± 0.005	68.550 ± 0.010		69.5845 ± 0.0015	70.070 ± 0.020
127.7		68.370 ± 0.020	68.680 ± 0.040		69.5540 ± 0.0015	70.105 ± 0.007
144.0		68.210 ± 0.015	68.416 ± 0.010	69.244 ± 0.005	69.432 ± 0.001	69.929 ± 0.005
168.0		67.990 ± 0.010	68.190 ± 0.010	69.065 ± 0.003	69.238 ± 0.001	69.677 ± 0.007
198.0	67.652 ± 0.008	67.686 ± 0.007	67.875 ± 0.008	68.803 ± 0.003	68.975 ± 0.001	69.370 ± 0.020
236.7	67.095 ± 0.005	67.130 ± 0.005	67.310 ± 0.005	68.393 ± 0.004	68.570 ± 0.001	68.870 ± 0.010
298.0	65.920 ± 0.007	65.988 ± 0.005	66.121 ± 0.004	67.470 ± 0.002	67.662 ± 0.001	67.831 ± 0.002

Table E.5: Temperature dependences of spectral signal frequencies of the sample Ti3 - part 1

Temperature	**Frequency** f [MHz]				
T [K] ± 0.5	$\mathbf{B_1}$	sat 2	**B**	$\mathbf{B_2}$	sat 4
95.3			67.00 ± 0.40		
109.0			66.65 ± 0.20		
124.0	65.70 ± 0.20			66.33 ± 0.15	
128.0	65.65 ± 0.15			66.39 ± 0.10	
144.0	65.30 ± 0.10			66.230 ± 0.050	
198.0	64.390 ± 0.050			65.480 ± 0.025	65.960 ± 0.060
237.0	63.780 ± 0.050	64.280 ± 0.070		64.770 ± 0.025	65.240 ± 0.060
299.4	62.480 ± 0.030	62.820 ± 0.050		63.320 ± 0.015	63.660 ± 0.040

Table E.6: Temperature dependences of spectral signal frequencies of the sample Ti3 - part 2

Temperature	**Frequency** f [MHz]				
T [K] ± 0.5	sat 6	sat 7	sat 8	**A**	sat 13
95.0	68.360 ± 0.040	68.680 ± 0.025		69.727 ± 0.007	70.260 ± 0.010
108.6	68.350 ± 0.025	68.645 ± 0.040		69.694 ± 0.006	70.210 ± 0.020
123.2 ± 1.0		68.430 ± 0.050		69.592 ± 0.006	70.125 ± 0.025
128.3	68.370 ± 0.040	68.510 ± 0.050		69.558 ± 0.007	70.080 ± 0.015
144.0	68.210 ± 0.040	68.360 ± 0.040		69.426 ± 0.005	69.920 ± 0.020
198.0	67.670 ± 0.040	67.860 ± 0.030	68.798 ± 0.004	68.966 ± 0.003	69.338 ± 0.020
237.0	67.110 ± 0.040	67.310 ± 0.025	68.370 ± 0.005	68.555 ± 0.003	68.840 ± 0.015
299.0	65.810 ± 0.040	66.000 ± 0.020	67.415 ± 0.006	67.612 ± 0.002	67.777 ± 0.015

Appendix F

Temperature Dependences of HWHM of the A Lines of Titanium Substituted Magnetite Samples - Tables

Table F.1: Temperature dependence of half width at half maximum of the A line of the sample Ti1

Temperature T [K] ± 0.5	**A HWHM** [kHz] ± 0.20
116.0	26.55
116.5	25.55
118.0 ± 1.0	25.50
124.0	23.70
128.0	22.75
136.0	19.60
144.0	17.50
168.0	12.10
198.0	9.30
215.7	8.70
237.0	7.35
273.0	7.30
299.0	6.70

Table F.2: Temperature dependence of half width at half maximum of the A line of the sample Ti2

Temperature T [K] ± 0.5	**A HWHM** [kHz] ± 0.20
116.2	29.20
123.8	17.60
127.7	17.40
144.0	12.45
168.0	9.75
198.0	8.60
236.7	6.50
298.0	6.30

Table F.3: Temperature dependence of half width at half maximum of the A line of the sample Ti3

Temperature T [K] ± 0.5	**A HWHM** [kHz] ± 0.20
95.0	128.30
108.6	110.30
123.2 ± 1.0	99.75
128.3	92.10
144.0	74.85
198.0	44.75
237.0	34.15
299.0	26.80

Bibliography

[1] Mizoguchi M. (2001): *Charge and Orbital Ordering Structure of Fe_3O_4 in the Low-Temperature Phase as Deduced from NMR Study*, J. Phys. Soc. Jpn. 70, 2333–2344.

[2] Novák P., Štěpánková H., Englich J., Kohout J., Brabers V. A. M. (2000): *NMR in magnetite below and around the Verwey transition*, Phys. Rev. B 61, 1256–1260.

[3] Gamaliy E., Štěpánková H., Englich J., Kohout J., Snezhko A., Novák P., Brabers V.A.M. (2002): *NMR of ^{57}Fe above the Verwey transition in Al-substituted magnetite*, J. Magn. Magn. Mater. 242–245, 732–734.

[4] Kohout J., Gamaliy E., Štěpánková H., Englich J., Novák P., Brabers V.A.M. (2004): *NMR of ^{57}Fe below and around the Verwey transition in Al-substituted magnetite*, J. Magn. Magn. Mater. 272–276, e1687–e1688.

[5] Kohout J., Gamaliy E., Štěpánková H., Englich J., Procházka V., Chlan V., Brabers V.A.M. (2005): *NMR of ^{57}Fe, ^{69}Ga and ^{71}Ga in Ga substituted magnetite*, J. Magn. Magn. Mater. 290–291, 1018–1020.

[6] Chlan V., Gamaliy E., Štěpánková H., Kouřil K., Englich J., Kohout J., Brabers V. (2007): *Nuclear magnetic resonance of ^{57}Fe in Al-, Ga- and Ti-substituted magnetite above Verwey temperature*, J. Magn. Magn. Mater. 310, 2555–2557.

[7] Řezníček R.: *Spektra jaderné magnetické rezonance magnetitu se substitucí zinku*, bachelor thesis, MFF UK, Prague, 2008.

[8] Sedlák B., Kuz'min R. N.: *Jaderné resonanční metody ve fyzice pevných látek*, Státní pedagogické nakladatelství, Praha, 1978.

[9] Meiboom S., Gill D. (1958): *Modified Spin-Echo Method for Measuring Nuclear Relaxation Times*, Rev. Sci. Instrum. 29, 688–691.

[10] Walz F. (2002): *The Verwey transition–a topical review*, J. Phys.: Condens. Matter 14, R285–R340.

[11] García J., Subías G. (2004): *The Verwey transition–a new perspective*, J. Phys.: Condens. Matter 16, R145–R178.

[12] Brabers V. A. M.: *Progress in spinel ferrite research. Handbook of Magnetic Materials*, ed. K. H. J. Buschow, Elsevier, Amsterdam, 1995.

[13] Kakol Z.: *Effect of Titanium and Zinc Doping and Influence of Stoichiometry Changes on Physical Properties of Magnetite*, AGH University, Faculty of Physics and Nuclear Techniques, Kraków, 1994.

[14] Krupička S.: *Fyzika feritů a příbuzných magnetických kysličníků*, Academia, Praha, 1969.

[15] Aroyo M. I., Perez-Mato J. M., Capillas C., Kroumova E., Ivantchev S., Madariaga G., Kirov A., Wondratschek H. (2006): *Bilbao Crystallographic Server: I. Databases and crystallographic computing programs*, Zeitschrift für Kristallographie 221, 1, 15–27.

[16] Iizumi M., Koetzle T. F., Shirane G., Chikazumi S., Matsui M., Todo S. (1982): *Structure of magnetite (Fe_3O_4) below the Verwey transition temperature*, Acta Cryst. B 38, 2121–2133.

[17] Wright J. P., Attfield J. P., Radaelli P. G. (2002): *Charge ordered structure of magnetite Fe_3O_4 below the Verwey transition*, Phys. Rev. B 66, 214422.

[18] De Grave E., Persoons R. M., Vandenberghe R. E., de Bakker P. M. A. (1993): *Mössbauer study of the high-temperature phase of Co-substituted magnetites, $Co_xFe_{3-x}O_4$. I. $x \leq 0.04$*, Phys. Rev. B 47, 5881—5893.

[19] Loos J., Novák P. (2002): *Double exchange and superexchange in a ferrimagnetic half-metal*, Phys. Rev. B 66, 132403.

[20] Kubo K., Ohata N. (1972): *A Quantum Theory of Double Exchange. I*, J. Phys. Soc. Jpn. 33, 21.

[21] Štěpánková H.: *Anizotropie hyperjemného pole ve ferimagnetických oxidech*, habilitační práce, MFF UK, Praha, 1999.

[22] Chlan V., Novák P., Štěpánková H., Řezníček R., Kouřil K., Kozłowski A. (2009): *Electronic structure and hyperfine fields in non-stoichiometric magnetite above the Verwey transition*, J. Magn. Magn. Mater., article in press, doi:10.1016/j.jmmm.2009.03.026

[23] Novák P., Štěpánková H., Englich J., Kohout J., Brabers V. A. M. (2000): *Temperature Dependence of NMR in Magnetite*, Ferrites, Proceedings of the Eight International Conference on Ferrites, 2000, Kyoto, p. 131–134.

[24] Kakol Z., Sabol J., Stickler J., Honig J. M. (1992): *Effect of low-level titanium(IV) doping on the resistivity of magnetite near the Verwey transition*, Phys. Rev. B 46, 1975–1978.

[25] Honig J. M. (1995): *Analysis of the Verwey transition in magnetite*, J. Alloys Compd. 229, 24–39.

[26] Gamaliy O.: *Hyperfine interactions in magnetic iron oxides with nonmagnetic substitutions*, Doctoral Thesis, MFF UK, Prague, 2006.

[27] Kokalj. A. (2003): *Computer graphics and graphical user interfaces as tools in simulations of matter at the atomic scale*, Comp. Mater. Sci. 28, 155–168. Code available from http://www.xcrysden.org/.

[28] Bałanda M., Wiecheć A., Kim D., Kakol Z., Kozłowski A., Niedziela P., Sabol J., Tarnawski Z., Honig J. M. (2005): *Magnetic AC susceptibility of stoichiometric and low zin doped magnetite single crystals*, Eur. Phys. J. B 43, 201–212.

[29] Brabers V. A. M., Whall T. E., Knapen P. S. A. (1984): *Preparation of polycrystalline and monocrystalline* $Fe_{3-x}Ti_xO_4$ *spinels*, J. Cryst. Growth 69, 101-107.

[30] Kohout J., Kouřil K., Chlan V., Štěpánková H.: Unpublished results on a gallium substituted magnetite

[31] Kovtun N. M., Koteleva A. M., Moskvin A. S., Shemyakov A. A. (1989): *Navedennye sverchtonkie vzaimodejstvija na jadrach ionov* O^{2-} *v ferritach-spinelach*, Zhurnal eksperimentalnoi i teoreticheskoi fiziki 95, 1459–1466

[32] Novák P., Englich J., Štěpánková H., Kohout J., Lütgemeier H., Wagner K., Tolksdorf W. (1997): *Antisite defects in yttrium iron garnet*, J. Phys. IV France 7, C1-283 – C1-287